

IDŐJÁRÁS

QUARTERLY JOURNAL OF THE HUNGAROMET
HUNGARIAN METEOROLOGICAL SERVICE

CONTENTS

<i>Nikola R. Bačević, Milica G. Radaković, Milena Nikolić, Aleksandar Valjarević, Vladica Stevanović, Dušan Kićović, Ružica Božović, Rastko S. Marković, Slobodan B. Marković, and Tin Lukić: Precipitation during the vegetation period in Central Serbia over 70 years</i>	107
<i>Marie Budíková, Jan Holub, Ladislav Budík, Lenka Příbylová, and Ivana Horová: Five-parameter log-normal distribution and its modification.....</i>	133
<i>Slobodan Gnjato, Igor Leščešen, Tatjana Popov, and Goran Trbić: Comprehensive flood frequency analysis of major Sava River affluents in Bosnia and Herzegovina: risks, and implications for water resources management</i>	161
<i>Kornél Komjáti, Kálmán Csirmaz, and Hajnalka Breuer: Examination of ERA5 thermodynamic profiles and hodographs in the pre-storm environment of severe thunderstorms producing large hail in Hungary between 2019 and 2023.....</i>	177
<i>Krisztina Labancz, László Bozó, and Gábor Kis-Kovács: Evaluation of long-term temporal variations in Hungarian PM₁₀ and PM_{2.5} emissions based on national inventories applied for air quality management</i>	193
<i>Dorottya Szám, Gábor Keve, Árpád Fekete, and Zsolt Hetesi: Changing rainfall patterns and their impact on cereal crops in the Szentes district.....</i>	201
<i>Peter Zaujec and Martin Halaj: Changes in precipitation conditions in Slovakia during northern and southern cyclonic situations in the 1991–2020 period.....</i>	219

IDŐJÁRÁS

Quarterly Journal of the HungaroMet Hungarian Meteorological Service

Editor-in-Chief

LÁSZLÓ BOZÓ

Executive Editor

KRISZTINA LABANCZ

EDITORIAL BOARD

- | | |
|---------------------------------------|--|
| ANTAL, E. (Budapest, Hungary) | MIKA, J. (Budapest, Hungary) |
| BARTHOLY, J. (Budapest, Hungary) | MERSICH, I. (Budapest, Hungary) |
| BATCHVAROVA, E. (Sofia, Bulgaria) | MÖLLER, D. (Berlin, Germany) |
| CZELNAI, R. (Dörcicse, Hungary) | PINTO, J. (Res. Triangle Park, NC, U.S.A.) |
| FERENCZI, Z. (Budapest, Hungary) | PRÁGER, T. (Budapest, Hungary) |
| GERESDI, I. (Pécs, Hungary) | PROBÁLD, F. (Budapest, Hungary) |
| HASZPRA, L. (Budapest, Hungary) | RADNÓTI, G. (Súrány, Hungary) |
| HORVÁTH, Á. (Siófok, Hungary) | S. BURÁNSZKI, M. (Budapest, Hungary) |
| HORVÁTH, L. (Budapest, Hungary) | SZEIDL, L. (Budapest, Hungary) |
| HUNKÁR, M. (Keszthely, Hungary) | SZUNYOGH, I. (College Station, TX, U.S.A.) |
| LASZLO, I. (Camp Springs, MD, U.S.A.) | TAR, K. (Debrecen, Hungary) |
| MAJOR, G. (Budapest, Hungary) | TOTH, Z. (Camp Springs, MD, U.S.A.) |
| MÉSZÁROS, E. (Veszprém, Hungary) | VALI, G. (Laramie, WY, U.S.A.) |
| MÉSZÁROS, R. (Budapest, Hungary) | WEIDINGER, T. (Budapest, Hungary) |

*Editorial Office: Kitaibel P.u. 1, H-1024 Budapest, Hungary
P.O. Box 38, H-1525 Budapest, Hungary
E-mail: journal.idojaras@met.hu*

**Indexed and abstracted in Science Citation Index Expanded™ and
Journal Citation Reports/Science Edition
Covered in the abstract and citation database SCOPUS®
Included in EBSCO's database**

*Subscription by mail:
IDŐJÁRÁS, P.O. Box 38, H-1525 Budapest, Hungary
E-mail: journal.idojaras@met.hu*

IDOJÁRÁS

*Quarterly Journal of the HungaroMet Hungarian Meteorological Service
Vol. 129, No. 2, April – June, 2025, pp. 107–132*

Precipitation during the vegetation period in Central Serbia over 70 years

Nikola R. Bačević¹, Milica G. Radaković², Milena Nikolić^{1,*}, Aleksandar Valjarević³, Vladica Stevanović¹, Dušan Kićović⁴, Ružica Božović⁵, Rastko S. Marković⁶, Slobodan B. Marković^{2,7,8}, and Tin Lukić²

¹ *University of Pristina, Faculty of Sciences and Mathematics, Department of Geography, 38220 Kosovska Mitrovica, Serbia*

² *University of Novi Sad, Faculty of Sciences, Department of Geography, Tourism and Hotel Management, Trg Dositeja Obradovica 3, 21000 Novi Sad, Serbia*

³ *University of Belgrade, Faculty of Geography, Department of Geospatial and Environmental Science, Studentski Trg 3/III, 11000 Belgrade, Serbia*

⁴ *Academy for applied studies Belgrade, The College of Tourism, 11000 Belgrade, Serbia*

⁵ *University of Pristina in Kosovska Mitrovica, Faculty of Technical Sciences, Department of Architecture, Knjaza Miloša 7, 38220 Kosovska Mitrovica, Serbia*

⁶ *University of Nis, Department of Geography and Tourism, Natural Sciences and Mathematics, Visegradska 11, 18000 Nis, Serbia*

⁷ *Serbian Academy of Sciences and Arts, Kneza Mihaila 35, 11000 Belgrade, Serbia*

⁸ *University of Montenegro, Cetinjska 2, 81000 Podgorica, Montenegro*

**Corresponding Author e-mail: milena.nikolic@pr.ac.rs*

(Manuscript received in final form May 22, 2024)

Abstract— In this study, the trend for a category of variables, that is, for the total average annual amount of precipitation for the vegetation period (P-VP) from April to October is presented. Moreover, with the help of Geographic Information System (GIS) numerical analysis, geospatial distribution of the obtained results on the territory of the Central Serbia is described. The main objective of this study is the possible changes in trends for the total average annual amount of precipitation for the vegetation period in the observed area. In terms of methodology, trend testing was conducted using the Mann-Kendall trend test (M-K), trend equation, and trend magnitude. The data used for the necessary analysis were taken from the Meteorological Yearbooks of the Republic Hydrometeorological Institute

of Serbia, with a total of 24 meteorological stations, for the observed time period from 1949 to 2018. A total of 24 time series were analyzed. The average annual amount of precipitation for the vegetation period of the observed area is 427.6 mm. The values range from 362.3 mm to 625.5 mm. The lowest value was recorded in Nis, while the highest value was recorded in Zlatibor. Based on the obtained results, a statistically significant positive trend was recorded in 2 time series, whereas in the remaining 22 time series there was no trend. Furthermore, the results obtained by the trend equation, and trend magnitude indicate a slight increase in the total average annual precipitation in 21 time series and a decrease was recorded in the remaining 3 time series. A decrease in the average annual amount of precipitation for the vegetation period was recorded in three cities, namely: Jagodina (-15.9 mm), Bujanovac (-4.6 mm), and Zajecar (-0.5 mm). Comprehending the interaction between precipitation and vegetation period is crucial for implementing adaptation and mitigation measures in terrestrial ecosystems. The preliminary findings of this study can offer a technical foundation and valuable reference for water resource and sustainable ecological management strategies in the Republic of Serbia, benefiting policymakers and stakeholders involved.

Key-words: climate change, variability, Central Serbia, average annual precipitation trends, vegetation period, Mann-Kendall trend test, GIS

1. Introduction

Both in the rest of the world and in Serbia, climate change is being talked about more and more often, and we are witnessing more and more frequent changes, especially when it comes to two key climate elements – temperature and precipitation. These changes are becoming more and more dynamic, faster, and intense during the last two decades, which is confirmed by many scientific studies devoted to this issue and this very current topic all over the world.

Changes in total average annual precipitation, especially during the vegetation period, can have significant consequences in various sectors, including agriculture, biodiversity, human health, hydrology, forestry, water resources, and others. This kind of research has not been carried out so far, so this study is gaining in importance. Each climate element is variable, to a greater or lesser extent, while spatiotemporal variability is particularly distinctive in precipitation (*Jones, 1999*).

The intensity, distribution, and frequency of precipitation vary around the world and are often subject to climate change, which is confirmed by the results of modern scientific studies by a group of authors (*Musellman et al., 2018; Pall et al., 2019; Roderick et al., 2019, 2020; Ali et al., 2021; Chen et al., 2021; Visser et al., 2021; Masamichi and Sugimoto, 2022; Derdour et al., 2022; Kimberley and Barkdoll, 2023; Salazar et al., 2023; Nosratpour and Rahimzadegan, 2023; Konstali et al., 2023; Lai, et al., 2023; Hines et al., 2023; Ghanghas et al., 2023*). Observing the influence of the general air circulation in the atmosphere on precipitation variability, it is concluded that changes in the total amount of precipitation are greater in the tropical and subtropical zones than in the temperate zone (*Morales, 1977*). In addition, global warming has a major impact on precipitation patterns, leading to extreme weather conditions such as droughts or

heavy rainfall (IPCC, 2018). The total amount of precipitation in most of the world will increase due to climate change, which also applies to the intensity of extreme events (Masamichi, 2021).

This study tries to answer the following questions: (1) if the total annual precipitation for the vegetation period in Central Serbia changed in the period from 1949–2018; (2) whether precipitation trends for the vegetation period are decreasing or increasing; (3) if the obtained trends are statistically significant, and finally, (4) what is the regional representation of precipitation changes for the vegetation period in Serbia. The answers to these questions are provided by the analysis of the annual amounts of precipitation for the vegetation period at 24 meteorological stations located in the observed area. The main goal of this study is to perform the necessary analysis of the variability of the change in the total average annual precipitation for the vegetation period in Central Serbia for the time period from 1949–2018, using the Mann Kendall trend test, trend equation, and trend magnitude. Also, with the help of GIS numerical analysis, the geospatial distribution of the obtained results in the observed area is shown.

1.1. Overview of previous research

The earliest research related to climate change and precipitation variability in Europe shows us that the European continent has the smallest range of variability compared to other continents (Conrad, 1941). In the past decade, many researches related to climate change in Europe, and the variability of the total amount of precipitation have been conducted.

In the north of Europe (Norway) there are no sudden changes in the distribution of precipitation, but a noticeable growing trend has been recorded (Zhou *et al.*, 2022). In the southern part of Europe (Italy), the precipitation trend shows a slight increase of an average of 5.42 mm per year, but none of the analyzed trends is statistically significant (Faqueseh and Grossi, 2024). In the central part of Europe (Hungary), the results of previous research indicate that trend analysis for medium and extreme precipitation rarely shows significant trends (Maheras *et al.*, 2018). The results obtained in the western part of the European continent (Southeast of France) indicate that there is no statistically significant trend (Ramesh *et al.*, 2010). The same case was recorded on the territory of Belgium as well (De Jongh *et al.*, 2006). In the eastern part of the European continent (Lithuania and Belarus), it was determined that the amount of precipitation in Lithuania slightly increased by 10 mm, while in Belarus it significantly decreased by 109 mm (Tripolskaja and Pirogovskaja, 2013).

Meanwhile, a positive trend is present in almost the entire part of southeast Europe (Leščešen *et al.*, 2023). Similar results were obtained in the Balkan Peninsula, the Balkan region, and Serbia (Ducić and Luković, 2005; Đorđević, 2008; Ducić *et al.*, 2009, 2010; Stanojević, 2012; Hrnjak *et al.*, 2013; Radevski *et al.*, 2013; Luković *et al.*, 2014; Gavrilov *et al.*, 2015; Ivanova and Radeva, 2016;

Bačević *et al.*, 2017; Popov *et al.*, 2018; Gavrilov *et al.*, 2019; Alsafadi *et al.*, 2020; Culafić *et al.*, 2020; Porja and Nunaj, 2020; Živanović *et al.*, 2020; Gocić *et al.*, 2020; Erić *et al.*, 2021; Milentijević *et al.*, 2021; Popov and Svetozarević, 2021; Spiridonov and Balabanova, 2021; Amiri and Gocić, 2023; Barbulescu and Postolache, 2023), indicating that in most cases there is no significant trend, and that there are no major changes in the geospatial distribution of precipitation, possibly in some cases a slight increase in the total amount of precipitation was recorded, which coincides with this study and with most of the other studies referring to the entire European continent and being quoted in this chapter.

Such obtained results are a manifestation of several factors, namely: climate changes (increase in average air temperature), the influence of the Atlantic Ocean and the Mediterranean, and the orography of the observed territory. Wu *et al.* (2015) noted a widespread agreement among scholars regarding the significant spatial heterogeneity in vegetation response to precipitation variability. White *et al.* (2005) demonstrated that the dynamic response of terrestrial vegetation in the United States to precipitation changes relies on various topographic attributes such as elevation, slope, and aspect. Propastin *et al.* (2008) attributed the considerable spatial variability in the relationship between vegetation growth and precipitation in Central Asia to distinct vegetation types. Chamailié-Jammes and Fritz (2009) calculated correlations between normalized difference vegetation index (NDVI) and precipitation fluctuations in eastern and southern African savannas, revealing that mean annual precipitation (MAP) actively determines the spatial distributions of vegetation sensitivity to altered precipitation patterns.

Recent studies have attempted a more comprehensive analysis of the spatial patterns of vegetation response to precipitation variability, considering multiple external factors simultaneously. Zeraatkar *et al.* (2022) investigated vegetation response to climatic parameters using zonal statistics, finding a decrease in annual precipitation from 1990 to 2020 with an increase in 2020. They observed a positive relationship between NDVI and precipitation at the annual scale, indicating a decrease in vegetation growth by approximately 90% between 2000 and 2010 due to observed climatic variations. Camberlin *et al.* (2007) examined the response of NDVI to precipitation variations in tropical Africa, associating the spatially heterogeneous vegetation response with MAP, vegetation type, and soil properties. Hawinkel *et al.* (2016) analyzed the precipitation-vegetation relationship over East Africa, highlighting MAP, vegetation type, and elevation as primary controllers of vegetation sensitivity to precipitation variability. Ayanlade *et al.* (2021) assessed spatial and temporal changes in precipitation and their effects on vegetation greenness across six ecological zones in Nigeria, finding that rainfall seasonality significantly influences vegetation greenness in all ecological zones. Chen *et al.* (2020) investigated vegetation response to precipitation anomalies in East Asia (China) and explored factors influencing varied vegetation responses to precipitation variability, including precipitation frequency, and distribution. Soomro *et al.* (2021) studied the relationship between

precipitation and vegetation to devise sustainable management measures for fragile biomes. Their analysis of trends and correlations between precipitation and NDVI from 1982 to 2015 over the Kunhar River basin, Pakistan, suggested that precipitation is not the sole factor influencing vegetation growth, with other climatic and biogeographic factors also playing significant roles.

Eisfelder et al. (2023) conducted a systematic study of seasonal vegetation trends across Europe over 30 years using a novel NDVI time series, revealing varied spatial patterns: positive spring trends in Scandinavia, Russia, and parts of Europe; negative summer trends in southern Russia and western Kazakhstan; and positive autumn trends across the region. Overall, their findings support previous observations of vegetation greening in Europe during the growing season. Knowing the rainfall regime for the vegetation period has great scientific, but also practical importance in almost all domains of modern society, and it is of particular importance in water supply, ecology, flood protection, and agriculture.

2. Data and methods

2.1. Research area

The Republic of Serbia is divided into three main regions, namely: Vojvodina, Central Serbia, and Kosovo and Metohija. Central Serbia (observed area) covers the area of 55,967 km², which makes up three quarters of the total national territory and, in percents, it is about 63%. The observed territory consists of three statistical regions: 1) the city of Belgrade; 2) Sumadija and Western Serbia; and 3) Eastern and Southern Serbia. The observed area stretches between 42° 13' 51" N and 45° 05' 49" N and 19° 06' 27" E and 23° 11' 47" E (*Ilić and Stanković, 2007*).

The important geographical regions of Central Serbia are: Sumadija, Macva, Timocka dolina, Pomoravlje, Podunavlje, Posavina, Podrinje, Zlatibor, Raska region, Toplica, Ponisavlje, Jablanica, Vlasina, and Krajiste (*Drobnjaković and Čikić, 2020*). Also, in addition to administrative borders, it also has clearly defined natural borders to neighboring regions. The rivers Danube and Sava represent the natural border with Vojvodina. The Danube River separates Central Serbia from Romania in the northeast, whereas the Drina River represents the natural border with Bosnia and Herzegovina in the west. In the southwest, the natural border with Montenegro is represented by the Dinarides (mountain range), and in the south it is Kopaonik, the high mountains (Besna Kobilica, Kozjak and Starac) and the Pcinja river valley, which separate the observed territory from Kosovo and Metohija, and North Macedonia. In the east, the Carpatho-Balkanides form the border with Bulgaria (*Radaković et al., 2018*).

In terms of orography, three main mountain ranges can be distinguished, which are located within the observed territory (*Fig. 1*). These are the Dinarides, in the west and southwest parts of Central Serbia, the Carpatho-Balkanides in the east

and the Rhodopes in the southeast. Speaking of the hydrological objects in Central Serbia, the Velika Morava River (the longest river) and its tributaries the rivers Juzna Morava and Zapadna Morava stand out, representing the most important and largest river system of this territory at the same time. Furthermore, many artificial lakes can be singled out: the Celije, Djerdap, Zlatar, Gruza, Gazivode, Vlasina, and Sjenica lakes, and many others (Božić *et al.*, 2006).



Fig. 1. Geographical position of Central Serbia with the analyzed meteorological stations and their altitude.

2.2. Materials

The total amount of precipitation that was discharged during the vegetation period (P-VG) from 1949 to 2018 was calculated on the basis of publicly available data of the Republic Hydrometeorological Institute of Serbia (<https://www.hidmet.gov.rs/>). 24 meteorological stations were used, the data of

which are given in *Table 1* (Bačević, et al., 2021), while their position is given in *Fig. 1*. For the purposes of this research, data on precipitation from 24 meteorological stations were used. Details of station names, geographic coordinates, geographic position, and their altitude are shown in *Fig. 1* and *Table 1*.

Table 1. List of meteorological stations located in Central Serbia, names of time series, their geographic coordinates, and altitudes

No.	Meteorological station	Name of time series	ϕ (°N)	λ (°E)	<i>h</i> (m)
1.	Belgrade	BG-P	44°48′	20°28′	132
2.	Bujanovac	BU-P	42°27′	21°46′	399
3.	Cuprija	CU-P	43°56′	21°23′	123
4.	Dimitrovgrad	DI-P	43°01′	22°45′	450
5.	Jagodina	JA-P	43°59′	21°23′	115
6.	Knjazevac	KZ-P	43°34′	22°15′	263
7.	Kragujevac	KG-P	44°02′	20°56′	181
8.	Kraljevo	KV-P	43°43′	20°42′	215
9.	Krusevac	KS-P	43°37′	21°15′	166
10.	Kursunlija	KU-P	43°08′	21°16′	384
11.	Leskovac	LE-P	42°59′	21°57′	231
12.	Loznica	LO-P	44°32′	19°14′	121
13.	Negotin	NG-P	44°14′	22°32′	42
14.	Nis	NI-P	43°20′	21°54′	202
15.	Novi Pazar	NP-P	43°08′	20°31′	545
16.	Pirot	PI-P	43°09′	22°35′	373
17.	Pozega	PZ-P	43°51′	20°02′	311
18.	Sjenica	SJ-P	43°16′	20°00′	1038
19.	Smederevska Palanka	SP-P	44°22′	20°57′	121
20.	Valjevo	VA-P	44°17′	19°55′	174
21.	Veliko Gradiste	VG-P	44°45′	21°30′	80
22.	Vranje	VR-P	42°33′	21°55′	433
23.	Zajecar	ZA-P	43°53′	22°17′	144
24.	Zlatibor	ZL-P	43°44′	19°43′	1029

2.3. Methods

2.3.1. Statistical data processing

In this paper, three statistical approaches were used in the analysis of trends in the total average annual precipitation for the vegetation period, and the geospatial distribution of data (precipitation) in the observed area was determined. The trend equation represents the first approach, which is calculated for each time series separately (Bačević et al., 2022). The second approach (independently of the first approach) represents data testing using and applying the non-parametric MK trend

test (Papić *et al.*, 2020). The third approach consists of determining the trend magnitude obtained by means of the trend equation (Bačević *et al.*, 2020). Trend analyses were carried out with the help of the XLSTAT extension (<https://www.xlstat.com/en>) in the Excel Microsoft Office package.

The first method includes linear regression, which describes the equation of the vegetation period precipitation trend for each meteorological station, in general form:

$$y = ax + b, \quad (1)$$

where y represents the total amount of precipitation in the vegetative period in mm, a is a slope that can be positive, negative or non-existent, x is a time series, while b is the value of precipitation at the beginning of the analyzed period (Bačević *et al.*, 2018; Vukoičić *et al.*, 2018). After this analysis, a trend magnitude analysis was conducted (Gavrilov *et al.*, 2018):

$$\Delta y = y(P_b) - y(P_e), \quad (2)$$

where Δy represents the trend magnitude in mm, $y(P_b)$ is the value of precipitation during the vegetation period in the first analyzed year, while $y(P_e)$ is the same value in the last year of the time series. The trend magnitude can be zero in case the specified values are equal, positive, or negative. In the first case the trend magnitude does not exist, in the second it is increasing, and in the third it is decreasing.

The third analytical method used in this paper is the use of the Mann-Kendall test on the time series of precipitation of the vegetation period in Central Serbia (Mann, 1945; Kendall, 1975). Each data in the time series is assigned a rank. Mutual differences in pairs of ranks are used to calculate the trend direction and strength, after which the variance of the test statistic, i.e., the randomness of the variability in the data, is determined. If the variance is small, the data are slightly scattered and vice versa. The last step is to determine the significance of the trend. This process begins by comparing the calculated test statistic with the data distribution, assuming that there is no trend (H_0 hypothesis). If the test statistic exceeds the critical value from the distribution, it means that there is a statistically significant trend (H_a hypothesis). This value that tells how much the test statistic exceeds the critical value from the distribution is called *p-value*. If this value is less than 0.05 or 5%, the trend results are statistically significant and we have to reject H_0 (Gavrilov, 2016; Stojićević, 2016; Razavi *et al.*, 2016).

2.3.2. Spatial data analysis

All digital cartographic analyses were conducted using ArcGIS Pro: 3.2.0. Data, which are necessary for mapping, were taken from the Internet and from

established databases, obtained during statistical processing. GIS and data modeling are very powerful tools for evaluating and calculating meteorological data of an area (Tomazos and Butler, 2009; Blake et al., 2007; Valjarević et al., 2022). In this paper, preference is given to the kriging method within the interpolation to show the geographical distribution of the average amount of precipitation during the vegetation period in the analyzed period.

The results of the statistical analysis are spatially represented using the Create Thiessen Polygons tool of the Arc GIS software. This method was developed by Thiessen (Thiessen, 1911), a meteorologist, more than a century ago, and refers to the creation of a polygon in the center of which is the entered coordinate (Radaković, 2017), in this case the coordinate of a meteorological station. Using this method, the entire territory of Central Serbia is divided into areas where the results of the linear regression and the Mann-Kendall test are the same: the trend in precipitation during the vegetation period exists as positive, negative, or non-existent.

All procedures and approaches used for the purpose of this research are presented in the flow chart given in Fig. 2.

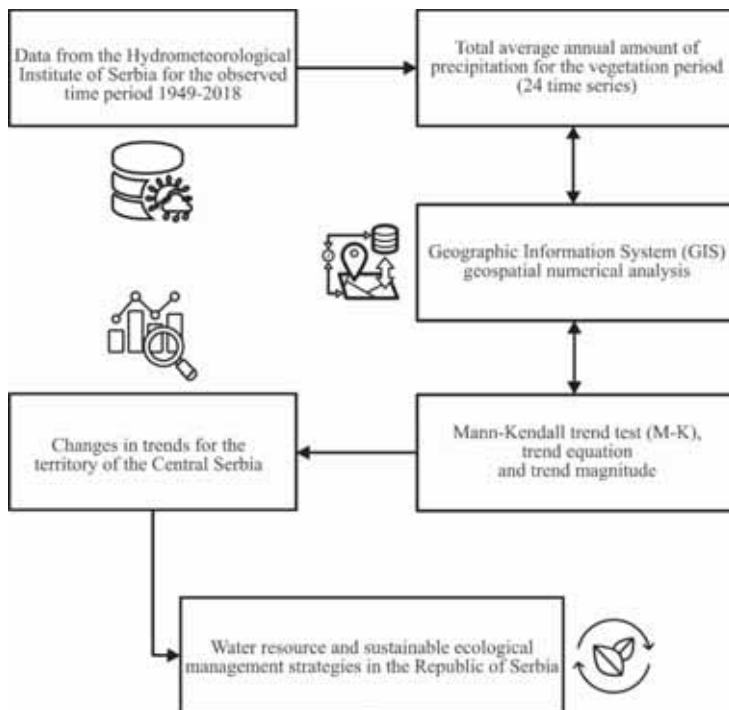


Fig. 2. Flow chart with all the procedures and methods used in this research.

3. Results

3.1. Trend parameters

In this scientific study, the obtained results are presented and summarized in *Table 2*, as well as in *Figs. 3, 4, 5, and 6*. Also, the analysis is presented for a total of 24 meteorological stations and the same number of time series, which are located in the territories of Central Serbia. Based on these variables, the values of the total annual amount of precipitation during the vegetation period (April-October) were calculated. Results for average annual precipitation (P-VP), trend equation results, linear trend equation, and trend magnitude are presented visually in *Table 2* and *Figs. 3 and 4*. The p-value, results of trend testing using the MK trend test and the evaluation of hypotheses for accepting or rejecting the trend are shown in *Fig. 4*, for each meteorological station, especially in the territory of Central Serbia, for the time interval from 1949 to 2018. The spatial distribution of the total annual amount of precipitation in Central Serbia is shown in *Fig. 6*.

Table 2. Names of time series, trend equation y , trend magnitude Δy , and average annual amount of precipitation for the vegetation period for 24 time series, which refer to the territory of Central Serbia.

Time series	Trend equation	Δy (mm)	Average amount of precipitation for the vegetation period (mm)
BG-P-VP	$y=0.3001x + 431.37$	20.7	442.0
BU-P-VP	$y=-0.0667x + 371.82$	-4.6	369.5
CU-P-VP	$y=0.2259x + 408.11$	15.6	416.1
DI-P-VP	$y=0.761x + 384.49$	52.5	411.5
JA-P-VP	$y=-0.2304x + 383.89$	-15.9	375.7
KZ-P-VP	$y=0.2966x + 366.77$	20.5	377.3
KG-P-VP	$y=0.3828x + 402.75$	26.4	416.3
KV-P-VP	$y=0.0792x + 489.06$	5.5	491.9
KS-P-VP	$y=0.0646x + 412.19$	4.5	414.5
KU-P-VP	$y=0.6421x + 378.99$	44.3	401.8
LE-P-VP	$y=0.7006x + 350.9$	48.3	375.8
LO-P-VP	$y=1.0137x + 502.1$	70.0	538.1
NG-P-VP	$y=0.1107x + 374.9$	7.6	378.8
NI-P-VP	$y=0.7311x + 336.36$	50.4	362.3
NP-P-VP	$y=1.1527x + 360.74$	79.5	401.7
PI-P-VP	$y=0.535x + 356.48$	37.0	375.5
PZ-P-VP	$y=0.4888x + 474.84$	32.7	492.2
SJ-P-VP	$y=1.5411x + 415.72$	106.3	470.4
SP-P-VP	$y=1.2584x + 370.19$	86.8	414.9
VA-P-VP	$y=0.8308x + 489.06$	57.3	518.6
VG-P-VP	$y=0.4541x + 430.82$	31.3	446.9
VR-P-VP	$y=0.0545x + 369.97$	3.7	371.9
ZA-P-VP	$y=-0.0073x + 374.55$	-0.5	374.3
ZL-P-VP	$y=1.9215x + 557.24$	132.5	625.5

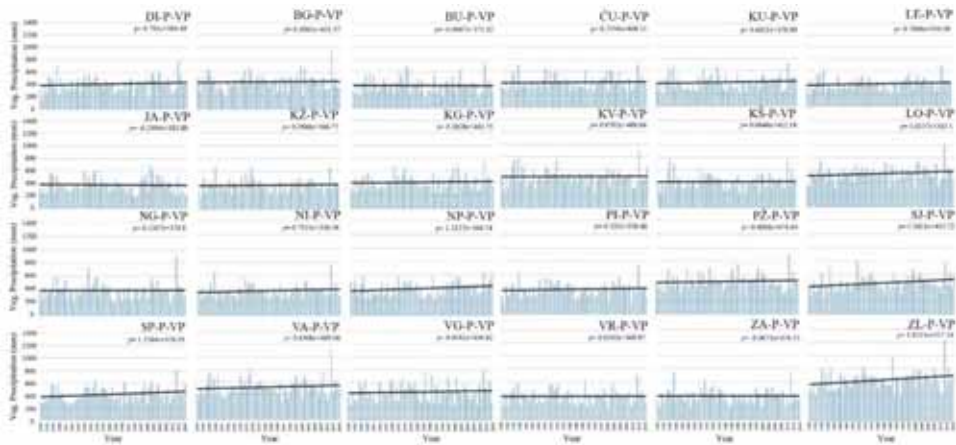


Fig. 3. Visual representation of the average annual precipitation for the vegetation period, trend equation, and linear trend for selected meteorological stations, which are arranged from the station with the lowest to the station with the highest average annual precipitation in Central Serbia for the observed time period from 1949 to 2018.

The obtained results of the abovementioned parameters, which are shown in Fig. 3 and Table 2, indicate a slight increase in the average total annual precipitation (P-VP) in the territory of Central Serbia, which is not the case for three time series (BU-P-VP, JA-P-VP, and ZA-P-VP) in which a negative balance was recorded. Out of a total of 24 time series, a slight increase in the average annual amount of precipitation for the vegetation period was recorded in 21 time series, while the total amount of precipitation for the vegetation period was decreasing in the remaining 3 time series. The highest increase in the average total annual precipitation of 132.5 mm was recorded in the time series ZI-P, followed by the time series SJ-P-VP and SP-P-VP, where the increases of 106.3 mm and 86.8 mm were recorded, respectively. The lowest increase in the average total annual precipitation of 3.7 mm was recorded in the time series VR-P-VP, followed by the time series KS-P-VP (4.5 mm) and KV-P-VP (5.5 mm). The highest decrease in the total average annual precipitation of -15.9 mm was recorded in the JA-P-VP time series. It is followed by the time series BU-P-VP and ZA-P-VP having the decrease of -4.6 mm and -0.5 mm respectively. Data on the total amount of precipitation from Table 2 for each meteorological station in Central Serbia are described and shown in more detail in Fig. 6 and in Section 3.3. GIS numerical analysis.

3.2. Trend assessment

The results obtained from the analysis of the MK trend test and the evaluation of hypotheses (p-values, type of hypothesis, risk of rejecting the hypothesis) are described spatially in *Fig. 4*. Out of a total of 24 time series, a significant statistically positive trend was recorded in 2 time series, where the H_a hypothesis prevails and where the p-value is lower than the significance level α , whose value is 0.05, whereas in 22 time series there is no trend. For these 2 time series in Sjenica and Zlatibor (SJ-P-VP and ZL-P-VP), where a significant positive statistical trend and H_a hypothesis prevails, there is a very small percentage of risk, ranging between 2.36% and 4.08%, that the given hypothesis will be rejected.

Out of a total of 22 time series, where there is no trend and where the H_0 hypothesis prevails, in most cases the risk of rejecting this hypothesis is very high. The risk values to reject this hypothesis range from 7.39% to 97.93%. A risk whose value is between 5.00% and 10.00% was recorded in one time series in Novi Pazar (NP-P-VP), which indicates that there will certainly be no trend in the future. Values between 10.00% and 50.00% were recorded in seven time series in Dimitrovgrad, Kursumlija, Leskovac, Loznica, Nis, Pirot, and Smederevska Palanka (DI-P-VP, KU-P-VP, LE-P-VP, LO-P-VP, NI-P-VP, PI-P-VP, and SP-P-VP), which indicates that the trend is in stagnation.

In the last 14 time series: Belgrade, Bujanovac, Cuprija, Jagodina, Knjazevac, Kragujevac, Kraljevo, Kursumlija, Negotin, Pozega, Valjevo, Veliko Gradiste, Vranje, and Zajecar (BG-P-VP, BU-P-VP, CU-P-VP, JA-P-VP, KZ-P-VP, KG-P-VP, KV-P-VP, KS-P-VP, NG-P-VP, PZ-P-VP, VA-P-VP, VG-P-VP, VR-P-VP, and ZA-P-VP), the risk value ranges between 50.00% and 93.93%. These results indicate that in the area of Central Serbia, the total annual amount of precipitation for the vegetation period is stagnant.

In most analyzed cases, the results of the trend equation deviate from the results of the MK trend test, more precisely in 17 time series. In 5 time series the results match each other. As far as non-matching is concerned, mostly the trend equation indicates a positive trend, and the MK test indicates no trend (14 time series). In 3 time series, the trend equation indicates a negative trend, while the MK test indicates that the trend does not exist. These results are shown in more detail in *Figs. 4* and *5*.

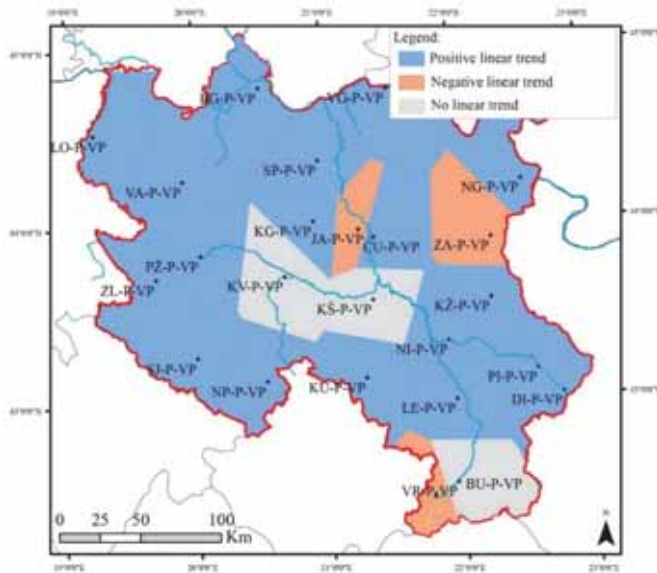


Fig. 4. Cartographic representation of the obtained results of the movement of the linear equation of the total annual amount of precipitation for the vegetation period in Central Serbia, from 1949 to 2018.

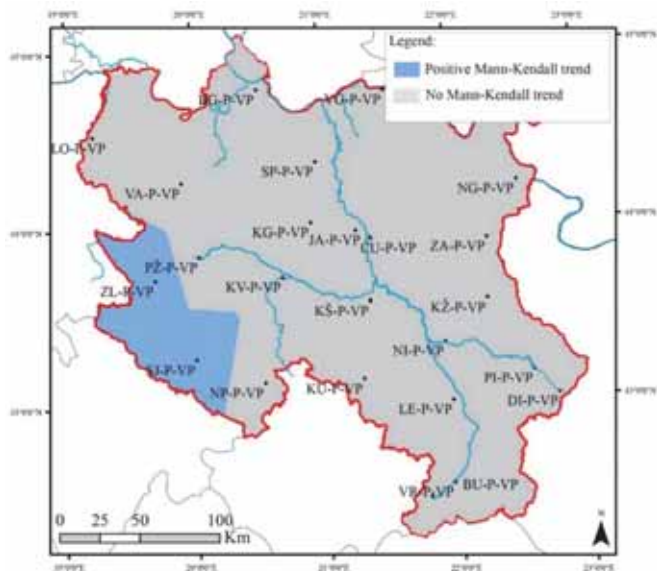


Fig. 5. Cartographic representation of the Mann-Kendall trend test results of the total annual precipitation for the vegetation period in Central Serbia, from 1949 to 2018.

3.3. GIS numerical analysis

The spatial distribution of the total annual amount of precipitation for the vegetation period in the time interval from 1949 to 2018 in Central Serbia is shown in more details in Fig. 6.

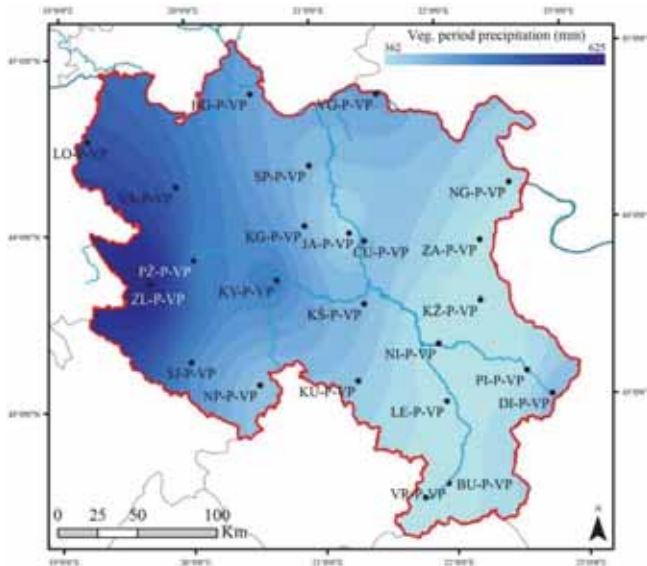


Fig. 6. Spatial distribution of average annual precipitation for the vegetation period from 1949 to 2018 in Central Serbia.

Fig. 6 shows geospatial distribution of the average annual precipitation for the vegetation period (P-VP) in the observed area. Interregional differences in the average annual amount of precipitation are caused by several reasons, among which the followings stand out: the effect of the influx of air masses from the Atlantic Ocean, the effect of the Mediterranean, and the effect of the terrain morphology. Because of this, higher average annual amount of precipitation was recorded in the western and northwestern parts of the observed area, while in the central, southern, and southeastern parts, lower average annual amount of precipitation was recorded for the vegetation period.

Values for the total annual amount of precipitation for the vegetation period in Central Serbia for the time interval from 1949 to 2018 are 427.6 mm ranging between 362.3 – 625.5 mm. The lowest value of the average annual precipitation (362.3 mm) was recorded in Nis and the highest value (625.5 mm) was recorded in Zlatibor. Other values for the average annual amount of precipitation are shown chronologically from the lowest to the highest, namely: Bujanovac (369.5 mm), Vranje (371.9 mm), Zajecar (374.3 mm), Pirot (375.5 mm), Jagodina (375.7 mm),

Leskovac (375.8 mm), Knjazevac (377.3 mm), Negotin (378.8 mm), Novi Pazar (401.7 mm), Kursumlija (401.8 mm), Dimitrovgrad (411.5 mm), Krusevac (414.5 mm), Smederevska Palanka (414.9 mm), Cuprija (416.1 mm), Kragujevac (416.3 mm), Beograd (442 mm), Veliko Gradiste (446.9 mm), Sjenica (470.4 mm), Kraljevo (491.9 mm), Pozeza (492.2 mm), Valjevo (518.6 mm), and Loznica (538.1 mm).

4. Discussion

The same or similar researches, referring to the total average amount of precipitation for the vegetation period in Central Serbia have not been conducted so far. Similarities and differences of the obtained results were compared with and commented based on previous researches which refer to the total annual amount of precipitation in Central Serbia, as well as to the territory of the Republic of Serbia, to the region, to Europe, and to the world.

This scientific study presents a detailed analysis of research results related to the total amount of precipitation during the vegetation period in Central Serbia. Based on the analyzed climate variable, several key aspects can be highlighted and the following can be stated: in this paper, a total of 24 time series were analyzed using trend equations, trend magnitude indicating an average increase or decrease in the value of the total annual precipitation, MK trend test, and GIS numerical analysis.

According to the results obtained from the trend equation and trend magnitude, an increase in the total amount of precipitation for the vegetation period was recorded in twenty-one cities of Central Serbia. A decrease in the average annual amount of precipitation for the vegetation period was recorded in three cities of Central Serbia (*Table 2*). The highest increase in the total amount of precipitation for the vegetation period (132.5 mm) in the past 70 years was recorded in the time series Zlatibor ZI-P-VG, and the lowest increase in the average amount of precipitation for the vegetation period (3.7 mm) was recorded in the time series Vranje VR-P-VP. A decrease in the average annual amount of precipitation for the vegetation period was recorded in three time series, namely: Jagodina JA-P-VP (-15.9 mm), Bujanovac BU-P-VP (-4.6 mm), and Zajecar ZA-P-VP (-0.5 mm). Using the MK test, the obtained results indicate that a statistically significant positive trend in the analyzed parameters was recorded in 2 time series. On the other hand, there is no change (no trend) in 22 time series. The spatial distribution of the average annual amount of precipitation in Central Serbia is 427.6 mm. Its range is between 362.3 – 625.5 mm.

In the paper of *Bačević et al. (2024)*, which refers to the same observed area (Central Serbia) and which has the same research methodology, but a different variable (total annual precipitation), the following results were obtained, which are very similar to the results of this scientific study, namely: a) based on the trend

equation and trend magnitude, an increase in the total annual amount of precipitation was recorded in seventeen time series. The highest average increase in the average annual precipitation of 233.3 mm was recorded in the case of ZL-YP. The lowest increase in total annual precipitation (10.7 mm) was recorded in the case of BG-YT. A decrease in the total annual amount of precipitation was recorded in seven time series related to the average annual amount of precipitation. The lowest decrease in total annual precipitation (-8.0 mm) was recorded in the case of ZA-YP, while the highest increase (-49.9 mm) was recorded in the case of NG-YP; b) Using the MK test, the obtained results indicate that in 5 time series a statistically significant positive trend in the analyzed parameters was recorded. On the other hand, in 19 time series there is no change (no trend); c) The spatial distribution of the average annual amount of precipitation in Central Serbia is 679.9 mm. Its range is between 591.4 – 973.9 mm (Table 3 and Fig. 7).

Table 3. Names of time series, trend equation y , trend magnitude Δy , probability p , for 24 time series (Bačević, et al., 2024).

Time series	Trend equation	Δy (rr)	Average amount of precipitation (rr)
BG-P	$y=0.1551x + 687.34$	10.7	692.8
BU-P	$y=-0.6316x + 646.14$	-43.6	623.7
CU-P	$y=0.5536x + 637.93$	38.2	658.1
DI-P	$y=0.8719x + 614.78$	60.2	644.4
JA-P	$y=-0.1305x + 596.07$	-9.0	591.4
KZ-P	$y=0.4094x + 598.74$	28.2	613.3
KG-P	$y=0.6743x + 612.23$	47.0	635.4
KV-P	$y=-0.1497x + 764.39$	-10.3	757.8
KS-P	$y=0.4411x + 640.38$	30.4	656
KU-P	$y=0.7866x + 630.65$	54.3	658.6
LE-P	$y=1.1444x + 591.42$	79.0	633.2
LO-P	$y=1.5447x + 790.19$	106.6	845
NG-P	$y=-0.6369x + 679.52$	-43.9	656.9
NI-P	$y=1.0139x + 561.62$	70.0	597.6
NP-P	$y=1.5142x + 585.9$	105.0	639.7
PI-P	$y=0.5151x + 575.32$	35.0	593.6
PZ-P	$y=0.2877x + 740.7$	19.9	750.9
SJ-P	$y=2.4294x + 653.17$	167.6	739.4
SP-P	$y=1.5509x + 591.91$	107.0	647
VA-P	$y=0.9847x + 756.25$	67.9	791
VG-P	$y=-0.188x + 694.84$	-13.0	688.2
VR-P	$y=-0.2131x + 621.29$	-14.7	613.7
ZA-P	$y=-0.1163x + 619.64$	-8.0	615.5
ZL-P	$y=3.3817x + 859.51$	233.3	973.9

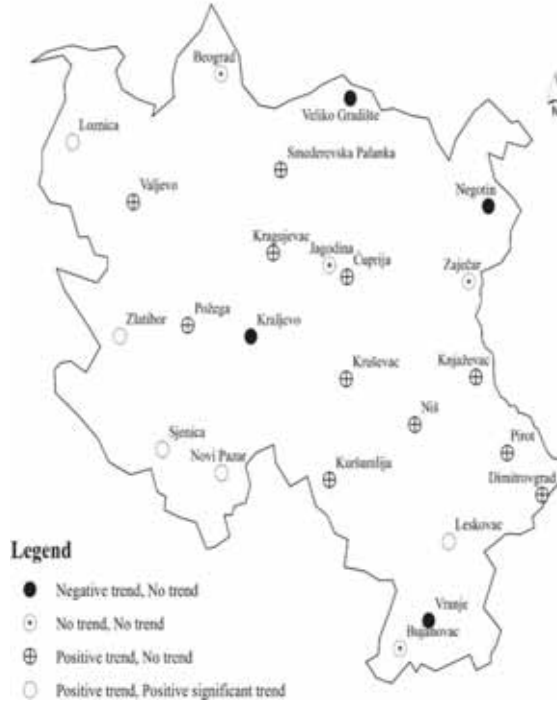


Fig. 7. Cartographic representation of the obtained results of the movement of linear equation and the Mann-Kendall trend test for the total annual amount of precipitation in Central Serbia for the time period from 1949 to 2018 (Bačević, et al., 2024).

The results of this research show a similarity with the research from 2024 in the paper of Bačević et al. (2024). In both researches, a slight increase was observed for climate variables related to the climate element of precipitation (mm) in most of the time series. In this paper, a slight increase in the average amount of precipitation for the vegetation period was recorded in 21 time series, while in the paper of Bačević et al. (2024) this increase was recorded in 17 time series. In the first case, negative balance for the analyzed variables was recorded in 3 time series, and in the second case in 7 time series, which is confirmed by the trend equation and trend magnitude.

Out of a total of 24 time series, the results are identical for 20 time series, while they differ in the remaining 4. For time series where results differ, positive balance is recorded in the first case, while, in the second case, the balance is negative. Furthermore, the MK trend test shows a lot of similarity between the results of both researches. The hypothesis H_0 (no trend) prevails in both cases, while positive trend was recorded in much fewer cases. In this paper, the total number of cases, where no trend was recorded, amounts to 22 time series, while in the paper of Bačević et al. (2024) this number amounts to 19 time series.

Positive trend was recorded in 2 time series in the first case, and in 5 time series in the second case.

Similarities and differences in the obtained results from these two researches arise from the fact that they include the same observed territory, apply the same methodology, and analyze the same number of time series. The only difference is in the variables (total precipitation for the vegetation period and average total annual precipitation).

This study can be used as a basis for future research, which would contribute to new additional knowledge about climate change in the observed territory.

In the paper of *Milentijević et al.* (2022), which includes the territory of Backa (northwestern part of Serbia), the trends of the average annual amount of precipitation for the vegetation period (for five meteorological stations) were analyzed. In all analyzed time series, a slight increase in the total amount of precipitation for the vegetation period was recorded, which is confirmed by the trend equation and trend magnitude. Out of a total of five time series, the hypothesis H_0 (no trend) prevails in four time series, while the hypothesis H_a (positive trend) prevails in only one time series, as shown in *Table 4*. These results match the results of this study because the distance between the observed meteorological stations is very small.

Table 4. Trend equation (y), trend magnitude (Δy) and probability of confidences (p) for precipitation time series (from 1949 to 2018) in Backa. Abbreviations are listed in Section 2.2. (*Milentijević et al.*, 2022).

Time series	Trend equation	Δy (mm)	p (%)
BP-YP	$y = -0.0792x + 616.86$	-5.5	0.8480
BP-P _E -VP	$y = 0.8409x + 365.96$	58.0	0.2438
B-YP	$y = 0.0684x + 590.86$	4.7	0.8520
B-P _E -VP	$y = 0.5936x + 365.6$	40.9	0.2954
N-YP	$y = 1.4727x + 572.45$	101.6	0.1455
N-P _E -VP	$y = 1.712x + 349.03$	118.1	0.0586
P-YP	$y = 1.4039x + 509.03$	96.9	0.0615
P-P _E -VP	$y = 1.3171x + 318.84$	90.9	0.0963
S-YP	$y = 1.2902x + 555.14$	89.0	0.1304
S-P _E -VP	$y = 1.2298x + 351.17$	84.9	0.0450

Similar results were obtained in most of the researches conducted in Serbia. Actually, a slight increase in the total amount of precipitation was recorded in the past period, which coincides with the results of these researches (*Unkašević and Tošić*, 2011; *Tošić et al.*, 2014, 2017; *Gavrilov et al.*, 2015; *Putniković et al.*, 2016;

Milovanović et al., 2017; *Anđelković et al.*, 2018; *Tošić and Putniković*, 2021; *Amiri and Gocić*, 2021a, 2021b; *Vujadinović et al.*, 2022; *Stošić et al.*, 2024).

The results obtained in these researches indicate a slight increase in the total annual amount of precipitation for the observed area, and that climate variability is not sufficiently pronounced. Also, they indicate a higher total annual amount of precipitation in the western part of Central Serbia compared to its eastern parts. Such results are consistent with these researches. Additionally, the findings of this study somewhat align with a more recent study by *Eisfelder et al.* (2023), which highlights that during the spring season, positive NDVI trends extend to Southeast Europe (including Hungary, Romania, Serbia, Bulgaria, North Macedonia, Albania, and Greece), suggesting a relationship between precipitation variability and seasonal vegetation trends.

These conditions are consistent with the observations of *Gončić and Trajković* (2013), who explained that the lack of significant trends in summer and winter precipitation series stemmed from increasing trends in both annual and seasonal minimum and maximum air temperatures, along with a significant decrease in relative humidity. The authors further noted that most stations showed no significant trends on an annual scale, yet a recent study by *Bačević et al.* (2024) reveals statistically positive trends for Loznica, Zlatibor, Sjenica, Novi Pazar, and Leskovac, respectively. This finding correlates with *Djordjević* (2008) discovery that precipitation quantities are increasing on an annual level, with the highest increase observed during winter.

5. Conclusion

This study presents the analyzed trends and geospatial distribution of the obtained results of the average annual amount of precipitation for the vegetation period (one category of variables) in Central Serbia. The observed time interval is from 1949 to 2018, which is a total period of 69 years. The data used for these researches were taken from the Meteorological Yearbooks of the Republic Hydrometeorological Institute of Serbia, with a total of 24 meteorological stations. The Mann-Kendall trend test was used for data processing and trend analyses. Furthermore, trend equations and trend magnitudes were calculated using appropriate formulas and the obtained results were displayed cartographically using GIS numerical analysis.

By analyzing the presented results of this study, it can be concluded that the total annual amount of precipitation for the vegetation period in the territory of Central Serbia is slightly increasing. Based on the trend magnitude, an increase in the average annual amount of precipitation was recorded in twenty-one cities of Central Serbia, while a decrease in the average annual amount of precipitation was recorded in three cities of Central Serbia (*Table 2*). The highest increase in the total amount of precipitation for the vegetation period in the past 69 years

(132.5 mm) was recorded in the time series ZI-P-VG, and the lowest increase in the average amount of precipitation in the vegetation period (3.7 mm) was recorded in the time series VR-P-VP. A decrease in the average annual amount of precipitation for the vegetation period was recorded in three time series, namely: JA-P-VP (-15.9 mm), BU-P-VP (-4.6 mm), and ZA-P-VP (-0.5 mm).

Based on the analysis of the MK trend test shown in *Figs. 5 and 6*, it is concluded that there are significant variations in the trends of the annual amount of precipitation for the vegetation period in Central Serbia. A significant statistically positive trend, where the H_a hypothesis prevails, was identified in only two time series, with a small percentage (2.36% – 4.08%) of the risk of rejecting this claim. In 22 time series, where the H_0 hypothesis prevails, there is no significant trend. The risk of rejecting this hypothesis is high in most cases (7.39% – 97.93). It can be concluded that there will be no trend in the observed territory in the future.

The distribution of the total amount of precipitation for the vegetation period in Central Serbia for a time interval of a total of 69 years (1949–2018) can be clearly seen in *Fig. 6*, providing a visual representation of regional differences, on the basis of which it can be concluded that it is greater in its western part in relation to the eastern parts. The average annual amount of precipitation for the vegetation period of the observed area is 427.6 mm. The values range from 362.3 mm to 625.5 mm. The lowest value was recorded in Nis, while the highest value was recorded in Zlatibor.

The general conclusion of the results obtained in this way, indicating a slight increase in the total amount of precipitation for the vegetation period in Central Serbia, significant variations and the lack of statistical significance in most time series emphasizes the complexity of climate changes in that area, which coincides with the results obtained at the global level.

The preliminary findings of this study can offer a technical foundation and valuable reference for water resource and sustainable ecological management strategies in the Republic of Serbia, benefiting policymakers and stakeholders involved.

Acknowledgement: MGR is grateful for L'Oréal-UNESCO For Women in Science award. SBM is grateful for grant F-178 of Serbian Academy of Sciences and Arts. TL and SBM acknowledge the support of the Ministry of Science, Technological Development and Innovation of the Republic of Serbia (Grant Nos. 451-03-65/2024-03/200123; 451-03-66/2024-03/200125 and 451-03-65/2024-03/200125).

References

- Ali, H., Peleg, N., and Fowler, H.J., 2021: Global scaling of rainfall with dewpoint temperature reveals considerable ocean-land difference. *Geophys. Res. Lett.* 48(15), e2021GL093798. <https://doi.org/10.1029/2021GL093798>
- Alsafadi, K., Mohammed, S.A., Ayugi, B., Sharaf, M., and Harsányi, E., 2020: Spatial–Temporal Evolution of Drought Characteristics Over Hungary Between 1961 and 2010. *Pure Appl. Geophys.* 177, 3961–3978. <https://doi.org/10.1007/s00024-020-02449-5>
- Amiri, M.A. and Gocić, M., 2021a: Analyzing the applicability of some precipitation concentration indices over Serbia. *Theor. Appl. Climatol.* 146(1–2), 645–656. <https://doi.org/10.1007/s00704-021-03743-5>
- Amiri, M.A. and Gocić, M., 2021b: Innovative trend analysis of annual precipitation in Serbia during 1946–2019. *Environ. Earth Sci.* 80(23), 777. <https://doi.org/10.1007/s12665-021-10095-w>
- Amiri, M.A. and Gocić, M., 2023: Analysis of temporal and spatial variations of drought over Serbia by investigating the applicability of precipitation-based drought indices. *Theor Appl Climatol.* 146, 645–656. <https://doi.org/10.1007/s00704-023-04554-6>
- Anđelković, G., Jovanović, S., Manojlović, S., Samardžić, I., Živković, L., Šabić, D., Gatarić, D. and Džinović, M., 2018: Extreme precipitation events in Serbia: defining the threshold criteria for emergency preparedness. *Atmosphere* 9(5), 188. <https://doi.org/10.3390/atmos9050188>
- Ayanlade, A., Jeje, O.D., Nwaezeigwe, J.O., Orimoojunje, O.O.I. and Olokeogun, O.S., 2021: Rainfall Seasonality Effects on Vegetation Greenness in Different Ecological Zones. *Environ. Challen.* 4, 100144. <https://doi.org/10.1016/j.envc.2021.100144>
- Bačević, N., Vukočić, D., Nikolić, M., Janc, N., Milentijević, N. and Gavrilov, M.G., 2017: Aridity in Kosovo and Metohija, Serbia. *Carpathian J. Earth Environ. Sci.* 12(2), 563–570.
- Bačević, R.N., Pavlović, M. and Rašljanin, I., 2018: Trend Assessing Using Mann-Kendall's Test for Pristina Meteorological Station Temperature and Precipitation Data, Kosovo and Metohija, Serbia. *The University Thought – Publ. Nat. Sci.* 8(2), 39–43. <https://doi.org/10.5937/univtho8-19513>
- Bačević, R.N., Valjarević, A., Milentijević, N., Kičović, D., Ivanović, M., and Mujević, M., 2020: Analysis of air temperature trends: City of Podgorica (Montenegro). *The University Thought – Publ. Nat. Sci.* 10(1), 31–36. <https://doi.org/10.5937/univtho10-24790>
- Bačević, R.N., Milentijević, M.N., Valjarević, A., Gicić, A., Kičović, D., Radaković, M., Nikolić, M., and Pantelić, M., 2021: Spatio-temporal variability of air temperatures in Central Serbia from 1949 to 2018. *Időjárás* 125(2):229–253. <https://doi.org/10.28974/idojaras.2021.2.4>
- Bačević, R.N., Milentijević, M.N., Valjarević, A., Nikolić, M., Stevanović, V., Kičović, D., Radaković, G.M., Papić, D., and Marković, B.S., 2022: The analysis of annual and seasonal surface air temperature of southern and southeastern Bosnia and Hercegovina from 1961 to 2017. *Időjárás* 126, 355–374. <https://doi.org/10.28974/idojaras.2022.3.5>
- Bačević, R.N., Valjarević, A., Nikolić, M., Stevanović, V., Dragojlović, J., Radaković, M., Kičović, D., Marković, S.R., Marković, B.S. and Lukić, T., 2024: Determination of changes in the total amount of precipitation using the Mann-Kendall trend test in Central Serbia for the period from 1949 to 2018. *Időjárás* 128, 451–472. <https://doi.org/10.28974/idojaras.2024.4.4>
- Bărbulescu, A. and Postolache, F., 2023: Are the Regional Precipitation and Temperature Series Correlated? Case Study from Dobrogea, Romania. *Hydrology* 10, 109. <https://doi.org/10.3390/hydrology10050109>
- Blake, A., Arbache, S.J., Sinclair, T.M. and Teles, V., 2007. Tourism and poverty relief. *Ann. Tourism Res.* 35(1), 107–126. <https://doi.org/10.1016/j.annals.2007.06.013>
- Božić, D.S., Simonović, P., Miljković Bojanić, E., Nikolić, K., Gavrilović, D., Merenik, S., Ferjančić, S., Vujović, B., Rajić, S., Garić, G., Stepić, M., Stanković, S., Veselinović, A., Gavrilović, Lj., Dimitrijević, R., Stamenković, S., Vlahović, P., Remetić, S., Stojanović, S., and Hamović, D., 2006: Morava, Prvo izdanje, Edicija, Zavod za udžbenike i nastavna sredstva, Beograd. (In Serbian)
- Camberlin, P., Martiny, N., Phillipp, N., and Richard, Y., 2007: Determinants of the interannual relationships between remote sensed photosynthetic activity and rainfall in tropical Africa. *Remote Sens.f Environ* 106, 199–216. <https://doi.org/10.1016/j.rse.2006.08.009>

- Chamaillé-Jammes, S. and Fritz, H., 2009: Precipitation-NDVI relationships in eastern and southern African savannas vary along a precipitation gradient. *Int. J. Remote Sens* 30(13), 3409–3422. <https://doi.org/10.1080/01431160802562206>
- Chen, F., Chen, J., and Huang, W., 2021: Weakened East Asian summer monsoon triggers increased precipitation in Northwest China. *Science China Earth Sciences* 64(5), 835–837. <https://doi.org/10.1007/s11430-020-9731-7>
- Chen, Z., Wang, W., Fu, J., 2020: Vegetation Response to Precipitation Anomalies under Different Climatic and Biogeographical Conditions in China. *Scientific Reports* 10, 830. <https://doi.org/10.1038/s41598-020-57910-1>
- Conrad, V., 1941: The variability of precipitation. *Month. Weather Rev.* 69, 5–11.
- Culafić, G., Popov, T., Gnjata, S., Bajić, D., Trbić, G. and Mitrović, L., 2020: Spatial and temporal patterns of precipitation in Montenegro. *Időjárás* 124, 499–519. <https://doi.org/10.28974/idojaras.2020.4.5>
- De Jongh, I.L.M., Verhoest, N.E.C., and De Troch, F.P., 2006: Analysis of a 105-year time series of precipitation observed at Uccle, Belgium. *Int. J. Climatol.* 26(14), 2023–2039. <https://doi.org/10.1002/joc.1352>
- Derdour, S., Ghenim, A., Megnounif, A., Tangang, F., Chung, J.X., and Ayoub, A.B. 2022: Bias Correction and Evaluation of Precipitation Data from the CORDEX Regional Climate Model for Monitoring Climate Change in the Wadi Chemora Basin (Northeastern Algeria). *Atmosphere* 13(11), 1876. <https://doi.org/10.3390/atmos13111876>
- Drobnjaković, M. and Čikić, J., 2020: The Socio-Spatial Aspect of Rurality - A Case Study of Rural Settlements in Central Serbia. *Mitteilungen der Österreichischen, Geographischen Gesellschaft*, 162. Jg., S. 469–494. <https://doi.org/10.1553/moegg162s469>
- Ducić, V. and Luković, J., 2005: Moguće veze između El Ninjo južne oscilacije (ENSO) i promena količine padavina u Srbiji. *Zbornik radova – Geografski fakultet Univerziteta u Beogradu* 53, 13–22. (In Serbian)
- Ducić, V., Luković, J., and Milovanović, B., 2009: Promene temperatura i padavina u Srbiji u drugoj polovini XX veka u sklopu globalnih klimatskih promena. *Zaštita prirode* 60 (1–2), 641–652. (In Serbian)
- Ducić, V., Luković, J., and Stanojević, G., 2010: Cirkulacija atmosfere i kolebanje padavina u Srbiji u periodu 1949–2004. *Glasnik Srpskog geografskog društva* 90 (2), 85–107. (In Serbian)
- Dorđević, V.S. 2008: Temperature and precipitation trends in Belgrade and indicators of changing extremes for Serbia. *Geographica Pannonica* 12(2), 62–68. <https://doi.org/10.5937/GeoPan0802062D>
- Eisfelder, C., Asam, S., Hirner, A., Reiners, P., Holzwarth, S., Bachmann, M., Gessner, U., Dietz, A., Huth, J., Bachofer, F., and Kuenzler C., 2023: Seasonal Vegetation Trends for Europe over 30 Years from a Novel Normalised Difference Vegetation Index (NDVI) Time-Series—The TIMELINE NDVI Product. *Remote Sens.* 15(14), 3616. <https://doi.org/10.3390/rs15143616>
- Erić, R., Kadović, R., Durđević, V., and Đukić, V., 2021: Future changes in extreme precipitation in central Serbia. *J. Hydrol. Hydromech.* 69(2), 196–208. <https://doi.org/10.2478/johh-2021-0006>
- Faquseh, H. and Grossi, G., 2024: Trend analysis of precipitation, temperature and snow water equivalent in Lombardy region, northern Italy. *Sustain. Water Resour. Manage.* 10, 18. <https://doi.org/10.1007/s40899-023-00992-2>
- Gavrilov, M.B., Marković, S.B., Mlađan, D., Subošić, D., Zarić, M., Pešić, A., Janc, N., Nikolić, M., Valjarević, A., Bačević, N. and Marković, S.I., 2015: Extreme Floods In Serbia Occurring Simultaneously With The High Water Levels And Heavy Rains - Case Study, International Scientific Conference “Archibald Reiss Days“, 3-4 March, Academy Of Criminological and Police Studies, Proceedings Of International Significance, 25-36, Belgrade, Serbia. <https://doi.org/10.1007/s00024-021-02688-0>
- Gavrilov, M.B., Tošić, I., Marković, S.B., Unkašević, M. and Petrović, P., 2016: The analysis of annual and seasonal temperature trends using the Mann-Kendall test in Vojvodina, Serbia. *Időjárás* 120:183–198.
- Gavrilov, M.B., Marković, S.B., Janc, N., Nikolić, M., Valjarević, A., Komac, B., Zorn, M., Punišić, M., and Bačević, N., 2018: Assessing average annual air temperature trends using the Mann–Kendall test in Kosovo. *Acta Geographica Slovenica* 58, 8–25. <https://doi.org/10.3986/AGS.1309>

- Gavrilov, M. B., Lukić, T., Janc, N., Basarin, B., and Marković, S. B., 2019: Forestry Aridity Index in Vojvodina, North Serbia. *Open Geosciences*, 11(1), 367–377. <https://doi.org/10.1515/geo-2019-0029>
- Ghanghas, A., Sharma, A., Dey, S., and Merwade, V., 2023: How Is Spatial Homogeneity in Precipitation Extremes Changing Globally? *Geophys. Res. Lett.* 50(16), 1–9. <https://doi.org/10.1029/2023GL103233>
- Gocić, M. and Trajković, S., 2013a: Analysis of changes in meteorological variables using Mann-Kendall and Sen's slope estimator statistical tests in Serbia. *Glob. Planet. Change* 100, 172–182. <https://doi.org/10.1016/j.gloplacha.2012.10.014>
- Gocić, M. and Trajković, S., 2013: Analysis of Precipitation and Drought Data in Serbia over the Period 1980–2010. *J. Hydrology* 494, 32–42. <https://doi.org/10.1016/j.jhydrol.2013.04.044>
- Gocić, M., Trajković, S., and Milanović, M., 2020: Precipitation and drought analysis in Serbia for the Period 1946–2017. In: (eds. Negm A, Romanescu G, Zelenakova M) *Water Resources Management in Balkan Countries*. Springer Water. Springer, Cham, 277–292. https://doi.org/10.1007/978-3-030-22468-4_11
- Gocić, M., Velimirović, L., Stanković, S.M., and Trajković, S., 2021: Determining the best fitting distribution of annual precipitation data in Serbia using L-moments method. *Earth Sci. Informat.* 14(2), 633–644. <https://doi.org/10.1007/s12145-020-00543-9>
- Hawinkel, P., Thiery, W., Lhermitte, S., Swinnen, E., Verbist, B., Orshoven, J.V., and Muys, B., 2016: Vegetation response to precipitation variability in East Africa controlled by biogeographical factors. *J. Geophys. Res.: Biogeosciences* 121(9), 2422–2444. <https://doi.org/10.1002/2016JG003436>
- Hines, B., Qian, G., Chu, T., and Tordesillas, A., 2023: Variability analysis of monthly precipitation vector time series in Australia by a new spatiotemporal entropy statistic. *Environ.Res.:Climate* 2(1), 011002. <https://doi.org/10.1088/2752-5295/acb5b8>
- Hrnjak, I., Lukić, T., Gavrilov, M. B., Marković, S. B., Unkašević, M., and Tošić, I., 2013: Aridity in Vojvodina, Serbia. *Theor. Appl. Climatol.* 115, 323–332. <https://doi.org/10.1007/s00704-013-0893-1>
- IPCC, 2018: Summary for Policymakers. In: (eds.: Masson-Delmotte, V., Zhai, P., Pörtner, H.O., Roberts, D., Skea, J., Shukla, P.R., Pirani, A., Moufouma-Okia, W., Péan, C., Pidcock, R., Connors, S., Matthews, J.B.R., Chen, Y., Zhou, X., Gomis, M.I., Lonnoy, E., Maycock, T., Tignor, M. and Waterfield, T.) *Global warming of 1.5 °C*. An IPCC Special Report on the impacts of global warming of 1.5 °C above pre-industrial levels and related global greenhouse gas emission pathways, in the context of strengthening the global response to the threat of climate change, sustainable development and efforts to eradicate poverty. WMO, Geneva, 3–24.
- Ilić, J. and Stanković, S., 2007: Geographical centers: Geographical centers of the Republic of Serbia, Central Serbia, the Autonomous Province of Vojvodina and the Autonomous Province of Kosovo and Metohia. *Zbornik Matice srpske za društvene nauke* 123, 109–122. <https://doi.org/10.2298/ZMSDN0723109I>
- Ivanova, V. and Radeva, S., 2016: Precipitation extremes trends in east and south Bulgaria from 1961 to 2010. In: 16th International Multidisciplinary Scientific GeoConference. SGEM, 507–514, Curran Associates, Inc.
- Jones, P., 1999: The Instrumental Data Record: Its Accuracy and Use in Attempts to Identify the "CO2 Signal", In: *Analysis of Climate Variability* (eds. Von Storch, H., Navarra, A.), Springer, Heidelberg, 53–76.
- Kendall, M.G., 1975: Rank correlation methods. Charles Griffin, London.
- Kimberley, M.P. and Barkdoll, B. 2023: Precipitation trends of major world cities with implications for sustainable water infrastructure management. *Sust. Water Resour. Manage.* 9(5), 171. <https://doi.org/10.1007/s40899-023-00950-y>
- Konstali, K., Spensberger, C., Spengler, T., and Sorteberg, A., 2023: Global Attribution of Precipitation to Weather Features. *J. Climate* 37(4), 1181–1196. <https://doi.org/10.1175/JCLI-D-23-0293.1>
- Lai, H., Chen, D. and Chen, H.W. 2023: Precipitation variability related to atmospheric circulation patterns over the Tibetan Plateau. *Int. J. Climatol.* 44, 91–107. <https://doi.org/10.1002/joc.8317>
- Leščešen, I., Basarin, B., Podrašćanin, Z., and Mészáros, M., 2023: Changes in Annual and Seasonal Extreme Precipitation over Southeastern Europe. *Environ. Sci. Proceed.* 26(1) 48.

- <https://doi.org/10.3390/environsciproc2023026048>.
- Luković, J., Bajat, B., Blagojević, D., and Kilibarda, M., 2014: Spatial pattern of recent rainfall trends in Serbia (1961–2009). *Regional Environ. Change* 14(5), 1789–1799.
<https://doi.org/10.1007/s10113-013-0459-x>
- Matheras, P., Tolika, K., Anagnostopoulou, C., Makra, L., Szpirosz, K. and Károssy, C., 2018: Relationship between mean and extreme precipitation and circulation types over Hungary. *Int. J. Climatol.* 38, 4518–4532. <https://doi.org/10.1002/joc.5684>
- Mann, H.B., 1945: Nonparametric tests against trend. *Econometrica* 13, 245–259.
- Masamichi, O. and Sugimoto, S. 2022: Dynamic and thermodynamic contributions of ENSO to winter precipitation in Japan: frequency and precipitation of synoptic weather patterns. *Climate Dynamics* 59(13), 1489–1504. <https://doi.org/10.1007/s00382-021-06052-9>
- Masamichi, O. 2021: Precipitation under climate change. *Precipitation. Earth Surface Respons. Proc.* 2021, 21–51. <https://doi.org/10.1016/B978-0-12-822699-5.00002-1>
- Milentijević, N., Bačević, N., Valjarević, A., Radaković, M. and Pantelić, M., 2021: Assessment of air temperature and precipitation trends: Case study of Macva (Serbia). The 5th Serbian congress of geographers. Novi Sad, Serbia. <https://doi.org/10.13140/RG.2.2.35542.16965>
- Milentijević, N., Valjarević, A., Bačević, R.N., Ristić, D., Kalkan, K., Cimbaljević, M., Dragojlović, J., Savić, S., and Pantelić, M., 2022: Assessment of observed and projected climate changes in Backa (Serbia) using trend analysis and climate modeling. *Időjárás* 126, 47–68.
<https://doi.org/10.28974/idojaras.2022.1.3>
- Milovanović, B., Schuster, P., Radovanović, M., Vakanjac, V.R., and Schneider, C., 2017: Spatial and temporal variability of precipitation in Serbia for the period 1961–2010. *Theor. Appl. Climatol.* 130, 687–700. <https://doi.org/10.1007/s00704-017-2118-5>
- Morales, C., 1977: Rainfall Variability – A Natural Phenomenon, *Ambio* 6, 30–33.
- Musselman, K.N., Lehner, F., Kyoko, I., Clark, M.P., Prein, F.P., Liu, C., Barlage, M., and Rasmussen, R., 2018: Projected increases and shifts in rain-on-snow flood risk over western North America. *Nat. Climate Change* 8(9), 808–812. <https://doi.org/10.1038/s41558-018-0236-4>
- Nosratpour, R. and Rahimzadegan, M., 2023: Clustering and assessment of precipitation climates using satellite precipitation products and improved machine learning precipitation models. *Int. J. Climatol* 43(16), 7819–7850. <https://doi.org/10.1002/joc.8294>
- Pall, P., Tallaksen, L.M., and Stordal, F., 2019: A Climatology of Rain-on-Snow Events for Norway. *Journal of Climate*, 32(20), 6995–7016. <https://doi.org/10.1175/JCLI-D-18-0529.1>
- Papić, D., Bačević, R.N., Valjarević, A., Milentijević, N., Gavrilov, B.M., Živković, M., and Marković, B.S., 2020: Assessment of air temperature trends in South and Southeast Bosnia and Herzegovina from 1961 to 2017. *Időjárás* 124, 381–399. <https://doi.org/10.28974/idojaras.2020.3.5>
- Popov, T., Gnjata, S., and Trbić, G., 2018: Analysis of Extreme Precipitation over the Peri-Pannonian Region of Bosnia and Hercegovina. *Időjárás* 122, 433–452.
<https://doi.org/10.28974/idojaras.2018.4.5>
- Popov, H. and Svetozarević, J., 2021: Changes and contemporary trends in the annual amounts of precipitation in Serbia. *J. Bulgarian Geograph. Soc.* 44, 73–79.
<https://doi.org/10.3897/jbgs.e77102>
- Proja, T and Nunaj L., 2020: Three decades of heat waves and extreme precipitation in Tirana. 11th International Conference of the Balkan Physical Union (BPU11), 28 August - 1 September 2022, Belgrade, Serbia.
- Propastin, P.A., Kappas, M., and Muratova, N.R., 2008: Inter-Annual Changes in Vegetation Activities and Their Relationship to Temperature and Precipitation in Central Asia from 1982 to 2003. *J. Environ. Informat.* 12(2), 75–87. <https://doi.org/10.3808/jei.200800126>
- Putniković, S., Tošić, I., and Đurđević, V., 2016: Circulation weather types and their influence on precipitation in Serbia. *Meteorol Atmos Phys*, 128, 649–662.
<https://doi.org/10.1007/s00703-016-0432-6>
- Radaković, G.M., Tošić, A.I., Bačević, R.N., Mladan, D., Marković S.B. and Gavrilov M.B., 2018: The analysis of aridity in Central Serbia from 1949–2015. *Theor. Appl. Climatol.* 133(3-4), 887–898.
<https://doi.org/10.1007/s00704-017-2220-8>

- Radaković, M., 2017: Utilizing Geographic Information System (GIS) for determining new locations of post office in Novi Sad, Serbia. *Zbornik radova Departmana za geografiju, turizam i hotelijerstvo* 46(2), 105–115.
- Radevski, I., Gorin, S., Markoski, B., Dimitrovska, O., and Todorovska, S., 2013: Spatial Precipitation Distribution in Prespa Basin (Republic Of Macedonia). Hilly-Mountain-Areas Problems and Perspectives, Ohrid, 12-15 IX 2013.
- Ramesh, A., Glade, T., and Malet, J., 2010: Evaluation of climate change on flood event by using parametric T-test and non-parametric Mann-Kendall test in Barcelonnette basin, France. EMS Annual Meeting. Abstracts, 7, 619.
- Razavi, T., Switzman, H., Arain, A., and Coulibaly, P., 2016: Regional climate change trends and uncertainty analysis using extreme indices: A case study of Hamilton, Canada. *Climate Risk Manage.* 13, 43–63. <https://doi.org/10.1016/j.crm.2016.06.002>
- Roderick, T.P., Wasko, C., and Sharma, A., 2019: Atmospheric moisture measurements explain increases in tropical rainfall extremes. *Geophys. Res. Lett.* 46(3), 1375–1382. <https://doi.org/10.1029/2018GL080833>
- Roderick, T. P., Wasko, C., and Sharma, A., 2020: An improved covariate for projecting future rainfall extremes? *Water Resour. Res.* 56(8), e2019WR026924. <https://doi.org/10.1029/2019WR026924>
- Salazar, Á., Thatcher, M., Goubanova, K., Bernal, P., Gutiérrez, J., and Squeo, F., 2023: CMIP6 precipitation and temperature projections for Chile. *Climate Dynamics* 62, 2475–2498. <https://doi.org/10.1007/s00382-023-07034-9>
- Soomro, S., Hu, C., Jian, S., Wu, Q., Boota, M., and Soomro, M.H.A.A., 2021: Precipitation Changes and Their Relationships with Vegetation Responses during 1982–2015 in Kunhar River Basin, Pakistan. *Water Supply* 21, 3657–3671. <https://doi.org/10.2166/ws.2021.129>
- Stanojević, G., 2012: Analiza godišnjih padavinskih suma na prostoru Srbije, Geografski institut „Jovan Cvijić“, SANU, Beograd. UDC: 911.2:551.58(497.11) <https://doi.org/10.2298/IJGI1202001S>
- Stojićević, G., 2016: Bioklimatska slika zapadne Srbije u funkciji turizma. Doktorska disertacija. Univerzitet u Novom Sadu, Prirodno-matematički fakultet, Departman za geografiju, turizam i hotelijerstvo. Novi Sad. (In Serbian)
- Stošić, T., Tošić, M., Lazić, I., da Silva, L., da Silva, A., Putniković, S., Đurđević, V., Tošić, I., and Stošić, B., 2024: Changes in rainfall seasonality in Serbia from 1961 to 2020. *Theor. Appl. Climatol.* 155, 4123–4138. <https://doi.org/10.1007/s00704-024-04871-4>
- Spiridonov, V. and Balabanova, S., 2021: The impact of climate change on intensive precipitation and flood types in Bulgaria. In (Ed. M.-M. Nistor), *Climate and Land Use Impacts on Natural and Artificial*, 153–169. <https://doi.org/10.1016/B978-0-12-822184-6.00001-6>
- Thiessen, A.H., 1911: Precipitation averages for large areas. *Monthly Weather Rev.* 39(7), 1082–1089.
- Tomazos, K. and Butler, R., 2009: Volunteer tourism: the new ecotourism? *Anatolia* 20(1), 196–211.
- Tošić, I., Hrnjak, I., Gavrilov, M.B., Unkašević, M., Marković, S.B., and Lukić, T., 2014: Annual and seasonal variability of precipitation in Vojvodina, Serbia. *Theor. Appl. Climatol.* 117, 331–341. <https://doi.org/10.1007/s00704-013-1007-9>
- Tošić, I., Unkašević, M., and Putniković, S., 2017: Extreme daily precipitation: the case of Serbia in 2014. *Theor. Appl. Climatol.* 128, 785–794. <https://doi.org/10.1007/s00704-016-1749-2>
- Tošić, I. and Putniković, S., 2021: Influence of the East Atlantic/West Russia pattern on precipitation over Serbia. *Theor. Appl. Climatol.* 146(3–4), 997–1006. <https://doi.org/10.1007/s00704-021-03777-9>
- Tripolskaja, L. and Prigovskaja, G., 2013: Impact of climate variability in Lithuania and Belarus on atmospheric precipitation infiltration: lysimetric study. *Zemdirbyste-Agriculture* 100(4), 369–376. <https://doi.org/10.13080/z-a.2013.100.047>
- Unkašević, M. and Tošić, I., 2011: A statistical analysis of the daily precipitation over Serbia: trends and indices. *Theor. Appl. Climatol.* 106, 69–78. <https://doi.org/10.1007/s00704-011-0418-8>
- Valjarević, A., Popovici, C., Štilić, A., and Radojković, M., 2022: Cloudiness and water from cloud seeding in connection with plants distribution in the Republic of Moldova. *Appl Water Sci*, 12, 262. <https://doi.org/10.1007/s13201-022-01784-3>
- Visser, J.B., Wasko, C., Sharma, A., and Nathan, R., 2021: Eliminating the “Hook” in precipitation–temperature scaling. *J. Climate* 34(23), 9535–9549. <https://doi.org/10.1175/JCLI-D-21-0292.1>

- Vujadinović Mandić, M., Vuković Vimić, A., Ranković Vasić, Z., Đurović, D., Ćosić, M., Sotonica, D., Nikolić, D., and Đurđević, V., 2022: Observed changes in climate conditions and weather-related risks in fruit and grape production in Serbia. *Atmosphere* 13(6), 948. <https://doi.org/10.3390/atmos13060948>
- Vukoičić, Z.D., Milosavljević, A.S., Penjišević, T.I., Bačević, R.N., Nikolić, M., Ivanović, D.R., and Jandžiković, M.B., 2018: Spatial analysis of temperature and its impact on the sustainable development of mountain in Central and Western Serbia. *Időjárás* 122(3), 259–283. <https://doi.org/10.28974/idojaras.2018.3.3>
- White, A. B., Kumar, P., and Tchong, D., 2015: A data mining approach for understanding topographic control on climate-induced inter-annual vegetation variability over the United States. *Remote Sens. Environ.* 98(1), 1–20. <https://doi.org/10.1016/j.rse.2005.05.017>
- Wu, D., X. Zhao, S. Liang, T. Zhou, K. Huang, B. Tang, Wenqian Zhaol., 2015: Time-lag effects of global vegetation responses to climate change. *Global Change Biol.* 21, 3520–3531. <https://doi.org/10.1111/gcb.12945>
- Zeraatkar, Z., Shahidi, A. and Memarian, H., 2024: Assessment and efficiency of CMIP6 models in simulation and prediction of climatic parameters of precipitation and temperature in the Samalghan basin, Iran. *Időjárás* 128, 59–75. <https://doi.org/10.28974/idojaras.2024.1.4>
- Zeroual, A., Meddi, M. and Bensaad, S., 2013: The impact of climate change on river flow in arid and semi-arid rivers in Algeria. *Hydrology Research* 48(2), 584–595. <https://doi.org/10.2166/nh.2016.244>
- Zhou, Y., Ruan, G., Xu, C., Xiong, L., Jain, S., and Li, L., 2022: Detection and Attribution of Norwegian Annual precipitation Variability Related to Teleconnections. *Adv. Earth Space Sci.* 9(3), 1–20. <https://doi.org/10.1029/2021EA001857>
- Živanović, S., Ivanović, R., Nikolić, M., Đokić, M., and Tošić, I., 2020: Influence of air temperature and precipitation on the risk of forest fires in Serbia. *Meteorology and Atmos. Phys.* 132(6), 869–883. <https://doi.org/10.1007/s00703-020-00725-6>

IDŐJÁRÁS

*Quarterly Journal of the HungaroMet Hungarian Meteorological Service
Vol. 129, No. 2, April – June, 2025, pp. 133–160*

Five-parameter log-normal distribution and its modification

Marie Budíková^{1,*}, Jan Holub², Ladislav Budík³, Lenka Příbylová¹, and Ivana Horová¹

¹*Department of Mathematics and Statistics, Faculty of Science, Masaryk University
Kotlářská 2, Brno, 611 37, Czech Republic*

²*Global Change Research Institute of the Czech Academy of Sciences
Bělidla 986/4a, Brno, 603 00, Czech Republic*

³*Czech Hydrometeorological Institute
Kroftova 2578/43, Brno, 616 67, Czech Republic*

* *Corresponding Author e-mail: budikova@math.muni.cz*

(Manuscript received in final form May 6, 2024)

Abstract— The introduction of the LN5 and mLN5 distributions extends the commonly used three-parameter log-normal distribution (LN3) by enhancing tail modeling, which is critical for accurate representation of extreme values in hydrology and climatology. This paper details two methods for parameter estimation: the established local maximum likelihood method and the newly developed triangular method, an adaptation of the relative least squares approach. The effectiveness of these distributions is demonstrated through their application to datasets from the Czech Hydrometeorological Institute, encompassing average daily flow, precipitation, atmospheric pressure, and air temperature. Results show significant improvements in modeling extreme events with LN5 and mLN5 over LN3, as well as over other compared distributions such as generalized Gamma and generalized Weibull, particularly in tail behavior, underscoring their potential for advancing environmental studies. Appendices include comprehensive derivations of the functional characteristics of LN5 and mLN5 and introduce an alternative parametrization for LN5.

Key-words: exceedance curve, five-parameter log-normal distribution, maximum likelihood estimate, modified five-parameter log-normal distribution, triangular method

Highlights:

Introduces LN5 distribution and its modification and derives their characteristics.
Applies LN5 to data, compares them with existing models with superior performance.
Enhances approximation of distribution tails to better represent extreme values.

1. Introduction

Exceedance curves are essential in analyzing hydrological and climatological data, offering insights into the likelihood of surpassing specific values, crucial for developing empirical or theoretical models. These curves, essentially inverse survival functions, often employ the three-parameter log-normal distribution (LN3) (*Sangal and Biswas, 1970*), Weibull or gamma distributions. Also more flexible alternatives to these classical choices as generalized Weibull distribution (*Mudholkar et al, 1996*), generalized gamma distribution (*Cox et al., 2007*), or two-piece distributions (*Rubio and Hong, 2016*) were suggested in literature. However, these distributions may not accurately represent all data ranges, especially in small drainage basins, and can lead to unrealistic extrapolations at extreme probabilities (*Budík, 2018*). We propose the five-parameter log-normal distribution (LN5) and its modified version (mLN5) as superior alternatives, providing better fits and more accurate extrapolations (*Budík, 2018, 2019*). Contributions, briefly suggested LN5 and mLN5 distributions, omitting the derivation of their functional characteristics. This paper details the functional characteristics of LN5 and mLN5 and their application to real-world data and shows the advantages of LN5 and mLN5 distributions compared to the aforementioned distributions used in hydrological and climatological practice.

The analysis of hydrological and precipitation data shows discrepancies between the theoretical curves and actual measurements for the different distributions mentioned above, especially for the LN3 distribution, which is commonly used in hydrological and climatological practice. Accurate midrange estimation is crucial, but with climate change causing shifts towards extreme events, estimating extremes becomes equally important. The LN5 distribution, based on our experience, effectively addresses these issues, offering several advantages:

- a) Near-accurate modeling of exceedance curves and quality extrapolations for large datasets across a range of probabilities, confirmed by a simulation study (*Budík and Budíková, 2020*).
- b) Enhanced modeling of extremely small and large values, crucial for estimating probabilities of significant climatic and hydrological events in the context of climate change.
- c) Greater flexibility in modeling exceedance curves, allowing for precise differentiation of regional climatic or hydrological characteristics.
- d) Ability to detect some primary data processing inaccuracies in hydrological data application.
- e) When applied to long-term climatological and hydrological data, LN5 or mLN5 parameters are interpretable and can reveal changes in these quantities, correlating with climate trends and landscape drying.

This paper presents the LN5 and mLN5 distributions' density and distribution functions, parameter estimation methods, and applications to real data. We also describe the triangulation method with inverse transformation, a robust estimation approach for natural process-generated data. Previously, LN5, mLN5, and the triangulation method were only suggested for one dataset in conference proceedings; this paper provides a theoretical foundation and shows its usefulness in broader context, specifically on applications on hydrology and climatology data.

The paper is structured as follows: The Methods section discusses the exceedance curve and its relationship to the survival function. The Theory section introduces the LN5 and mLN5 distributions and covers methods for parameter estimation. The Results section applies these findings to real data. The paper concludes with a discussion on the approach's advantages and limitations in the final section. The appendices include theoretical derivations, an explanation of alternative parameterizations, graphs of PDF and CDF functions, a comparison of LMLE estimates for the Morava and the Dyje Rivers, and results from a prior simulation study.

2. Methods

In practice, the empirical exceedance curve, theoretical exceedance curve (*Lane, 2002*), and survival function (see *Fig. 1*) are key concepts for analyzing the probability of an observed variable surpassing a certain threshold, commonly used in studying extreme events like floods, earthquakes, or financial market crashes. The empirical exceedance curve plots the descending values of a variable (on the vertical axis) against the estimated probabilities of exceeding these values (on the horizontal axis). The probability of exceeding a given threshold is estimated as the relative frequency of data points above each threshold. The theoretical exceedance curve, derived from a probability distribution model, arranges the quantiles of the chosen probability distribution in descending order on the vertical axis, and the corresponding exceedance probabilities are plotted on the horizontal axis. The theoretical exceedance curve can be used to estimate the probability of outliers beyond the observed data range. The survival function, inversely related to the theoretical exceedance curve, indicates the probability that the variable's realization will exceed a specific value. It is crucial in assessing survival probabilities or durations across various fields.

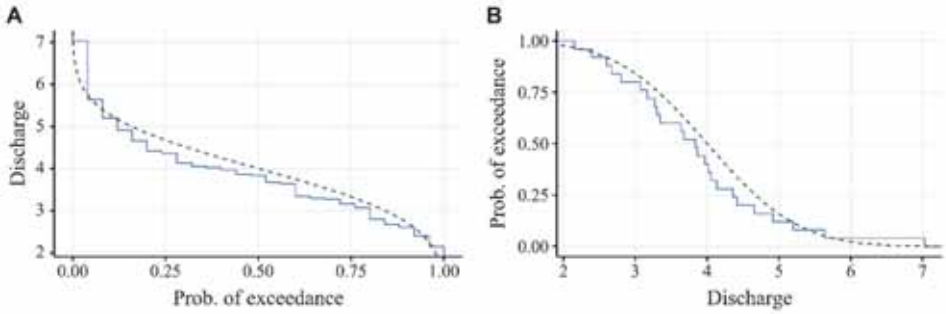


Fig. 1. **A.** The empirical exceedance curve (blue solid line) and the theoretical exceedance curve (black dashed line). **B.** The empirical survival function (blue solid line) and the theoretical survival function (black dashed line).

In summary, while the empirical exceedance curve is based on the measured data, the theoretical exceedance curve is based on a model of the underlying probability distribution, and the survival function is the inverse of the exceedance curve. Obtaining the best theoretical exceedance curve is necessary to estimate the magnitude of extreme events at a given probability of exceedance. To advance this modeling, we introduce the LN5 and mLN5 distributions for constructing exceedance curves. The upcoming Theory section will detail new results regarding the characteristics and parameter estimation methods of these distributions. Subsequently, in the Results section, we will demonstrate the application of these distributions to hydrology and climatology data.

3. Theory

In this section, we derive new LN5 distributions as generalizations of the three-parameter log-normal distribution LN3 (*Sangal and Biswas, 1970*).

3.1. Fundamental five-parameter log-normal distribution

Let $X \sim N(\mu, \sigma^2)$ be a normally distributed random variable with mean μ and variance σ^2 . Let $a, b \in \mathbb{R}^+, y_0 \in \mathbb{R}$. Random variable Y defined by the transformation

$$Y = a \exp(\text{sgn}X \cdot |X|^b) + y_0, \quad (1)$$

which follows the five-parameter log-normal distribution, i.e., $Y \sim \text{LN5}(a, b, \mu, \sigma^2, y_0)$, and the parameter vector is denoted by $\boldsymbol{\theta} = (a, b, \mu, \sigma^2, y_0)$.

It is important to recognize that the parameters influence the shape of the distribution function's graph. The location parameter y_0 shifts the distribution. Parameter a , shape parameter in general, is a parameter of scale if $y_0 = 0$. The remaining parameters b, μ, σ^2 are shape parameters. In particular, μ and σ^2 correspond to the mean and variance of an inversely transformed random variable

$$\text{sgn}(Y - a - y_0) \ln^{\frac{1}{b}} \left(\left(\frac{Y - y_0}{a} \right)^{\text{sgn}(Y - a - y_0)} \right).$$

The probability density, cumulative distribution, and quantile functions of the five-parameter log-normal distribution take the following form.

Probability density function

$$f(y, \boldsymbol{\theta}) = \begin{cases} \frac{1}{\sqrt{2\pi}\sigma} \cdot \frac{\ln^{\frac{1-b}{b}} \left(\frac{a}{y - y_0} \right)}{b(y - y_0)} \cdot \exp \left\{ -\frac{\left(-\ln^{\frac{1}{b}} \left(\frac{a}{y - y_0} \right) - \mu \right)^2}{2\sigma^2} \right\}, & y \in (y_0, y_0 + a), \\ \frac{1}{\sqrt{2\pi}\sigma} \cdot \frac{\ln^{\frac{1-b}{b}} \left(\frac{y - y_0}{a} \right)}{b(y - y_0)} \cdot \exp \left\{ -\frac{\left(\ln^{\frac{1}{b}} \left(\frac{y - y_0}{a} \right) - \mu \right)^2}{2\sigma^2} \right\}, & y \in (y_0 + a, \infty), \\ 0, & \text{otherwise.} \end{cases} \quad (2)$$

Cumulative distribution function

$$F(y, \boldsymbol{\theta}) = \begin{cases} 0, & y \in (-\infty, y_0), \\ \frac{1}{2} \left[1 + \text{erf} \left(\frac{-\ln^{\frac{1}{b}} \left(\frac{a}{y - y_0} \right) - \mu}{\sqrt{2}\sigma} \right) \right], & y \in [y_0, y_0 + a), \\ \frac{1}{2} \left[1 + \text{erf} \left(\frac{\ln^{\frac{1}{b}} \left(\frac{y - y_0}{a} \right) - \mu}{\sqrt{2}\sigma} \right) \right], & y \in [y_0 + a, \infty). \end{cases}$$

Quantile function

$$F^{-1}(\alpha, \boldsymbol{\theta}) = \begin{cases} a \exp\{-[-\mu - \sqrt{2}\sigma \operatorname{erf}^{-1}(2\alpha - 1)]^b\} + y_0, & \alpha \in I_1, \\ a \exp\{[\mu + \sqrt{2}\sigma \operatorname{erf}^{-1}(2\alpha - 1)]^b\} + y_0, & \alpha \in I_2, \end{cases}$$

where

$$I_1 = \left(0, \frac{1}{2} \left[1 + \operatorname{erf}\left(\frac{-\mu}{\sqrt{2}\sigma}\right)\right]\right),$$

$$I_2 = \left(\frac{1}{2} \left[1 + \operatorname{erf}\left(\frac{-\mu}{\sqrt{2}\sigma}\right)\right], 1\right),$$

erf is the error function and derivation of Eqs.(2)–(4) and further details on $f(y, \boldsymbol{\theta})$, $F(y, \boldsymbol{\theta})$, and $F^{-1}(\alpha, \boldsymbol{\theta})$ are listed in Appendix A of the Supplementary material, while probability density functions and cumulative distribution functions for various parameters are depicted in Appendix D of the Supplementary material.

3.2. Modified five-parameter log-normal distribution (mLN5)

The density of the LN5 distribution with parameter $b \neq 1$ is not a smooth function, which often does not align with the nature of the data. To address this issue, we have introduced a novel version of the LN5 distribution, the mLN5, which is achieved by modifying the transformation Eq.(1). Additional details can be found in Appendix B of the Supplementary material, while probability density functions and cumulative distribution functions for various parameters are depicted in Appendix D of the Supplementary material.

Let $X \sim N(\mu, \sigma^2)$ be a normally distributed random variable. Let $a, b \in \mathbb{R}^+$, and $y_0 \in \mathbb{R}$. Random variable Y , a transformation of X in the form

$$Y = \begin{cases} a \exp\{\operatorname{sgn}X \cdot |X|^b\} + y_0, & |X| \geq 1, \\ a \exp\{\operatorname{sgn}X \cdot |X|^{b+(1-b)(1-|X|)}\} + y_0, & |X| < 1, \end{cases} \quad (3)$$

follows the modified five-parameter log-normal distribution, i.e. $\text{mLN5}(a, b, \mu, \sigma^2, y_0)$, and the parameter vector is denoted by $\boldsymbol{\theta} = (a, b, \mu, \sigma^2, y_0)$.

We define function t that describes transformation Eq.(3) on open sets

$$t(x) = \begin{cases} t_1(x) = a \exp\{-(-x)^b\} + y_0, & x \in G_1 = (-\infty, -1), \\ t_2(x) = a \exp\{-(-x)^{b+(1-b)(1+x)}\} + y_0, & x \in G_2 = (-1, 0), \\ t_3(x) = a \exp\{x^{b+(1-b)(1-x)}\} + y_0, & x \in G_3 = (0, 1), \\ t_4(x) = a \exp\{x^b\} + y_0, & x \in G_4 = (1, \infty). \end{cases}$$

Let's denote the image of function t on a given set G_j as $H_j = t(G_j)$, $j = 1, \dots, 4$ and define a function τ_j as an inverse function to the t_j on H_j for $j = 1, \dots, 4$,

$$\tau_1(y) = -\ln^{\frac{1}{b}}\left(\frac{a}{y - y_0}\right), \quad y \in H_1 = (y_0, ae^{-1} + y_0)$$

$$\tau_4(y) = \ln^{\frac{1}{b}}\left(\frac{y - y_0}{a}\right), \quad y \in H_4 = (ae + y_0, \infty),$$

where $x = \tau_2(y)$ is the solution of equation $y = t_2(x)$ for $y \in H_2 = (ae^{-1} + y_0, a + y_0)$. Similarly, $x = \tau_3(y)$ is the solution of equation $y = t_3(x)$ for $y \in H_3 = (a + y_0, ae + y_0)$. Let $\tau'_j(y)$ denote derivatives of functions τ_j with respect to y for $j = 1, \dots, 4$.

The probability density, cumulative distribution, and quantile functions of the five-parameter log-normal distribution take the following form.

Probability density function

$$f(y, \theta) = \begin{cases} \frac{1}{\sqrt{2\pi}\sigma} \exp\left\{-\frac{1}{2\sigma^2}\left[\ln^{\frac{1}{b}}\left(\frac{a}{y - y_0}\right) + \mu\right]^2\right\} |\tau'_1(y)|, & y \in (y_0, ae^{-1} + y_0) \\ \frac{1}{\sqrt{2\pi}\sigma} \exp\left\{-\frac{1}{2\sigma^2}[\tau_2(y) - \mu]^2\right\} |\tau'_2(y)|, & y \in (ae^{-1} + y_0, a + y_0), \\ \frac{1}{\sqrt{2\pi}\sigma} \exp\left\{-\frac{1}{2\sigma^2}[\tau_3(y) - \mu]^2\right\} |\tau'_3(y)|, & y \in (a + y_0, ae + y_0), \\ \frac{1}{\sqrt{2\pi}\sigma} \exp\left\{-\frac{1}{2\sigma^2}\left[\ln^{\frac{1}{b}}\left(\frac{y - y_0}{a}\right) - \mu\right]^2\right\} |\tau'_4(y)|, & y \in (ae + y_0, \infty), \\ 0, & \text{otherwise.} \end{cases} \quad (4)$$

Cumulative distribution function

$$F(y, \theta) = \begin{cases} 0, & y \in (-\infty, y_0), \\ \frac{1}{2} \left[1 + \operatorname{erf} \left(\frac{-\ln^{\frac{1}{b}} \left(\frac{a}{y - y_0} \right) - \mu}{\sqrt{2}\sigma} \right) \right], & y \in [y_0, ae^{-1} + y_0), \\ \frac{1}{2} \left[1 + \operatorname{erf} \left(\frac{\tau_2(y) - \mu}{\sqrt{2}\sigma} \right) \right], & y \in [ae^{-1} + y_0, a + y_0), \\ \frac{1}{2} \left[1 + \operatorname{erf} \left(\frac{\tau_3(y) - \mu}{\sqrt{2}\sigma} \right) \right], & y \in [a + y_0, ae + y_0), \\ \frac{1}{2} \left[1 + \operatorname{erf} \left(\frac{\ln^{\frac{1}{b}} \left(\frac{y - y_0}{a} \right) - \mu}{\sqrt{2}\sigma} \right) \right], & y \in [ae + y_0, \infty). \end{cases} \quad (5)$$

Quantile function

$$F^{-1}(\alpha, \theta) = \begin{cases} a \exp\{-[-\mu - \sqrt{2}\sigma \operatorname{erf}^{-1}(2\alpha - 1)]^b\} + y_0, & \alpha \in I_1, \\ t_2(\mu + \sqrt{2}\sigma \operatorname{erf}^{-1}(2\alpha - 1)), & \alpha \in I_2, \\ t_3(\mu + \sqrt{2}\sigma \operatorname{erf}^{-1}(2\alpha - 1)), & \alpha \in I_3, \\ a \exp\{[\mu + \sqrt{2}\sigma \operatorname{erf}^{-1}(2\alpha - 1)]^b\} + y_0, & \alpha \in I_4, \end{cases}$$

where

$$\begin{aligned} I_1 &= \left(0, \frac{1}{2} \left[1 + \operatorname{erf} \left(\frac{-1 - \mu}{\sqrt{2}\sigma} \right) \right] \right), \\ I_2 &= \left(\frac{1}{2} \left[1 + \operatorname{erf} \left(\frac{-1 - \mu}{\sqrt{2}\sigma} \right) \right], \frac{1}{2} \left[1 + \operatorname{erf} \left(\frac{-\mu}{\sqrt{2}\sigma} \right) \right] \right), \\ I_3 &= \left(\frac{1}{2} \left[1 + \operatorname{erf} \left(\frac{-\mu}{\sqrt{2}\sigma} \right) \right], \frac{1}{2} \left[1 + \operatorname{erf} \left(\frac{1 - \mu}{\sqrt{2}\sigma} \right) \right] \right), \\ I_4 &= \left(\frac{1}{2} \left[1 + \operatorname{erf} \left(\frac{1 - \mu}{\sqrt{2}\sigma} \right) \right], 1 \right). \end{aligned}$$

3.3. Parameter estimation

Estimates of the unknown parameters of the chosen probability distribution are commonly obtained by the method of moments, the method of maximum likelihood, or the method of relative least squares (Cohen, 1951; Johnson et al, 1994). Here, we describe two possible methods for five-parameter log-normal distributions. Similar transformations define both discussed distributions. Hence, we describe methods of parameter estimation simultaneously. The idea of the first method is to minimize a specific loss function. The second method is based on maximum likelihood estimation.

Let $\mathbf{Y} = (Y_1, \dots, Y_n)$ be a random sample from the LN5 distribution or the mLN5 distribution and $\mathbf{y} = (y_1, \dots, y_n)$ be the realization of this random sample. The LN5 and mLN5 distributions have parameters given by vector $\boldsymbol{\theta} = (a, b, \mu, \sigma^2, y_0)$, and $\hat{\boldsymbol{\theta}} = (\hat{a}, \hat{b}, \hat{\mu}, \hat{\sigma}^2, \hat{y}_0)$ denotes the vector of estimated parameters.

3.3.1. Triangular method

The triangular method (see Fig. 2) is motivated by minimizing the difference between theoretical and empirical cumulative distribution functions over both probability and observed values. To accommodate for the non-symmetry of log-normal distribution, observed values are inversely transformed to normal distribution.

Estimated parameters $\hat{\boldsymbol{\theta}}$ minimize statistic K , i.e. $\hat{\boldsymbol{\theta}} = \arg \min_{\boldsymbol{\theta} \in \Theta} K(\mathbf{y}, \boldsymbol{\theta})$,

$$K(\mathbf{y}, \boldsymbol{\theta}) = \sum_{i=1}^n \left(\frac{u_i - u_{theor,i}}{u_{theor,i}} \right)^2 + \sum_{i=1}^n (p_i - p_{theor,i})^2. \quad (6)$$

Here, $p_i = \frac{i}{n+1}$ is an empirical probability; $p_{theor,i} = F(y_i, \boldsymbol{\theta})$ is a transformation of y_i to range (0,1), where $F(y, \boldsymbol{\theta})$ is the probability distribution function of the LN5 or the mLN5 distribution; any function $u_i = \frac{1}{\sigma}(\tau(y_i, a, b, y_0) - \mu)$ is an inverse transformation of observed values y_i to standardized normal distribution, where τ is an inverse function to the function t ; $u_{theor,i} = \Phi^{-1}(p_i)$ is transformation of p_i , where Φ is the cumulative distribution function of standardized normal distribution. The first term in K statistic Eq.(6) belongs to the relative least squares method, and the second term belongs to the probability optimization method. The triangular method described here differs from the one proposed in (Budík, 2019). In practice, it has been shown that using the value $u_{theor,i}$ in the denominator instead of u_i (see the method of relative least squares) leads to a more accurate estimation of the parameters.

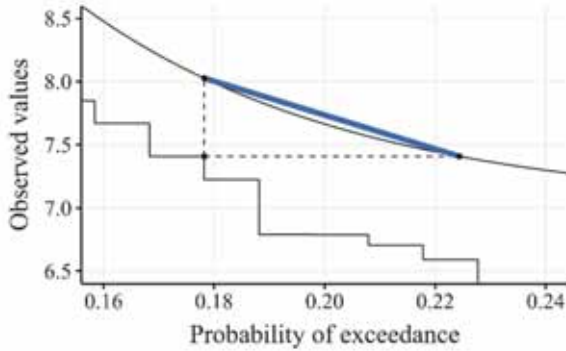


Fig. 2. Illustration of the triangular method.

3.3.2. Local maximum likelihood method

Maximum likelihood estimate of parameters $\boldsymbol{\theta}$ is a vector $\hat{\boldsymbol{\theta}}_{\text{MLE}} = (\hat{a}, \hat{b}, \hat{\mu}, \hat{\sigma}^2, \hat{y}_0)$, that satisfies $\mathcal{L}(\hat{\boldsymbol{\theta}}_{\text{MLE}}|\mathbf{Y}) \geq \mathcal{L}(\boldsymbol{\theta}|\mathbf{Y}), \forall \boldsymbol{\theta} \in \boldsymbol{\Theta}$, for a given random sample \mathbf{Y} and the likelihood function $\mathcal{L}(\boldsymbol{\theta}|\mathbf{Y}) = \prod_{i=1}^n f(Y_i, \boldsymbol{\theta})$. We refer to $l(\boldsymbol{\theta}|\mathbf{Y}) = \ln \mathcal{L}(\boldsymbol{\theta}|\mathbf{Y})$ as the log-likelihood function.

Likelihood function for a observation of a random sample $\mathbf{y} = (y_1, \dots, y_n)^\top$ is given by

$$\mathcal{L}(\boldsymbol{\theta}|\mathbf{y}) = \prod_{\substack{i=1 \\ y_i \in H}}^n \frac{1}{\sqrt{2\pi}\sigma} \exp\left\{-\frac{1}{2\sigma^2}[\tau_j(y_i) - \mu]^2\right\} |\tau'_j(y_i)|, \quad j = 1, \dots, J,$$

where $H = \bigcup_{j=1}^J H_j$, H_j are supports of the density function f from Eqs.(2) and (4), $J = 2$ for the LN5 distribution and $J = 4$ for the mLN5 distribution.

It was shown that under certain conditions log-likelihood function of LN3 distribution approaches infinity (Cohen, 1951). One of the possible parameter estimation methods is the local maximum likelihood estimate (LMLE). Convergence to a local maximum of the likelihood function has been shown for LN3 distribution (Wingo, 1975; Griffiths, 1980). As the LN5 and mLN5 distributions are generalizations of the LN3 distribution, the log-likelihood function $l(\boldsymbol{\theta}|\mathbf{y})$ approaches infinity when $y_0 \rightarrow \min(y_1, \dots, y_n)$ for both LN5 and mLN5 distributions. To find a reasonable parameter estimate, it is necessary to assume that $y_0 < \min(y_1, \dots, y_n)$. Then log-likelihood function takes the form

$$l(\boldsymbol{\theta}|\mathbf{y}) = -n \ln\sqrt{2\pi} - n \ln\sigma - \frac{1}{2\sigma^2} \sum_{i=1}^n [\tau_j(y_i) - \mu]^2 + \sum_{i=1}^n \ln|\tau'_j(y_i)|, \quad (7)$$

for $j = 1, \dots, J$. The local maximum likelihood estimate $\hat{\boldsymbol{\theta}}_{\text{LMLE}}$ is the solution of a system of equations

$$\frac{\partial l(\boldsymbol{\theta}|\mathbf{y})}{\partial \theta_p} = 0, \quad p = 1, \dots, 5, \quad \text{where} \quad \theta_p \in \boldsymbol{\theta} = (a, b, \mu, \sigma^2, y_0).$$

This system does not yield any analytical solution for all parameters. However, the estimates of parameters μ and σ^2 can be expressed as

$$\hat{\mu} = \frac{1}{n} \sum_{i=1}^n \tau_j(y_i), \quad \hat{\sigma}^2 = \frac{1}{n} \sum_{i=1}^n [\tau_j(y_i) - \mu]^2, \quad j = 1, \dots, J, \quad (8)$$

which imply a possibility to obtain profile log-likelihood (Spratt, 2000) from Eqs. (7) and (8) as follows:

$$l((a, b, \mu)|\mathbf{y}) = -n \ln\sqrt{2\pi} - n \ln\hat{\sigma} - \frac{n}{2} + \sum_{i=1}^n \ln|\tau'_j(y_i)|, \quad j = 1, \dots, J, \quad (9)$$

and estimate $\hat{\boldsymbol{\theta}}_{\text{LMLE}}$ as a maximization of expression Eq.(9).

4. Results

4.1. Application in hydrology

To illustrate the capabilities of the LN5 and mLN5 distributions, we apply the procedure described above to the data the Czech Hydrometeorological Institute provided. They are two datasets; the first consists of $n = 36160$ observations of the average daily flow (m^3s^{-1}) of the Morava River at the Kroměříž station, Czech Republic, the second set contains $n = 29190$ observations of the average daily flow (m^3s^{-1}) of the Dyje River at the Podhradí station, Czech Republic. The underlying process is time-based; however, long-term behavior is often studied in hydrological practice, and it is commonly assumed that data are

independent (*Sangal and Biswas, 1970*). Hence, we will consider provided data as a random sample. Discharge measurements are not exact, and provided data are rounded to two decimal places.

We compare the five-parameter log-normal distribution LN5 and its modification mLN5 with generalized gamma distribution (*Cox et al., 2007*), generalized Weibull distribution (*Mudholkar et al, 1996*), Cauchy two-piece distributions (*Rubio and Hong, 2016*) and the three-parameter variant LN3 (*Sangal and Biswas, 1970*). We estimate the parameters using the local maximum likelihood method with optimization by Nelder-Mead method, (*Millard, 2013*). Estimates of parameters for log-normal distributions for the Morava and the Dyje Rivers are given in *Table 1*.

The log-likelihood for the distribution of mLN5 is the highest, and the log-likelihood for the distribution of LN3 is the lowest. Moreover, all distributions are compared using Akaike information criteria listed in *Table 2*.

Table 1. LMLE parameter estimates and log-likelihood for the random sample of daily average discharge of the Morava and the Dyje Rivers for LN3, LN5, and mLN5 distributions.

		\hat{a}	\hat{b}	$\hat{\mu}$	$\hat{\sigma}^2$	\hat{y}_0	l
Morava	LN3	–	–	3.4550	0.8581	2.3797	-173 479.0
	LN5	98.4527	0.9610	-1.1396	0.8878	2.0099	-173 454.5
	mLN5	91.2712	0.9360	-1.0630	0.8983	1.7339	-173 439.9
Dyje	LN3	–	–	1.6497	0.8599	0.0928	-87 366.5
	LN5	2.5375	1.1975	0.7245	0.6311	-0.0874	-86 671.71
	mLN5	2.3037	1.2605	0.7673	0.6108	0.0199	-86 655.36

Table 2. Akaike information criteria (AIC) of the generalized gamma, generalized Weibull, Cauchy two-piece, LN3, LN5 and mLN5 distributions for the random sample of daily average discharge of the Morava and the Dyje Rivers. The lowest value is in bold.

	GenGamma	GenWeibull	Two-Piece	LN3	LN5	mLN5
Morava	346 985.0	348 146.1	350 879.4	346 964.0	346 919.0	346 889.8
Dyje	173 738.3	173 588.5	175 270.2	174 739.1	173 353.4	173 320.7

Figs. 3 and 4 show the relative differences between empirical and estimated exceedance curves. See Appendix E of the Supplementary material for a comparison of histograms with density estimates. The analysis of the relative errors of the exceedance shows that, of the tested distributions, the mLN5 distribution is able to most accurately model both the middle part and the tails of the exceedance curve, which is very important when describing extreme

hydrological and climatological events. Deviations on the left side of the curve are apparently caused by extreme values of flow rates, which do not correspond to the expected course of the curve due to the length of the observed period. At the right end of the curve, deviations are probably associated with measurement errors of low flows.

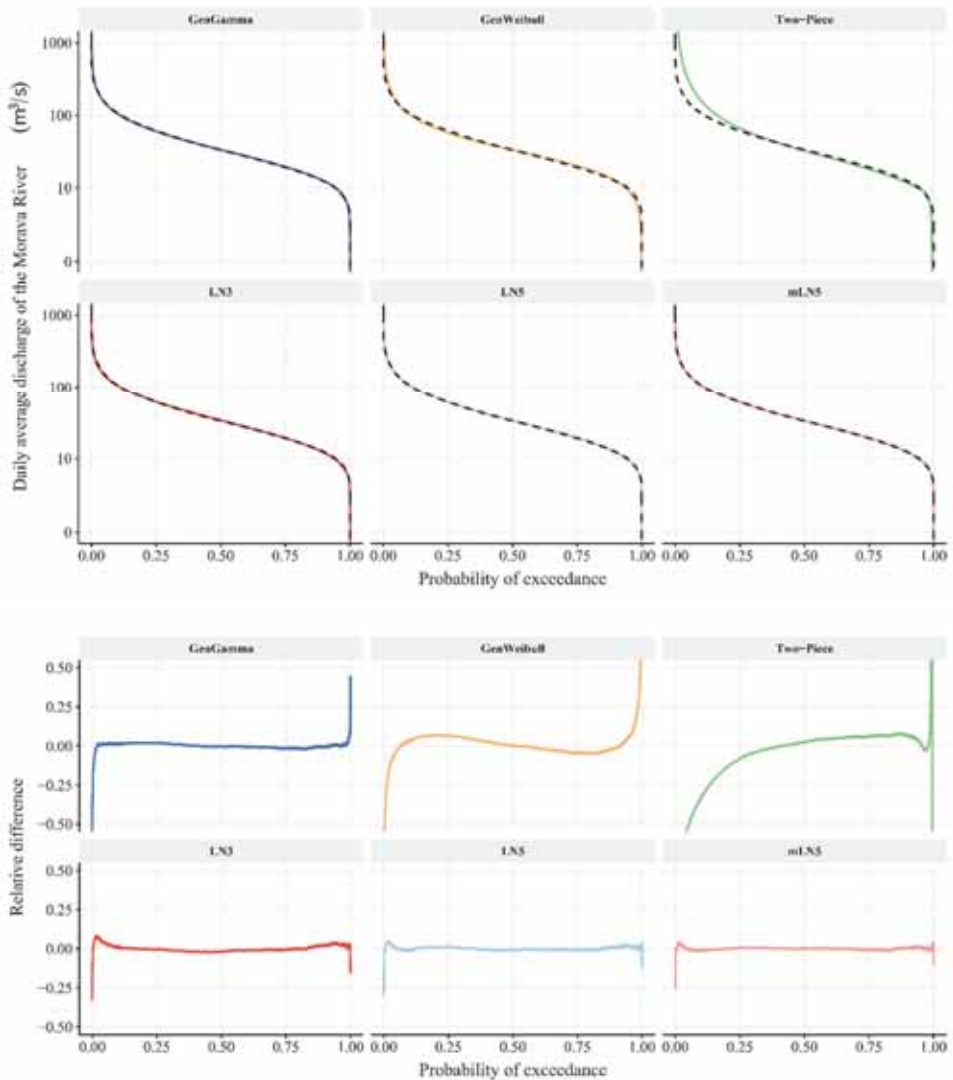


Fig. 3. Exceedance curves for the Morava River. Upper: The empirical exceedance curve (black dashed line) and fitted exceedance curves for the generalized gamma (blue line), generalized Weibull (orange line), Cauchy two-piece (green line), LN3 (red line), LN5 (light blue line) and mLN5 (pink line) distributions. Lower: Relative difference of estimated and empirical exceedance curves.

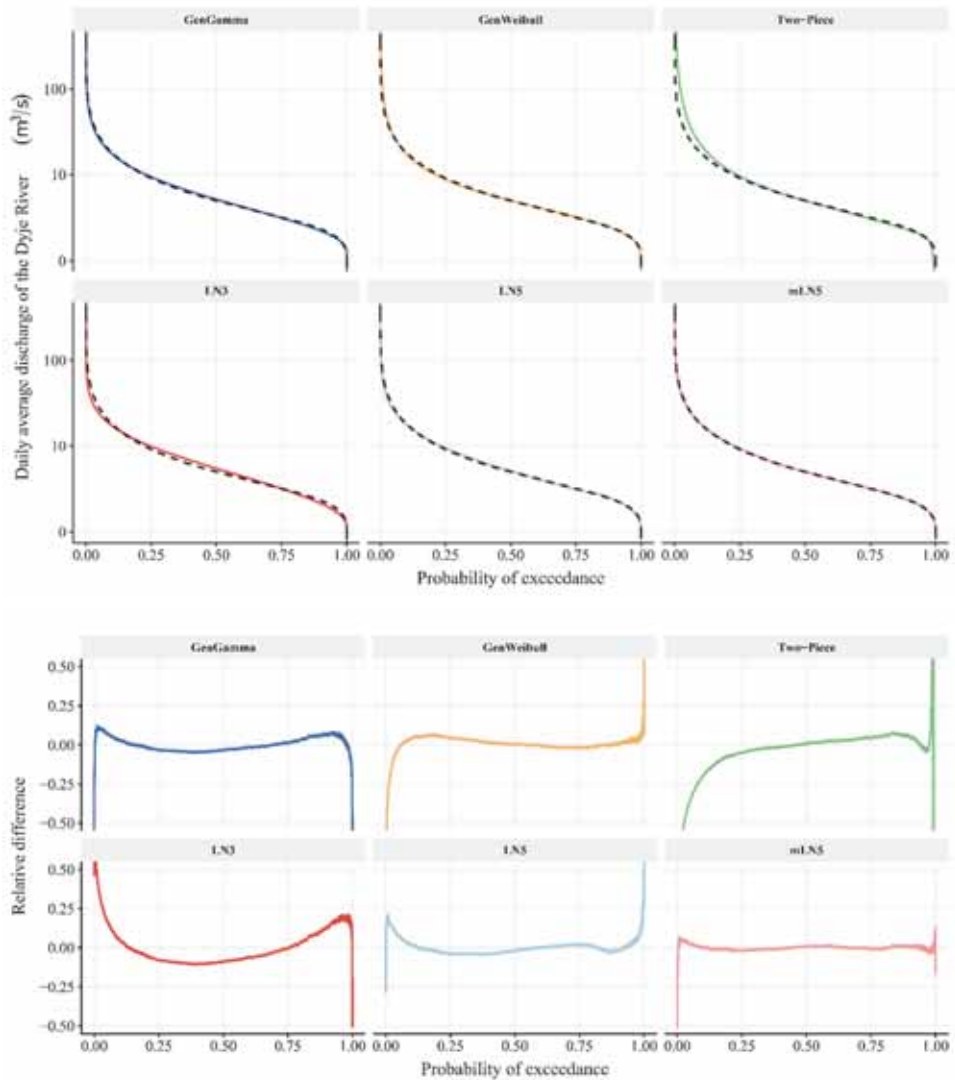


Fig. 4. Exceedance curves for the Dyje River. Upper: The empirical exceedance curve (black dashed line) and fitted exceedance curves for the generalized gamma (blue line), generalized Weibull (orange line), Cauchy two-piece (green line), LN3 (red line), LN5 (light blue line) and mLN5 (pink line) distributions. Lower: Relative difference of estimated and empirical exceedance curves.

4.2. Application in climatology

To illustrate the mLN5 distribution’s capabilities, we applied it to daily total precipitation, average daily atmospheric pressure, and average daily air

temperature datasets provided by the Czech Hydrometeorological Institute. The precipitation dataset (mm) from the Žatec station includes 44739 observations, with 17110 days of recorded precipitation. The atmospheric pressure dataset (hPa) from the Dukovany station comprises 13514 observations, and the temperature dataset (°C) from the Lysá hora station contains 21915 observations. For temperature data, an alternative parameterization (Appendix C of the Supplementary material) is necessary for the mLN5 distribution to prevent overflow during parameter estimation.

Fig. 5 displays the empirical and estimated exceedance curves for the Žatec station. Traditionally, exceedance curve estimation focused solely on days with measurable rainfall. However, the application of LN5 and mLN5 distributions enables parameter estimation for exceedance curves on both precipitation and non-precipitation days. While significant differences are evident between empirical and estimated curves using the LN3 distribution, such discrepancies are notably absent with the LN5 and mLN5 distributions.

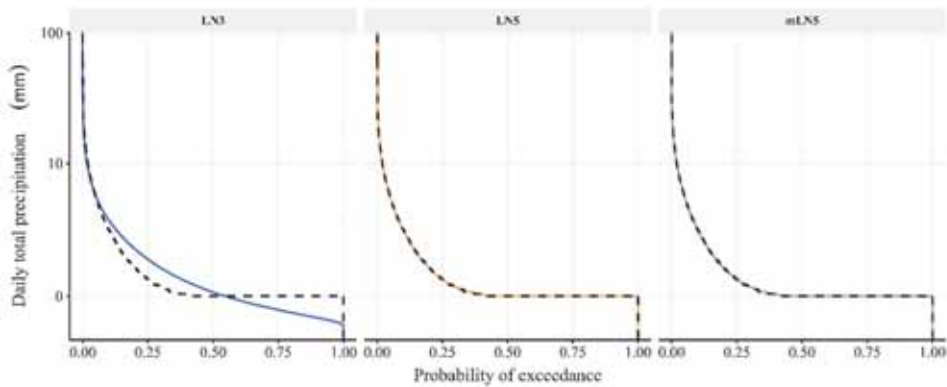


Fig. 5. The empirical exceedance curve (rain) for the Žatec station (black dashed line) and fitted exceedance curves for the LN3 (blue line), LN5 (orange line) and mLN5 (green line) distributions.

For average temperature, we found that using values proportional to potentially radiated energy (according to the Stephan-Boltzmann law) instead of Celsius degrees yields better empirical and estimated curve agreement. Fig. 6 shows the empirical and estimated exceedance curves for atmospheric pressure at Dukovany and temperature (converted to radiated energy) at Lysá hora. The graphs indicate a near-perfect match in the middle range, though a small sample size may cause imperfections at the margins for pressure data. This mLN5 transformation can be extended to other climatological data, considering factors like air humidity and sunshine duration and intensity.

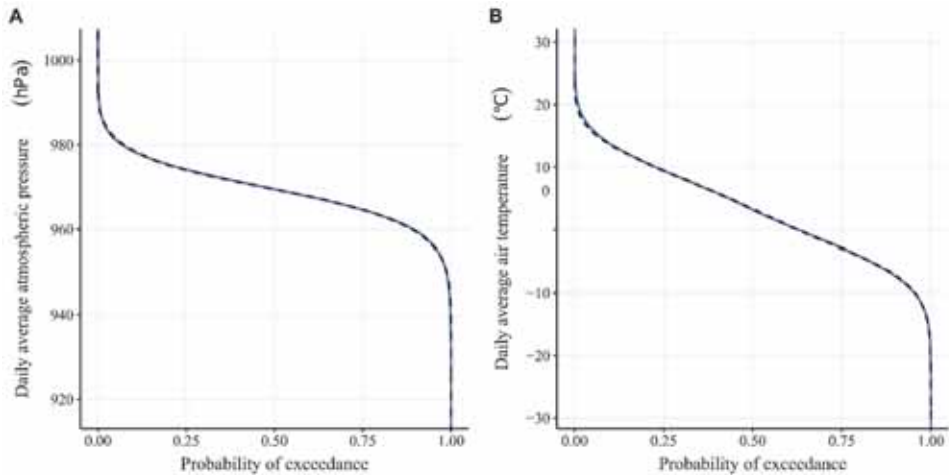


Fig. 6. The empirical exceedance curve (black dashed line) and fitted exceedance curves for the mLN5 (blue line) distribution for atmospheric pressure **A** for Dukovany, and temperature **B** for Lysá hora.

5. Discussion and conclusions

In this paper, we introduced the five-parameter log-normal distribution (LN5) and its modification (mLN5), offering alternatives to the commonly used three-parameter log-normal distribution (LN3) (*Sangal and Biswas, 1970*), generalized Weibull distribution (*Mudholkar et al., 1996*), generalized gamma distribution (*Cox et al., 2007*) or Cauchy two-piece distributions (*Rubio and Hong, 2016*) for hydrological and climatological data analysis. We provided formulas for their probability density, cumulative distribution, and quantile functions, and outlined parameter estimation methods. Future research could enhance these models, exploring methods like moments estimation and properties of local maximum likelihood estimates.

Hydrological and climatological data have unique characteristics, with uncertainties in both measured values and exceedance probabilities. Traditional least squares methods assume accurate exceedance probabilities but error-prone values, while probability optimization assumes precise values but uncertain probabilities. Our triangular method, minimizing deviations in both dimensions, emerges as particularly suitable for such data. It is also effective for asymmetric exceedance curves, common in hydrology and climatology. As part of exploring the practical applications of the mLN5 distribution, we endeavored to model the exceedance curves for medical data, and once again, we observed a highly favorable agreement between the empirical and theoretical exceedance curves.

The triangular method, particularly with inverse transformation, requires data compatible with normal distribution transformation (e.g., LN2, LN3). While this paper doesn't delve into the triangular method's theoretical aspects, our simulation study (Budík and Budíková, 2020) (see Appendix F of the Supplementary material) indicates its effectiveness, especially in challenging extrapolations. Its computational efficiency is proven in processing extensive Central European climatological and hydrological datasets, with detailed results to be published separately.

Natural processes often produce data that mixes distributions. For example, flood-induced flow changes affect exceedance curve parameters and may even lead to changes in the distribution itself due to natural causes such as overtopping of reservoirs that may change flow mechanisms from groundwater to surface, etc. We are currently developing a heuristic approach to enhance the accuracy of modeling in such complex scenarios and anticipate publishing the results later. Based on the analysis of hundreds of datasets on average daily flows, we have concluded that there is a certain degree of inverse dependency between the parameters b and σ . As b increases, σ decreases, and vice versa. Furthermore, for streams with large catchment areas (on the order of 10^4 km²), the parameter b is close to 1. In contrast, for streams with smaller catchment areas, the parameter b can deviate from 1 in both directions. Its values are influenced by the geological characteristics of the catchment, the quantity and quality of vegetation, and the precipitation regime.

This study has several limitations. The LN5 and mLN5 distributions mark a significant step in modeling exceedance curves, particularly for extreme event probabilities, aiding in understanding and adapting to climate change. However, the analyzed data may not always meet independence and identical distribution assumptions. Our proposed procedures, considering data heterogeneity, autocorrelation, and seasonality, have shown promising results in modeling exceedance curves, but further research is needed in this direction. We focused on two parameter estimation methods: the triangular method and local maximum likelihood. Other methods like Bayesian estimation or L-moments could be explored, though they assume precise exceedance probabilities, often unmet in real data. We acknowledge that utilizing a five-parameter distribution typically involves significant computational intensity. A specific challenge in parameter estimation arises from the non-smooth nature of the probability densities associated with the LN5 and mLN5 distributions. Nevertheless, these drawbacks are counterbalanced by the fact that both distributions effectively capture not only the central tendency but also the entire exceedance curve. While analyzing the average daily discharge on the Morava River and the Dyje River, it was revealed that the mLN5 distribution yielded the lowest AIC value among the six distributions investigated (refer to

Table 2). Furthermore, it exhibited the most favorable trajectory of relative estimation errors, as depicted in Figures 3b and 4b. It's important to note that

unlike earlier distributions used for exceedance curves, the LN5 and mLN5 distributions enable concurrent analysis of days with precipitation and those without precipitation. Further research should aim to refine the mLN5 distribution and investigate other potential models for better approximating hydrological and climatological data.

Average daily precipitation totals, average daily temperature, and average daily air pressure from the CHMI stations can be found at the following address: <https://www.chmi.cz/historicka-data/pocasi/denni-data/Denni-data-dle-z.-123-1998-Sb>. Average daily flow rates are available for download at [https://isvs.chmi.cz/ords/f?p=11002:HOME:9046927352185:::~:](https://isvs.chmi.cz/ords/f?p=11002:HOME:9046927352185:::). The source code related to this research is available on GitLab at <https://gitlab.ics.muni.cz/9607/ln5>.

Acknowledgements: This research was funded by the Ministry of Education, Youth, and Sports of the Czech Republic for SustES—Adaptation strategies for sustainable ecosystem services and food security under adverse environmental conditions project [grant number CZ.02.1.01/0.0/0.0/16 019/0000797] and Mathematical and Statistical Modeling project [grant number MUNI/A/1132/2022].

MB: conceptualization, methodology, writing – original draft, validation, project administration. JH: conceptualization, formal analysis, investigation, writing – original draft, software, computations, visualization. LB: conceptualization, investigation, methodology, data curation, writing – original draft, computations, validation. LP: conceptualization, writing – review & editing. IH: conceptualization, validation, supervision.

The authors thank Gejza Wimmer for constructive criticism of the manuscript and Ondřej Pokora for careful checking of the mathematical part of the text.

References

- Budík, L., 2018: Hydrological and meteorological data and modifications of statistical distributions - heuristic approach. 17th Conference on Applied Mathematics, APLIMAT 2018 Proceedings, Bratislava: STU, 165–172.
- Budík, L., 2019: Progress in heuristic approach to stochastic modeling of hydrological and meteorological data. 18th Conference on Applied Mathematics, APLIMAT 2019 Proceedings, Bratislava: STU, 109–119.
- Budík, L., and Budíková, M., 2020: Comparison of various methods of parameters estimation of mLN5 distribution using simulation study. 19th Conference on Applied Mathematics, APLIMAT 2020 Proceedings, Bratislava: STU, 170–179.
- Cohen, A., 1951: Estimating parameters of logarithmic-normal distributions by maximum likelihood. *J. Amer. Stat. Soc.* 46(1), 206–212. <https://doi.org/10.1080/01621459.1951.10500781>
- Cox, C., Chu, H., Schneider, M. F., and Munoz, A. (2007). Parametric survival analysis and taxonomy of hazard functions for the generalized. *Stat. medicine* 26(23), 4352–4374. <https://doi.org/10.1002/sim.2836>
- Griffiths, D.A., 1980: Interval estimation for the three-parameter lognormal distribution via the likelihood function. *J. Roy. Stat. Soc.. Series C (Applied Statistics)* 29(1) , 58–68. <https://doi.org/10.2307/2346411>
- Johnson, N.L., Kotz, S., and Balakrishnan, N., 1994: Continuous Univariate Distributions, vol. 1. New York: Wiley-Interscience.
- Lane, B., 2002: Statistical methods in hydrology, vol. 496. Iowa: Iowa State Press.
- Millard, S.P., 2013: EnvStats: An R Package for Environmental Statistics. New York: Springer. <https://doi.org/10.1007/978-1-4614-8456-1>

- Mudholkar, G.S., Srivastava, D.K., and Kollia, G.D., 1996: A generalization of the weibull distribution with application to the analysis of. J. Amer. Stat. Assoc. 91(436), 1575–1583. <https://doi.org/10.1080/01621459.1996.10476725>*
- Rubio, F. J., and Hong, Y., 2016: Survival and lifetime data analysis with a flexible class of distributions. J. Appl. Stat. 43(10), 1794–1813. <https://doi.org/10.1080/02664763.2015.1120710>*
- Sangal, B., and Biswas, A., 1970: The 3-parameter log normal distribution and its applications in hydrology. Water Resour. Res. 6, 505–515. <https://doi.org/10.1029/WR006i002p00505>*
- Sprott, D. A., 2000: Statistical Inference in Science. New York: Springer.*
- Wingo, D. R., 1975: The use of interior penalty functions to overcome lognormal distribution parameter estimation anomalies. J. Stat. Comput. Simul. 4(1), 49–61. <https://doi.org/10.1080/00949657508810109>*

Supplementary material

Five-parameter log-normal distribution and its modification

Marie Budíková^{a*}, Jan Holub^b, Ladislav Budík^c, Lenka Přibylková^a, Ivana Horová^a

^aDepartment of Mathematics and Statistics, Faculty of Science, Masaryk University, Kotlářská 2, Brno, 602 00, Czech Republic

^bGlobal Change Research Institute of the Czech Academy of Sciences, Belidla 986/4a, Brno, 603 00, Czech Republic

^cCzech Hydrometeorological Institute, Kroftova 2578/43, Brno, 616 67, Czech Republic

Appendices

A Five-parameter log-normal distribution (LN5)

Let t be a real function $t(x) = a \exp\{\text{sgn}x \cdot |x|^b\} + y_0$. Let τ_1 be an inverse function to the function t on $H_1 = t(G_1) = (y_0, a + y_0)$, where $G_1 = (-\infty, 0)$, in the form $\tau_1(y) = -\ln^{\frac{1}{b}}(\frac{a}{y-y_0})$, and its derivative $\tau_1'(y) = \frac{1}{b(y-y_0)} \ln^{\frac{1-b}{b}}(\frac{a}{y-y_0})$. Similarly, let τ_2 be an inverse function to the function t on $H_2 = t(G_2) = (a + y_0, \infty)$, where $G_2 = (0, \infty)$, in the form $\tau_2(y) = \ln^{\frac{1}{b}}(\frac{y-y_0}{a})$, $\tau_2'(y) = \frac{1}{b(y-y_0)} \ln^{\frac{1-b}{b}}(\frac{y-y_0}{a})$.

Let $X \sim N(\mu, \sigma^2)$ be a normally distributed random variable and $g_X(x)$ be its probability density function. The function $t(x)$ is regular on open and disjoint intervals G_1, G_2 , and function $f(y) = \sum_{i=1}^2 f_j(y)$ is a **probability density function** of transformed random variable $Y = t(X)$ that has **LN5 distribution**, where

$$f_j(y) = \begin{cases} g_X(\tau_j(y))|\tau_j'(y)| = \frac{1}{\sqrt{2\pi\sigma^2}} \exp\left\{-\frac{1}{2\sigma^2}[\tau_j(y) - \mu]^2\right\} |\tau_j'(y)|, & y \in H_j, \\ 0, & \text{otherwise.} \end{cases}$$

Function $f(y)$ can be expressed as

$$f(y) = \begin{cases} \frac{1}{\sqrt{2\pi\sigma^2}} \cdot \frac{\ln^{\frac{1-b}{b}}(\frac{a}{y-y_0})}{b(y-y_0)} \cdot \exp\left\{-\frac{(-\ln^{\frac{1}{b}}(\frac{a}{y-y_0}) - \mu)^2}{2\sigma^2}\right\}, & y \in (y_0, y_0 + a), \\ \frac{1}{\sqrt{2\pi\sigma^2}} \cdot \frac{\ln^{\frac{1-b}{b}}(\frac{y-y_0}{a})}{b(y-y_0)} \cdot \exp\left\{-\frac{(\ln^{\frac{1}{b}}(\frac{y-y_0}{a}) - \mu)^2}{2\sigma^2}\right\}, & y \in (y_0 + a, \infty), \\ 0, & \text{otherwise.} \end{cases}$$

Let $F(y, \theta) = \int_{-\infty}^y f(t, \theta) dt$ denote the cumulative distribution function for the probability density function $f(y, \theta)$ of LN5 distribution with parameters $\theta = (a, b, \mu, \sigma^2, y_0)^T$. Let $U \sim N(0, 1)$ be a random variable with its cumulative distribution function $\Phi(u) = \frac{1}{2}[1 + \text{erf}(\frac{u}{\sqrt{2}})]$ where erf is the error function $\text{erf}(x) = \frac{2}{\sqrt{\pi}} \int_0^x \exp(-t^2) dt$. For transformations

*Corresponding author

Email address: budikova@math.muni.cz (Marie Budíková)

w_1, w_2 , we have

$$\begin{aligned} w_1 &= \frac{-\ln^{\frac{1}{b}}\left(\frac{a}{t-y_0}\right) - \mu}{\sigma}, & w_2 &= \frac{\ln^{\frac{1}{b}}\left(\frac{t-y_0}{a}\right) - \mu}{\sigma}, \\ dw_1 &= \frac{\ln^{\frac{1}{b}}\left(\frac{a}{t-y_0}\right)}{\sigma b(t-y_0)} dt, & dw_2 &= \frac{\ln^{\frac{1}{b}}\left(\frac{t-y_0}{a}\right)}{\sigma b(t-y_0)} dt, \\ y_0 &\xrightarrow{w_1} -\infty, & a+y_0 &\xrightarrow{w_2} -\frac{\mu}{\sigma}, \\ z_1 &\xrightarrow{w_1} v_1 := \frac{-\ln^{\frac{1}{b}}\left(\frac{a}{z_1-y_0}\right) - \mu}{\sigma}, & z_2 &\xrightarrow{w_2} v_2 := \frac{\ln^{\frac{1}{b}}\left(\frac{z_2-y_0}{a}\right) - \mu}{\sigma}. \end{aligned}$$

Let $z_1 \in H_1$, then

$$\begin{aligned} F(z_1) &= \int_{-\infty}^{y_0} 0 dt + \int_{y_0}^{z_1} \frac{1}{\sqrt{2\pi}\sigma} \cdot \frac{\ln^{\frac{1}{b}}\left(\frac{a}{t-y_0}\right)}{b(t-y_0)} \cdot \exp\left(-\frac{\left(-\ln^{\frac{1}{b}}\left(\frac{a}{t-y_0}\right) - \mu\right)^2}{2\sigma^2}\right) dt = \\ &= \int_{-\infty}^{v_1} \frac{1}{\sqrt{2\pi}} \exp\left(-\frac{1}{2}w_1^2\right) dw_1 = \frac{1}{2} \left[1 + \operatorname{erf}\left(\frac{-\ln^{\frac{1}{b}}\left(\frac{a}{z_1-y_0}\right) - \mu}{\sqrt{2}\sigma}\right) \right], \end{aligned}$$

Let $z_2 \in H_2$, then

$$\begin{aligned} F(z_2) &= \int_{-\infty}^{y_0} 0 dt + \int_{y_0}^{a+y_0} \frac{1}{\sqrt{2\pi}\sigma} \cdot \frac{\ln^{\frac{1}{b}}\left(\frac{a}{t-y_0}\right)}{b(t-y_0)} \cdot \exp\left(-\frac{\left(-\ln^{\frac{1}{b}}\left(\frac{a}{t-y_0}\right) - \mu\right)^2}{2\sigma^2}\right) dt + \\ &+ \int_{a+y_0}^{z_2} \frac{1}{\sqrt{2\pi}\sigma} \cdot \frac{\ln^{\frac{1}{b}}\left(\frac{t-y_0}{a}\right)}{b(t-y_0)} \cdot \exp\left(-\frac{\left(\ln^{\frac{1}{b}}\left(\frac{t-y_0}{a}\right) - \mu\right)^2}{2\sigma^2}\right) dt = \Phi\left(-\frac{\mu}{\sigma}\right) - \Phi(-\infty) + \\ &+ \Phi\left(\frac{\ln^{\frac{1}{b}}\left(\frac{z_2-y_0}{a}\right) - \mu}{\sigma}\right) - \Phi\left(-\frac{\mu}{\sigma}\right) = \Phi\left(\frac{\ln^{\frac{1}{b}}\left(\frac{z_2-y_0}{a}\right) - \mu}{\sigma}\right) = \frac{1}{2} \left[1 + \operatorname{erf}\left(\frac{\ln^{\frac{1}{b}}\left(\frac{z_2-y_0}{a}\right) - \mu}{\sqrt{2}\sigma}\right) \right]. \end{aligned}$$

Combining terms $F(z_1), F(z_2)$, we obtain **cumulative distribution function**

$$F(y, \theta) = \begin{cases} 0, & y \in (-\infty, y_0), \\ \frac{1}{2} \left[1 + \operatorname{erf}\left(\frac{-\ln^{\frac{1}{b}}\left(\frac{a}{y-y_0}\right) - \mu}{\sqrt{2}\sigma}\right) \right], & y \in [y_0, a+y_0), \\ \frac{1}{2} \left[1 + \operatorname{erf}\left(\frac{\ln^{\frac{1}{b}}\left(\frac{y-y_0}{a}\right) - \mu}{\sqrt{2}\sigma}\right) \right], & y \in [a+y_0, \infty), \end{cases}$$

Let $X \sim N(\mu, \sigma^2)$ and $F_X^{-1}(\alpha)$ its quantile function $F_X^{-1}(\alpha) = \mu + \sqrt{2}\sigma \operatorname{erf}^{-1}(2\alpha-1)$, for $\alpha \in (0, 1)$. Then the transformed random variable $Y = t(X), Y \sim \text{LN5}(a, b, \mu, \sigma^2, y_0)$, has **quantile function**

$$F^{-1}(\alpha) = t(F_X^{-1}(\alpha)) = a \cdot \exp\left\{\operatorname{sgn}(F_X^{-1}(\alpha))|F_X^{-1}(\alpha)|^b\right\} + y_0, \quad \alpha \in (0, 1).$$

This is equivalent to

$$F^{-1}(\alpha, \theta) = \begin{cases} a \exp \{ - [-\mu - \sqrt{2}\sigma \operatorname{erf}^{-1}(2\alpha - 1)]^b \} + y_0, & \alpha \in I_1, \\ a \exp \{ [\mu + \sqrt{2}\sigma \operatorname{erf}^{-1}(2\alpha - 1)]^b \} + y_0, & \alpha \in I_2, \end{cases}$$

where

$$I_1 = \left(0, \frac{1}{2} \left[1 + \operatorname{erf} \left(\frac{-\mu}{\sqrt{2}\sigma} \right) \right] \right), \quad I_2 = \left[\frac{1}{2} \left[1 + \operatorname{erf} \left(\frac{-\mu}{\sqrt{2}\sigma} \right) \right], 1 \right).$$

B Modified five-parameter log-normal distribution (mLN5)

Let function t be a transformation

$$t(x) = \begin{cases} t_1(x) = a \exp \{ - (-x)^b \} + y_0, & x \in G_1 = (-\infty, -1), \\ t_2(x) = a \exp \{ - (-x)^{b+(1-b)(1+x)} \} + y_0, & x \in G_2 = (-1, 0), \\ t_3(x) = a \exp \{ x^{b+(1-b)(1-x)} \} + y_0, & x \in G_3 = (0, 1), \\ t_4(x) = a \exp \{ x^b \} + y_0, & x \in G_4 = (1, \infty). \end{cases}$$

Now, the following expressions hold for the inverse functions:

Function $\tau_1(y) = -\ln^{\frac{1}{b}} \left(\frac{a}{y-y_0} \right)$ is an inverse function to t_1 on $H_1 = t(G_1) = (y_0, ae^{-1} + y_0)$, and its derivative satisfies $\tau_1'(y) = \frac{1}{b(y-y_0)} \ln^{\frac{1-b}{b}} \left(\frac{a}{y-y_0} \right)$. Function τ_2 is an inverse function to t_2 on $H_2 = t(G_2) = (ae^{-1} + y_0, a + y_0)$ and $\tau_2(y) = x$ solves equation $y = t_2(x)$ in form of equation

$$\ln \left[\ln \left(\frac{a}{y-y_0} \right) \right] = [b + (1-b)(1+x)] \ln(-x).$$

Moreover, its derivative satisfies $\tau_2'(y) = \left[t_2'(x)|_{x=\tau_2(y)} \right]^{-1}$, where

$$t_2'(x) = a \exp \{ - (-x)^{1+x-bx} \} (-x)^{x-bx} [1 + x(1-b)(1 + \ln(-x))].$$

Function τ_3 is as an inverse function to the function t_3 on $H_3 = t(G_3) = (a + y_0, ae + y_0)$, and $\tau_3(y) = x$ solves equation $y = t_3(x)$ in form of equation

$$\ln \left[\ln \left(\frac{y-y_0}{a} \right) \right] = [b + (1-b)(1-x)] \ln(x),$$

with derivative with respect to y given as $\tau_3'(y) = \left[t_3'(x)|_{x=\tau_3(y)} \right]^{-1}$, where

$$t_3'(x) = a \exp \{ x^{1-x+bx} \} x^{-x+bx} [1 - x(1-b)(1 + \ln(x))].$$

Function τ_4 is an inverse function to the function t_4 on $H_4 = t(G_4) = (ae + y_0, \infty)$, that is $\tau_4(y) = \ln^{\frac{1}{b}} \left(\frac{y-y_0}{a} \right)$, and its derivative is $\tau_4'(y) = \frac{1}{b(y-y_0)} \ln^{\frac{1-b}{b}} \left(\frac{y-y_0}{a} \right)$.

Let $X \sim N(\mu, \sigma^2)$ be a normally distributed random variable and $g_X(x)$ be its probability density function. Let

function $t(x)$ be regular on open and disjoint intervals G_1, \dots, G_4 . Then function $f(y) = \sum_{j=1}^4 f_j(y)$ is a **probability density function** of transformed random variable $Y = t(X)$ that has **mLN5 distribution**, where

$$f_j(y) = \begin{cases} g_x(\tau_j(y)) |t'(y)| = \frac{1}{\sqrt{2\pi\sigma}} \exp\left\{-\frac{1}{2\sigma^2}[\tau_j(y) - \mu]^2\right\} |t'_j(y)|, & y \in H_j, \\ 0, & \text{otherwise.} \end{cases}$$

It can be shown that $t'_2(x) > 0, \forall x \in G_2$, and $t'_3(x) > 0, \forall x \in G_3$, if $b < b_{\max} \doteq 8,389$. Hence function t is regular on intervals G_1, \dots, G_4 for $0 < b < b_{\max}$.

To obtain cumulative distribution function $F(y, \theta)$ from known probability density function $f(y, \theta)$, we evaluate non-negative parts $f_j(y, \theta)$. Let $z_j \in H_j$ denote endpoints of interval $H_j = (H_j^L, H_j^U)$, $j = 1, \dots, 4$, then

$$\int_{H_j^L}^{z_j} f(t) dt = \int_{H_j^L}^{z_j} \frac{1}{\sqrt{2\pi\sigma}} \exp\left\{-\frac{1}{2\sigma^2}[\tau_j(t) - \mu]^2\right\} |t'_j(t)| dt.$$

Let $w_j = \frac{\tau_j(t) - \mu}{\sigma}$ be transformations that modify this expression. Then we have for the bounds

$$z_j \xrightarrow{\tau_j^L} \frac{\tau_j(z_j) - \mu}{\sigma}, y_0 \xrightarrow{\tau_1} -\infty, a e^{-1} + y_0 \xrightarrow{\tau_1, \tau_2} \frac{-1 - \mu}{\sigma}, a + y_0 \xrightarrow{\tau_2, \tau_3} \frac{-\mu}{\sigma}, a e + y_0 \xrightarrow{\tau_3, \tau_4} \frac{1 - \mu}{\sigma}, \infty \xrightarrow{\tau_4} \infty.$$

Then integrating density $f(t, \theta)$ over sets H_1, \dots, H_4 gives

$$\begin{aligned} \int_{H_1} f(t, \theta) dt &= \frac{1}{2} [1 + \operatorname{erf}(\frac{-1 - \mu}{\sqrt{2}\sigma})] - 0, \\ \int_{H_2} f(t, \theta) dt &= \frac{1}{2} [1 + \operatorname{erf}(\frac{-\mu}{\sqrt{2}\sigma})] - \frac{1}{2} [1 + \operatorname{erf}(\frac{-1 - \mu}{\sqrt{2}\sigma})] \\ \int_{H_3} f(t, \theta) dt &= \frac{1}{2} [1 + \operatorname{erf}(\frac{1 - \mu}{\sqrt{2}\sigma})] - \frac{1}{2} [1 + \operatorname{erf}(\frac{-\mu}{\sqrt{2}\sigma})] \\ \int_{H_4} f(t, \theta) dt &= 1 - \frac{1}{2} [1 + \operatorname{erf}(\frac{1 - \mu}{\sqrt{2}\sigma})] \end{aligned}$$

Hence

$$F(z_j, \theta) = \int_{H_j^L}^{z_j} f(t) dt = \int_{-\infty}^{y_0} 0 dt + \int_{H_1} f(t) dt + \dots + \int_{H_j^L}^{z_j} f(t) dt = \frac{1}{2} \left[1 + \operatorname{erf}\left(\frac{z_j - \mu}{\sqrt{2}\sigma}\right) \right],$$

for $j = 1, \dots, 4$. This yields full form of **cumulative distribution function** $F(y, \theta)$

$$F(y, \theta) = \begin{cases} 0, & y \in (-\infty, y_0), \\ \frac{1}{2} \left[1 + \operatorname{erf}\left(\frac{\tau_j(y) - \mu}{\sqrt{2}\sigma}\right) \right], & y \in H_j, j = 1, \dots, 4. \end{cases}$$

Quantile function $F^{-1}(y, \theta)$ is obtained as an inverse function of cumulative distribution function $F(y, \theta)$. Let $y \in H_j$, $j = 1, \dots, 4$, then for $\alpha = \frac{1}{2} [1 + \operatorname{erf}(\frac{\tau_j(y) - \mu}{\sqrt{2}\sigma})] \in I_j$, we have

$$\tau_j(y) = \mu + \sqrt{2}\sigma \operatorname{erf}^{-1}(2\alpha - 1) \text{ and } y = t_j(\mu + \sqrt{2}\sigma \operatorname{erf}^{-1}(2\alpha - 1)),$$

where

$$\begin{aligned}
 I_1 &= (F(y_0), F(ae^{-1} + y_0)) = \left(0, \frac{1}{2} \left[1 + \operatorname{erf}\left(\frac{-1-\mu}{\sqrt{2}\sigma}\right)\right]\right), \\
 I_2 &= [F(ae^{-1} + y_0), F(a + y_0)] = \left[\frac{1}{2} \left[1 + \operatorname{erf}\left(\frac{-1-\mu}{\sqrt{2}\sigma}\right)\right], \frac{1}{2} \left[1 + \operatorname{erf}\left(\frac{-\mu}{\sqrt{2}\sigma}\right)\right]\right), \\
 I_3 &= [F(a + y_0), F(ae + y_0)] = \left[\frac{1}{2} \left[1 + \operatorname{erf}\left(\frac{-\mu}{\sqrt{2}\sigma}\right)\right], \frac{1}{2} \left[1 + \operatorname{erf}\left(\frac{1-\mu}{\sqrt{2}\sigma}\right)\right]\right), \\
 I_4 &= [F(ae + y_0), F(\infty)] = \left[\frac{1}{2} \left[1 + \operatorname{erf}\left(\frac{1-\mu}{\sqrt{2}\sigma}\right)\right], 1\right).
 \end{aligned}$$

C Alternative parametrization

The five-parameter log-normal distribution and its modification can be written with alternative parametrization with the potential to improve the numerical optimization of estimation methods.

Let $\mu' = \frac{\mu}{\sigma}$, $\sigma' = \sigma^b$, then $\operatorname{sgn}X|X|^b$ can be written as $\operatorname{sgn}(U + \mu')U + \mu'^b\sigma'$, where $X = \mu + \sigma U$ and U is a random variable with a standardized normal distribution, $U \sim N(0, 1)$. Then random variable Y from the LN5 distribution is in the form of

$$Y = a \exp\{\operatorname{sgn}(U + \mu')\sigma'|U + \mu'^b\} + y_0.$$

If $|X| < 1$, then $|X|^{b+(1-b)(1-|X|)} = |U + \mu'|^{b+(1-b)(1-|X|)}(\sigma')^{(1+(\frac{1}{2}-1)(1-|X|))}$. Hence a random variable Y from the mLNS distribution can be written as follows

$$Y = \begin{cases} a \exp\{\operatorname{sgn}(U + \mu')\sigma'|U + \mu'^b\} + y_0, & |X| \geq 1, \\ a \exp\{\operatorname{sgn}(U + \mu')|U + \mu'|^{b+(1-b)(1-|X|)}(\sigma')^{(1+(\frac{1}{2}-1)(1-|X|))}\} + y_0, & |X| < 1. \end{cases}$$

D PDF and CDF functions for LNS and mLNS

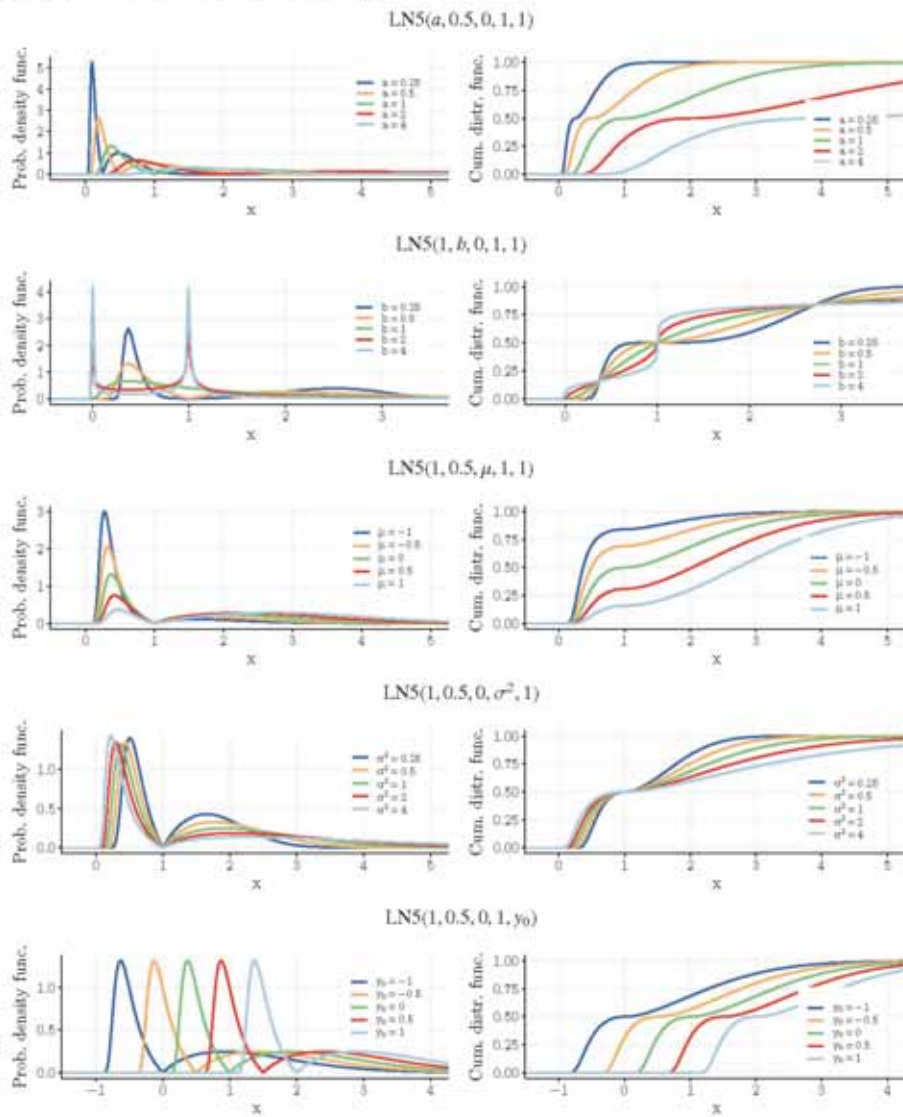


Figure 1: Probability density and cumulative distribution functions of the LNS distribution.

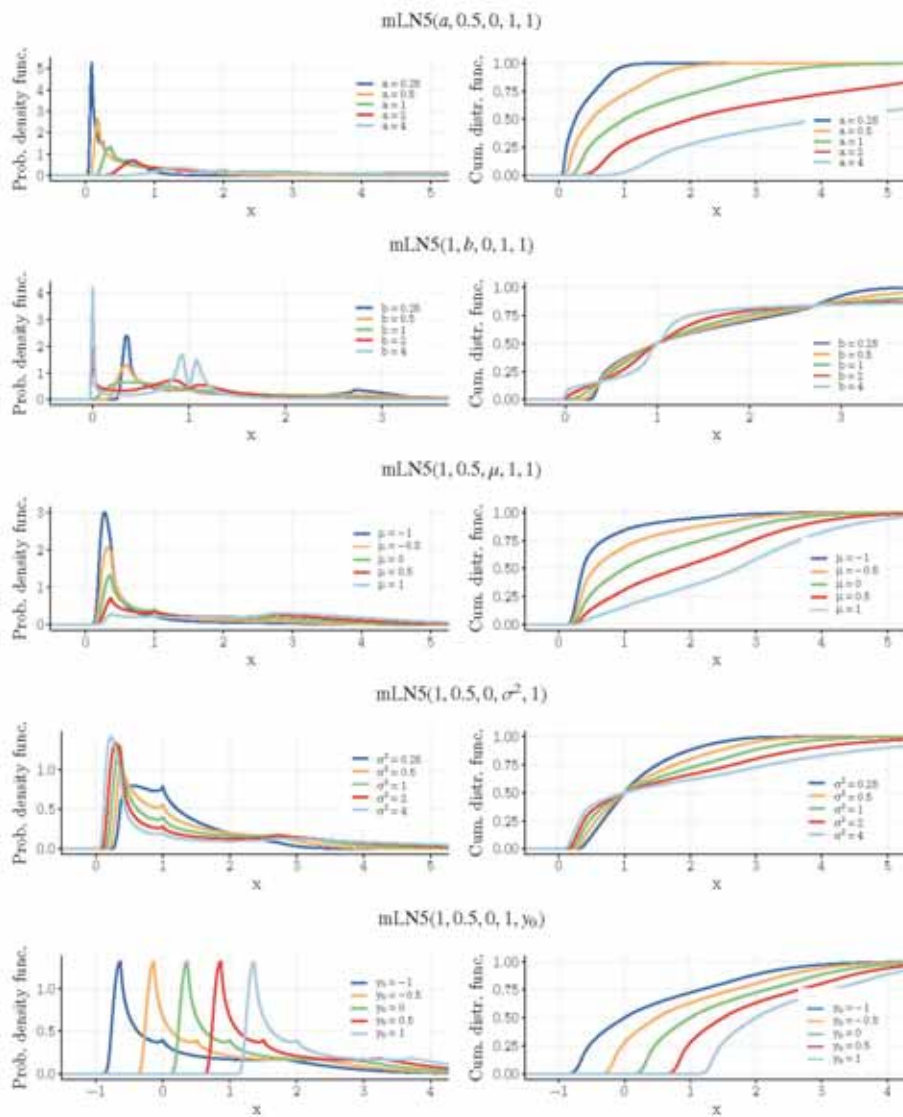


Figure 2: Probability density and cumulative distribution functions of the mLN5 distribution.

E Comparison of LMLE estimates for Morava nad Dyje rivers

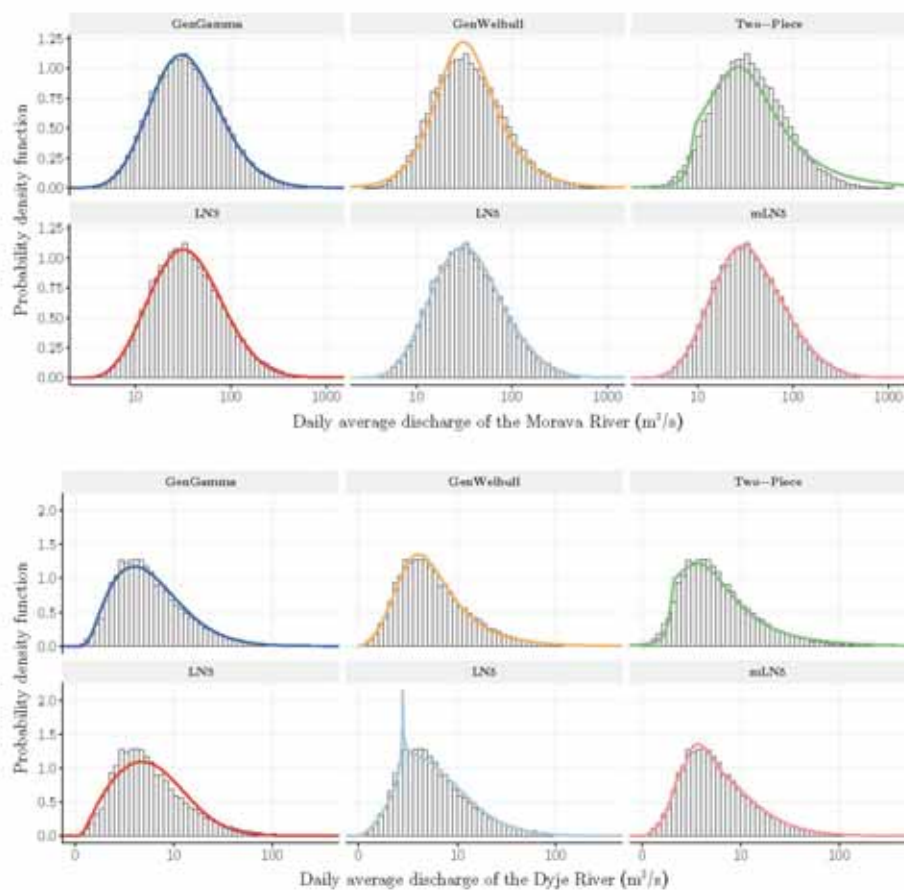


Figure 3: Histograms and superposed fitted probability density functions for the generalized gamma (blue line), generalized Weibull (orange line), Cauchy two-piece (green line), LN3 (red line), LN5 (light blue line) and mLNS (pink line) distributions.

F Simulation study results from [1]

A set of 100,000 values was generated from a standardized normal distribution $N(0, 1)$. Seven distinct random samples were selected from this foundational dataset, each encompassing 10,000 data points. Values within these samples transformed $Y = a \exp\{\text{sgn}X \cdot |X|^b\} + y_0$ to derive values consistent with the LN5 distribution.

Throughout the sampling, the parameters were kept constant at the following values: $b = 0.8$, $\mu = 1$, $\sigma = 1$, and $y_0 = 0$. These parameters closely emulate the real cumulative frequency curves for daily water discharges. Here, $y_0 = 0$ represents scenarios where the watercourse becomes dry. The parameter a was set as 0.294528, for more details [1]. The simulation analysis revealed that among the methods evaluated in terms of parameter estimates (see 1) and extrapolation (see [1]), Triangular Method, Variant 2, emerged as the most optimal.

References

[1] Budík, L. and Budíková, M. (2020). Comparison of various methods of parameters estimation of mLN5 distribution using simulation study. In *19th Conference on Applied Mathematics, APLIMAT 2020 Proceedings*, pages 170–179, Bratislava. STU.

Table 1: Parameter estimations computed for simulation samples of dataset with parameters $a = 0.294528$, $b = 0.8$, $\mu = 1$, and $\sigma = 1$. The best fit is denoted in bold. For the estimation of parameters, the methods employed were: Relative Least Squares Method (RLSM), Probability Optimization Method (POM), Triangular Method, Variant 1: combination of RLSM and POM (TM1), and Triangular Method, Variant 2: combination of LSM and POM incorporating an inverse transformation (TM2).

Method	\hat{a}	\hat{b}	$\hat{\mu}$	$\hat{\sigma}$
Sample no. 1				
RLSM	0.243358	0.782592	1.24503	1.057016
POM	0.223280	0.770924	1.384804	1.104462
TM1	0.274504	0.783096	1.094912	1.026296
TM2	0.275616	0.789582	1.085200	1.015933
Sample no. 2				
RLSM	0.238844	0.790799	1.269184	1.033957
POM	0.210920	0.777133	1.442264	1.090935
TM1	0.268627	0.792766	1.121960	1.004279
TM2	0.269994	0.798859	1.111332	0.994402
Sample no. 3				
RLSM	0.236678	0.789933	1.271358	1.054050
POM	0.210268	0.775730	1.438383	1.110359
TM1	0.270639	0.789515	1.106404	1.022046
TM2	0.275251	0.795143	1.081732	1.101214
Sample no. 4				
RLSM	0.238529	0.788103	1.267800	1.041082
POM	0.210255	0.772953	1.446264	1.08990
TM1	0.273279	0.787952	1.103734	1.016186
TM2	0.275736	0.793663	1.084771	1.050257
Sample no. 5				
RLSM	0.255029	0.777143	1.193399	1.050257
POM	0.227308	0.770170	1.345661	1.096242
TM1	0.281798	0.779331	1.067624	1.021678
TM2	0.286431	0.784197	1.044230	1.010946
Sample no. 6				
RLSM	0.235462	0.786703	1.283621	1.056514
POM	0.205117	0.774641	1.473530	1.117418
TM1	0.259347	0.790325	1.159128	1.028999
TM2	0.262668	0.794762	1.139972	1.019406
Sample no. 7				
RLSM	0.245514	0.769837	1.255831	1.059999
POM	0.213389	0.760617	1.448668	1.119533
TM1	0.276621	0.773506	1.102148	1.022328
TM2	0.283040	0.778053	1.070653	1.009546

IDŐJÁRÁS

*Quarterly Journal of the HungaroMet Hungarian Meteorological Service
Vol. 129, No. 2, April – June, 2025, pp. 161–175*

Comprehensive flood frequency analysis of major Sava River affluents in Bosnia and Herzegovina: risks, and implications for water resources management

Slobodan Gnjato^{1,*}, Igor Leščesen², Tatjana Popov¹, and Goran Trbić¹

¹ *University of Banja Luka, Faculty of Natural Sciences and Mathematics
Mladena Stojanovića 2, 78000 Banja Luka, Bosnia and Herzegovina*

² *Institute of Hydrology SAS
Dúbravská cesta 9, 841 04 Bratislava, Slovak Republic*

**Corresponding Author email: slobodan.gnjato@pmf.unibl.org*

(Manuscript received in final form May 24, 2024)

Abstract— This study addresses the pressing issue of flood frequency analysis in Bosnia and Herzegovina (BH), focusing on major rivers—Una, Sana, Vrbas, and Bosna. In light of the global impact of floods on lives, property, and infrastructure, the research aims to understand and predict these events, particularly considering climate change and socioeconomic development. Employing goodness-of-fit tests such as Kolmogorov-Smirnov and Cramér-Von Mises, the study identifies the most suitable probability distributions for modeling river discharge data. Pearson 3, generalized extreme value (GEV), and Gumbel distributions emerge as best fits, demonstrating variations across rivers. The research emphasizes the importance of tailoring models to specific hydrological characteristics, with the Bosna River best modeled by the Pearson 3 distribution and the Sana River by the GEV distribution. Calculated return periods for extreme flood events provide valuable insights into potential discharge magnitudes, highlighting the crucial role of accurate probability distributions in informed risk management and infrastructure planning. This study fills a critical gap in flood frequency analysis for selected rivers in BH, offering essential information for water resource management and flood risk assessment in the context of ongoing climate change.

Key-words: flood frequency analysis, flood, L-moments, Bosnia and Herzegovina, river discharge modeling

1. Introduction

Floods are the most widespread and destructive natural disasters, endangering many lives and causing damage to property, agriculture, and infrastructure worldwide (Blöschl, 2022; Chen et al., 2021; Heinrich et al., 2023). In addition, the damage caused by floods has increased in recent decades and is expected to increase further, mainly due to socioeconomic progress and climate change (Nguyen et al., 2020; Steinhausen et al., 2022). With an average of 163 events per year, floods have contributed to 44% of all natural disasters affecting 1.6 billion people around the world in the last two decades (CRED and UNDRR, 2020). The total economic loss from weather-related natural disasters in the European Economic Area amounted to 487 billion euros in the period 1980-2020 and can be attributed to weather-related extremes (Snizhko et al., 2023). Fluctuations in river flow regimes are primarily caused by climate change and human-induced impacts (Khoi et al., 2019).

Recording the frequency of flooding events is necessary but challenging due to the lack of hydrological stations and their limited geographical coverage (Benito et al., 2023). Numerous studies conducted over the last decade have investigated changes in flood events, their seasonality, and trends in Europe (Arnell and Gosling, 2016; Alfieri et al., 2015; Bertola et al., 2020; Blöschl et al., 2019; Lehmkühl et al., 2022; Trambly et al., 2023). Flood events in northwestern Europe have increased due to increased autumn and winter precipitation, while lower precipitation and less snow cover, together with a significant warming of the air, have led to a decrease in flood events in southern and eastern Europe (Blöschl et al., 2019). Fang et al. (2022) reported a distinct regional pattern of average flood dates in summer (Jun-Aug) in the Alps and in winter (Dec-Feb) across western Europe and the Mediterranean region. Flood-related studies have also increased in the southeastern region of Europe in the last decade. Some authors used regional flood frequency analysis (Kavcic et al., 2014; Leščešen et al., 2022), while other studies for the same area focused on using a general flood frequency and seasonality analysis (Ilinca and Anghel, 2022; Morlot et al., 2019; Trobec, 2017). Overall, it can be said that a significant amount of flood studies is still missing (especially in the Western Balkans region), which makes this problem even more important, especially as floods have become more frequent in the region.

Accurate and consistent forecasting of river flows is essential for many purposes, such as water resources management, modernization strategies, maneuvers, and maintenance activities (Samantaray and Sahoo, 2020). Flood risk assessment is often carried out to reduce the damage caused by floods in a particular location (Ahmed et al., 2023). In this regard, flood frequency analysis (FFA) is crucial for flood risk assessment and management, as it provides predictions of the frequency and intensity of flood events, which are essential for planning infrastructure and defining risk-related measures (Pan et al., 2023). To

ensure that flood dynamics and magnitude are accurately assessed, the most accurate FFA requires a significant number of accurately observed peak discharges (*Bartens and Haberlandt, 2024*). A statistical method such as FFA is commonly used to determine the extent of flooding within a given return period (*Šraj et al., 2016*) and is often used in water management studies (*Ahn and Palmer, 2016*). The conventional FFA approach extrapolates the tails of the distribution to determine the probability and magnitude of extreme events by fitting mathematical functions to the given data (*Leščičešen et al., 2022*). FFA is essential to engineering practice to establish links between design variables that correlate to a chosen hydrological risk (*Šraj et al., 2016*).

In Bosnia and Herzegovina (BH), FFA is almost non-existent given that numerous evaluations of flood frequency covering the 1961–1990 period were created, mostly for project studies, and they are not accessible to the general public. For this analysis, we selected four hydrological profiles on the largest right affluents of the Sava River (SR) in BH (Una, Sana, Vrbas, and Bosna rivers). Four out of five selected profiles have near-natural streamflow regimes, whereas the only station influenced by the dam is Delibašino Selo on the Vrbas River. In BH, the two main causes of flooding are sudden snowmelt that happens in the late winter/early spring or cyclone-originated precipitation. There has been a noticeable increase in the frequency of flooding events since the year 2000. Since the SR basin is made up primarily of impermeable rock layers with a dense hydrographic system (*Gnjato et al., 2023*), most floods in BH have taken place in this part of the country (*Gnjato et al., 2024*). Consequently, FFA is of great importance for engineering practice, since severe floods in the SR basin in BH are predicted to be generated more frequently as a result of climate warming. Hence, the principal task of this research was to perform a comprehensive flood frequency analysis for the main affluents of the SR in BH for the period 1961–2020.

2. Study area

Roughly 40% of the SR basin encloses the BH area, while the entire basin encompasses territories of several adjacent countries. Starting in Croatia at the mouth of the Una River and finishing at the mouth of the Drina River, the Sava River flows 345 km through BH. The SR basin in BH encompasses central mountainous (Dinaric) and northern mostly plain (Peripannonian) areas which make up around 75% of BH (*Fig. 1*). The northern lower areas of the basin experience a moderate continental climate. In contrast, the mid and southern areas of the basin are exposed to continental and mountain climates. The biggest Sava tributaries in BH are the Una, Vrbas, Bosna, and Drina rivers. All aforementioned tributaries of the SR experience pluvial-nival river regimes with maximum streamflow values in the spring season, while minimum streamflows occur in the summer (*Gnjato et al., 2021*).



Fig. 1. Location of the Sava River basin along with analyzed hydrological stations.

3. Data and methods

In this paper, a 60-year (1961–2020) database of the maximum peak discharge for each month for four gauging stations that are located in the BH (Fig. 1) was used. Discharge data was obtained from the Republic Hydrometeorological Service – Republic of Srpska. Statistical characteristics of these data sets and the whole period are presented in Table 1.

Table 1. Descriptive statistics of monthly maximum discharge (m^3/s) at the selected rivers

Parameter	River			
	Una	Sana	Vrbas	Bosna
Mean annual discharge (m^3/s)	499.13	220.69	262.85	473.00
Standard error (m^3/s)	13.05	6.14	11.48	15.53
Median (m^3/s)	436.30	185.10	208.00	387.00
Standard deviation (m^3/s)	350.32	164.84	228.46	416.77
Kurtosis	0.874	0.838	0.79	0.82
Skewness	0.957	0.961	2.68	2.51
Minimum annual discharge (m^3/s)	42.80	8.80	29.00	22.00
Maximum annual discharge (m^3/s)	2059	1014	1752	4205

To define the flood frequency at a specific site, the selection of a suitable probability distribution is of crucial importance. We have considered the generalized extreme value (GEV), Pearson type-III (P3), Log Pearson type III (LP3) and Gumbel (GUM) distributions for the analysis of flood frequency at four gauging stations at the four rivers in the northern part of BH. The probability density function (pdf) and quantile function $y(F)$ of these distributions are presented in *Table 2*. These distributions are most commonly used for FFA in the literature and are frequently applied in many countries (*Petrović et al., 2024; Cassalho et al., 2019; Drissia et al., 2019; Ul Hassan et al., 2019*).

Table 2. Probability density and quantiles functions of the probability distributions

Distribution	Probability density function $f(y)$	Quantile function $y(F)$
GEV	$\frac{1}{\alpha} = \left[1 - k \left(\frac{y - \mu}{\alpha}\right)\right]^{\frac{1}{k} - 1} \exp\left\{-\left[1 - k \left(\frac{y - \mu}{\alpha}\right)\right]^{\frac{1}{k}}\right\}$	$\mu + \frac{\alpha}{k} [1 - (-\log F)^k]$
P3	$\frac{1}{\beta^\alpha \Gamma \alpha} (y - \mu)^{\alpha - 1} \exp\left\{-\frac{(y - \mu)}{\beta}\right\}$	Explicit analytical form is not available
LP3	$f(y) = \frac{1}{\sigma(y)\sqrt{2\pi}} \exp\left[-\frac{1}{2}\left(\frac{y - \mu(y)}{\sigma(y)}\right)^2\right]$	$y(f) = \mu(y) + \sigma(y)x \left[Z + \frac{1}{2}\left(\frac{Z^2 - 1}{3}\right)\right]$
GUM	$\frac{1}{\alpha} \exp\left[-\frac{y - \mu}{\alpha} - \exp\left(-\frac{y - \mu}{\alpha}\right)\right]$	$\mu - \alpha \log(-\log F)$

Hosking and Wallis (1997) introduced L-moments as linear functions of probability weighted moments (PWM's), offering an alternative to conventional moments. Computed from linear combinations of order statistics, L-moments can be defined for any random variable Y with an existing mean. PWM was applied for L-moments calculation as outlined by *Hosking and Wallis (1997)*:

$$\beta_r = E\{X[F_x(x)]^r\}, \tag{1}$$

where, β_r is the r th order PWM and $F_x(x)$ characterizes the cumulative distribution function (CDF) of X . Sample estimators (β_i) of the first four PWMs are explained in *Hosking and Wallis (1997)*:

$$\beta_0 = m = \frac{1}{n} \sum_{j=1}^n X_j, \quad (2)$$

$$\beta_1 = \sum_{j=1}^{n-1} \left[\frac{n-j}{n(n-1)} \right] x_{(j)}, \quad (3)$$

$$\beta_2 = \sum_{j=1}^{n-2} \left[\frac{(n-1)(n-j-2)}{n(n-1)(n-2)} \right] X_{(j)}, \quad (4)$$

$$\beta_3 = \sum_{j=1}^{n-3} \left[\frac{(n-j)(n-j-1)(n-j-2)}{n(n-1)(n-2)(n-3)} \right] X_{(j)}, \quad (5)$$

where, $X_{(j)}$ is the rank of AMS with $X_{(1)}$ which represents the highest value and $X_{(n)}$ that represents the lowest value. Regarding PWMs, the initial four L-moments, signifying the mean, scale, skewness, and kurtosis of the distributions, are established through linear combinations of PWMs (*Hosking and Wallis, 1997*):

$$\lambda_1 = \beta_0, \quad (6)$$

$$\lambda_2 = 2\beta_1 - \beta_0, \quad (7)$$

$$\lambda_3 = 6\beta_2 - 6\beta_1 + \beta_0, \quad (8)$$

$$\lambda_4 = 20\beta_3 - 30\beta_2 + 12\beta_1 - \beta_0. \quad (9)$$

Finally, the L-moment ratios defined by *Hosking and Wallis (1993)* are specified below:

$$L - C_v = \tau_2 = \frac{\lambda_2}{\lambda_1}, \quad (10)$$

$$L - C_s = \tau_3 = \frac{\lambda_3}{\lambda_2}, \quad (11)$$

$$L - C_k = \tau_4 = \frac{\lambda_4}{\lambda_2}, \quad (12)$$

where τ_2 is the L coefficient of variation, τ_3 is the L coefficient of skewness, τ_4 is the L coefficient of kurtosis.

The optimal distribution function was determined by employing the Kolmogorov-Smirnov (K-S) and Cramer-von Mises (CvM) tests. These tests were selected for their robustness and reliability at different sample sizes, making them particularly suitable for flood frequency analysis where sample sizes may be limited. K-S and CvM tests are known for their ability to accurately assess

goodness of fit even at minimum cell frequencies and provide a sound methodological basis for determining the optimal distribution function (Petrović *et al.*, 2024; Leščešen *et al.*, 2022; Kousar *et al.*, 2020). The K-S test is frequently employed method for assessing the consistency of probability distribution methods, delivering reliable results even with limited samples and minimal cell frequencies. The approach involves computing the value of D_{max} that represents the maximum unconditional deviation between the cumulative extent of two distributions, followed by comparison with the critical value of D to either accept or reject the proposed set hypothesis (Bhat *et al.*, 2019). In comparing two or more theoretical distributions, the distribution exhibiting lower values of the D_{max} statistics is considered the optimal fit with the empirical data. The K-S test goes as follows:

$$D_{max} = \max |F_e(x) - F_t(x)| . \quad (13)$$

Similarly, the Cramer–von Mises test evaluates the concordance between empirical and theoretical distributions, with a diminished value of $N\omega$ indicating a closer conformity of the distribution with the empirical data:

$$N\omega^2 = \frac{1}{12N} + \sum_{i=1}^N [F_e(x) - F_t(x)]^2 . \quad (14)$$

For further confirmation, the Monte Carlo approach was employed to assess the performance of different probability distributions in modeling river discharge data (Zorzetto *et al.*, 2016). The analysis involved conducting 1000 simulations to evaluate the Mean Absolute Error (MAE) and root mean squared error (RMSE) for each distribution, which are defined as follows:

$$MAE = \frac{1}{3} \sum_{i=1}^n |y_i - \hat{y}_i| , \quad (15)$$

$$RMSE = \sqrt{\frac{1}{n} \sum_{i=1}^n (y_i - \hat{y}_i)^2} , \quad (16)$$

where n is the number of data points, y_i is the observed discharge value, and \hat{y}_i is the estimated discharge value from the probability distribution. For each simulation, random data were generated using the parameters obtained from fitting the Pearson 3, log-Pearson 3, generalized extreme value (GEV), and Gumbel distributions to the observed discharge data. The MAE and RMSE were calculated for each distribution, providing insights into their ability to accurately represent the observed discharge values.

4. Results and discussion

When analyzing the flood frequency, the main objective is to accurately and rigorously determine the quantile values that define the range of low exceedance probabilities, as there are usually no observed values. The goodness-of-fit tests were performed to assess the suitability of different probability distributions for modelling the discharge data of the Bosna, Vrbas, Una, and Sana rivers, with further validation using the Monte Carlo approach (Table 3).

Table 3. Fit statistics and distribution selection for river discharge data

River	Distribution	Goodness-of-Fit Test				Monte Carlo Approach	
		Kolmogorov-Smirnov		Cramer-von Mises		MAE	RMSE
		Stat	P-value	Stat	P-value		
Una	GEV	0.058	0.019	0.641	0.017	391.33	525.40
	P3	0.061	0.008	0.751	0.009	400.56	533.40
	LP3	0.754	0.000	161.2	0.000	1331.00	3028.60
	GUM	0.058	0.013	0.635	0.018	377.23	487.70
Bosna	GEV	0.076	0.000	0.752	0.009	440.54	768.10
	P3	0.033	0.400	0.103	0.568	409.29	577.00
	LP3	0.632	0.000	0.104	0.567	1817.68	4584.40
	GUM	0.066	0.003	0.811	0.007	384.71	532.00
Sana	GEV	0.042	0.137	0.511	0.037	184.84	251.52
	P3	0.048	0.065	0.512	0.037	188.02	250.78
	LP3	0.590	0.000	96.315	0.000	2318.91	5907.70
	GUM	0.050	0.050	0.682	0.014	176.06	227.55
Vrbas	GEV	0.085	0.006	0.479	0.045	230.96	382.37
	P3	0.056	0.166	0.174	0.324	221.52	317.40
	LP3	0.778	0.000	96.24	0.000	356.84	1993.68
	GUM	0.091	0.003	0.547	0.030	205.74	289.00

In this study, no single distribution was identified as the best fit for all gauging station locations. Similar results have been reported in several other studies (Petrović *et al.*, 2024; Drissia *et al.*, 2019; UI Hassan *et al.*, 2019; Castellarin *et al.*, 2012) For the Una River, the LP3 distribution was found to be the best fit, as it had the lowest values in both the Kolmogorov-Smirnov and Cramér-Von Mises statistics. The P3 distribution was also identified as the best fitting model for the Bosna river, which was confirmed by its superior

performance in both tests. Conversely, the Gumbel distribution showed the best fit for the Sana River and had the lowest statistics in both goodness-of-fit tests. Finally, for the Vrbas River, the P3 distribution also performed the best and had the lowest statistics in both tests. Graphical confirmation of the goodness-of-fit results was achieved through a box plot analysis, which further underpins the identified best-fit probability distributions for each river system (*Fig. 2*).

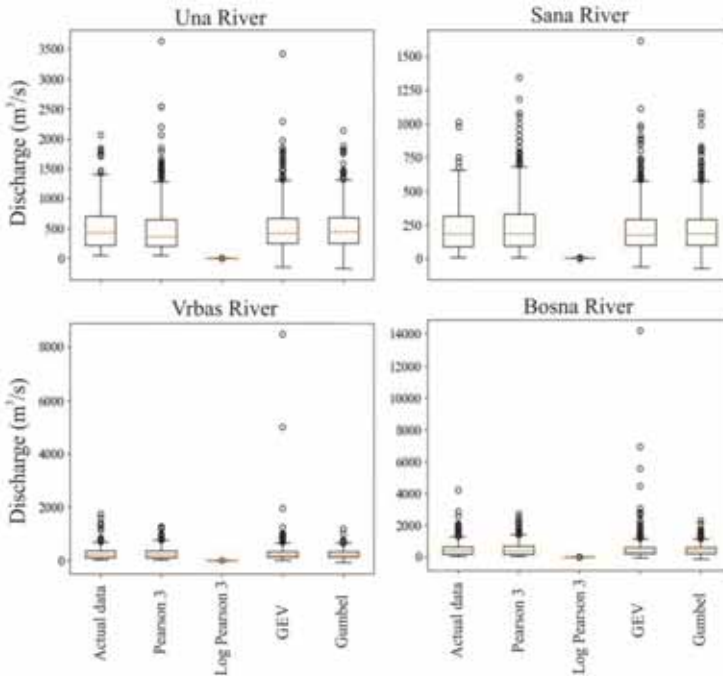


Fig. 2. Box plot presentation of the fitting results for all considered distribution functions.

For clarity, a cumulative distribution function (CDF) chart was created to further validate the results and strengthen their credibility (*Fig. 3*). This diagram visually compares the distribution of observed discharge values with those estimated using different probability distributions. The x-axis represents the discharge values, while the y-axis indicates the cumulative probability of occurrence. The CDF diagram shows that the log-Pearson 3 distribution along the x-axis deviates significantly from the observed discharge values, indicating a lack of fit. In contrast, other distributions show a considerable overlap with the observed discharge data, indicating a better fit. Consistent with the conclusions drawn from the CvM test and the KS test, the CDF plot confirms that the generalized extreme value (GEV) distribution, the Pearson 3 distribution, and the

Gumbel distribution are best suited for modeling river discharge data. These distributions not only have a good statistical fit but also closely match the observed discharge values, which clearly demonstrates their suitability for the analysis.

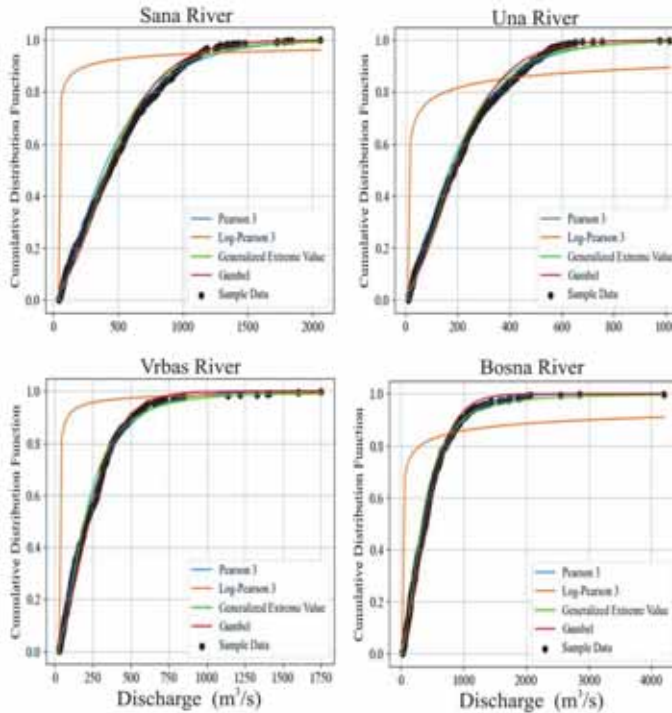


Fig. 3. Cumulative distribution function (CDF) analysis.

Even though results from FFA analysis in Slovenia (*Zabret and Brilly, 2014*), overall Sava River basin (*Leščičen et al., 2022*) suggest that GEV distribution is the most appropriate for this region, from the presented results a single distribution does not appear as the best fitting distribution for all rivers. The size of the sample does not play a decisive role in favoring any specific distribution or estimation method. The Bosna River has the highest average of monthly maximum discharge, and it is best modeled by Pearson 3 distribution, while the Sana River has the lowest average of the monthly maximum and is best modeled by GEV distribution (see *Table 1*). The results for Sana River are in good accordance with the results presented by *Morlot et al. (2019)*. The Pearson 3 distribution is more suitable for rivers that have lower values of the coefficient of kurtosis and low values of the coefficient of skewness (see *Table 1*). These sentences should be rephrased as follows: A crucial difference between our study and that of *Morlot et al. (2019)* lies in the suitability of the log-Pearson 3

distribution for the observed flows. Our results show that this distribution is not suitable for the fluxes investigated, whereas *Morlot et al.* (2019) indicate that it is most suitable for the rivers Una, Vrbas, and Bosna. This discrepancy could be due to differences in the data sets used for the analyses. In our study, monthly maximum values were used, while *Morlot et al.* used daily discharge values. This discrepancy raises interesting questions that should be investigated in future research projects.

To improve the robustness of our study, we conducted a Monte Carlo simulation to evaluate the performance of different probability distributions in modeling runoff data. This approach provided valuable information on the accuracy of the distribution fit and the reliability of the runoff estimates (*Table 4*). This comprehensive analysis ensures a more thorough understanding of the predictive capabilities of the selected distributions and thus increases the reliability of flood estimation, even for different return periods.

Table 4. MAE and RMSE comparison with Monte Carlo approach

River	Monte Carlo approach	
	MAE	RMSE
Una	370.81	734.81
Bosna	320.74	127.12
Sana	434.82	480.35
Vrbas	113.23	342.62

The results of the Monte Carlo simulation, presented in *Table 4*, show the performance of the model in simulating runoff data for the Sana, Vrbas, Una, and Bosna rivers. The MAE values range from 113.23 to 434.82 cubic meters per second (m³/s), while the RMSE values range from 127.12 to 734.82 m³/s. Lower MAE and RMSE values indicate better agreement between observed and simulated runoff values. The results indicate that the model works relatively well, especially for the rivers Vrbas and Bosna, where the MAE and RMSE values are comparatively lower. For the Una River, however, the model shows slightly higher errors, indicating that the discharge dynamics for this river can only be captured with limited accuracy. Although the model shows varying degrees of accuracy on the different rivers, its ability to approximate the discharge data with reasonable precision underlines its usefulness for the FFA.

A key objective of the flood frequency analysis is to determine the quantile in the extreme upper tail of the best-fit distribution for the Una, Sana, Vrbas, and Bosna rivers. Using the quantile function and the parameter values specific to the best-fit distribution at each gauging station, we calculate the quantile estimates

corresponding to return periods of 5, 10, 25, 50, 100, 200, 500, and 1000 years, with 95% confidence intervals (Fig. 4). The confidence intervals for each distribution were determined as depicted in Anghel and Ilinca (2023).

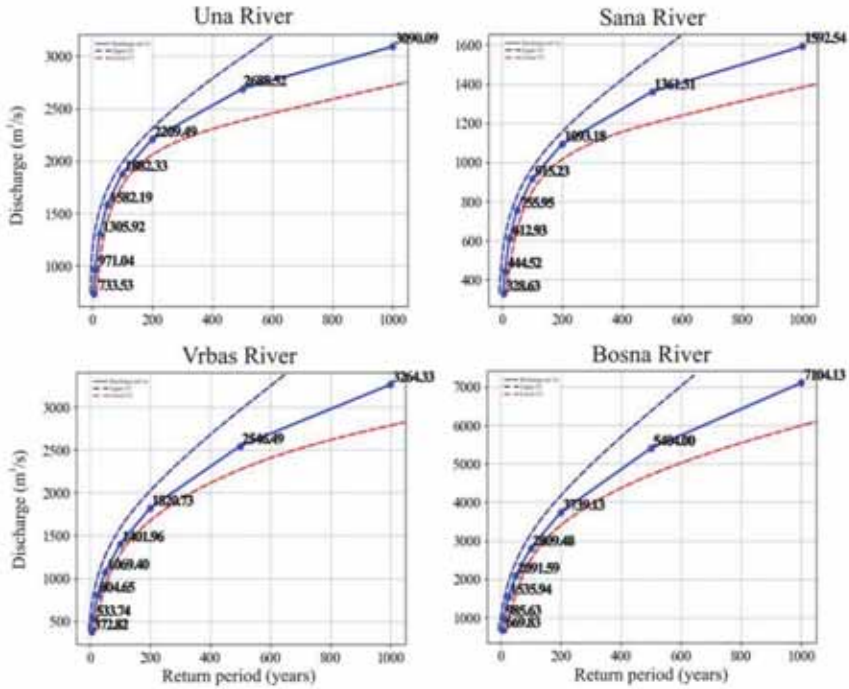


Fig. 4. Calculated return periods for selected rivers.

The analysis shows increasing discharge values for different return periods across several rivers, including the Una, Sana, Vrbas and Bosna. These results emphasize the importance of accurate probability distributions for estimating extreme flood magnitudes, which are crucial for effective risk management strategies in the northern parts of BH.

5. Conclusion

This study addressed the critical issue of flood frequency analysis in Bosnia and Herzegovina, focusing on the major rivers-Una, Sana, Vrbas, and Bosna. The global impact of floods on lives, property, and infrastructure underscores the urgency of understanding and predicting these events, especially in the context of climate change and socioeconomic development.

The comprehensive analysis included goodness-of-fit tests, including Kolmogorov-Smirnov and Cramér-Von Mises tests, to identify the most appropriate probability distributions for modeling river discharge data. The results showed differences between rivers, with the Pearson 3, generalized extreme value (GEV) and Gumbel distributions emerging as the best fits for different cases. Graphical analyzes using box plots and cumulative distribution function (CDF) diagrams visually confirmed the statistical results and substantiated the appropriateness of the identified distributions for each river system.

The study also highlighted that a single distribution is not universally appropriate for all rivers, emphasizing the importance of tailoring the models to specific hydrological characteristics. The Bosna River, characterized by the highest average monthly discharge, showed the best fit with the Pearson 3 distribution, while the Sana River, with the lowest average, was best modeled by the GEV distribution.

In addition, the calculated return periods for extreme flood events provided valuable insights into potential runoff magnitudes for different return intervals. The results emphasize the importance of accurate probability distributions in estimating extreme flood magnitudes, which are essential for sound risk management and infrastructure planning.

This research fills a critical gap in the analysis of flood frequency for the selected rivers in Bosnia and Herzegovina and provides valuable information for water resource management and flood risk assessment. As climate change continues to impact hydrological patterns, the results of this study contribute to our understanding of how different rivers respond to extreme events, helping to develop robust flood mitigation and adaptation strategies in the region.

Future research could focus on extending the scope of this analysis to other rivers and integrating more recent climate data to improve the robustness of flood prediction models. In addition, the inclusion of socioeconomic factors and land use changes could lead to a more comprehensive understanding of flood risks and enable more effective management strategies.

Acknowledgements: The results presented in this paper are part of the scientific research project “Flood Frequency Analysis in the Sava River Basin in the Republic of Srpska” (Contract No. 19.032/961-27/24), funded by the Ministry of Scientific and Technological Development and Higher Education of the Republic of Srpska.

References

- Ahmed, A., Yildirim, G., Haddad, K., and Rahman, A., 2023: Regional Flood Frequency Analysis: A Bibliometric Overview. *Water* 15(9), 1658. <https://doi.org/10.3390/w15091658>
- Ahn, K-H. and Palmer, R., 2016: Regional flood frequency analysis using spatial proximity and basin characteristics Quantile regression vs. parameter regression technique. *J. Hydrol.* 540, 515–526. <https://doi.org/10.1016/j.jhydrol.2016.06.047>

- Alfieri, L., Burek, P., Feyen, L., and Forzieri, G., 2015: Global warming increases the frequency of river floods in Europe. *Hydrol. Earth Syst. Sci.* 19, 2247–2260. <https://doi.org/10.5194/hess-19-2247-2015>
- Anghel, C.G. and Ilinca, C., 2023: Predicting Flood Frequency with the LH-Moments Method: A Case Study of Prigor River, Romania. *Water* 15(11), 2077. <https://doi.org/10.3390/w15112077>
- Arnell, N.W. and Gosling, S.N., 2016: The impacts of climate change on river flood risk at the global scale. *Clim. Change* 134, 387–401. <https://doi.org/10.1007/s10584-014-1084-5>
- Bartens, A., and Haberlandt, U., 2024: Flood frequency analysis using mean daily flows vs. instantaneous peak flows. *Hydrol. Earth Syst. Sci.* 28, 1687–1709. <https://doi.org/10.5194/hess-2023-144>
- Benito, G., Ballesteros-Cánovas, J.A., and Díez-Herrero, A., 2023: Chapter 2 - Paleoflood hydrology: reconstructing rare events and extreme flood discharges. In (Eds. Shroder, J.F., Paron, P., & Di Baldassarre, G.), *Hydro-Meteorological Hazards, Risks, and Disasters*. Elsevier. 33-83.
- Bertola, M., Viglione, A., Lun D., Hall, J., and Blöschl, G., 2020: Flood trends in Europe: are changes in small and big floods different? *Hydrol. Earth Syst. Sci.* 24, 1805–1822. <https://doi.org/10.5194/hess-24-1805-2020>
- Blöschl, G., 2022: Three hypotheses on changing river flood hazards. *Hydrol. Earth Syst. Sci.* 26, 5015–5033. <https://doi.org/10.5194/hess-26-5015-2022>
- Blöschl, G., Hall, J., Viglione, A., Perdigão, R.A.P., Parajka, J., Merz, B., ... and Živković, N., 2019: Changing climate both increases and decreases European river floods. *Nature*, 573, 108–111. <https://doi.org/10.1038/s41586-019-1495-6>
- Bhat, M.S., Alam, A., Ahmad, B., Koilia, B.S., Farooq, H., Taloor, A.K., and Ahmad, S., 2019: Flood frequency analysis of river Jhelum in Kashmir basin. *Quat. Int.* 507, 288–294. <https://doi.org/10.1016/j.quaint.2018.09.039>
- Cassalho, F., Beskow, S., de Mello, C. R., and de Moura, M.M., 2019: Regional flood frequency analysis using L-moments for geographically defined regions: An assessment in Brazil. *J. Flood Risk Manag.* 12. <https://doi.org/10.1111/jfr3.12453>
- Castellarin, A., Kohnova, S., Gaal, L., Fleig, A., Salinas, J.L., Toumazis, A., Kjeldsen, T. R., and Macdonald, N., 2012: Review of applied-statistical methods for flood-frequency analysis in Europe. NERC/Centre for Ecology & Hydrology.
- Centre for Research on the Epidemiology of Disasters & United Nations Office for Disaster Risk Reduction, 2020. The human cost of disasters: an overview of the last 20 years (2000-2019). https://www.preventionweb.net/files/74124_humancostofdisasters20002019reportu.pdf
- Chen, M., Papadakis, K., and Jun, C., 2021: An investigation on the non-stationarity of flood frequency across the UK. *J. Hydrol.* 597. <https://doi.org/10.1016/j.jhydrol.2021.126309>
- Drissia, T.K., Jothiprakash, V., and Anitha, A.B., 2019: Flood Frequency Analysis Using L Moments: a Comparison between At-Site and Regional Approach. *Water Resour. Manag.* 33, 1013–1037. <https://doi.org/10.1007/s11269-018-2162-7>
- Fang, G., Yang, J., Li, Z., Chen, Y., Duan, W., Amory, C., and De Maeyer, P., 2022: Shifting in the global flood timing. *Sci. Rep.* 12. <https://doi.org/10.1038/s41598-022-23748-y>
- Gnjato, S., Leščičen, I., Basarin, B., and Popov, T., 2024: What is happening with frequency and occurrence of the maximum river discharges in Bosnia and Herzegovina? *Acta geography. Sloven.* 64, 129–149. <https://doi.org/10.3986/AGS.13461>
- Gnjato, S., Popov, T., Ivanišević, M., and Trbić, G., 2023: Long-term streamflow trends in Bosnia and Herzegovina (BH). *Environ. Earth Sci.* 82. <https://doi.org/10.1007/s12665-023-11040-9>
- Gnjato, S., Popov, T., Adžić, D., Ivanišević, M., Trbić, G., and Bajić, D., 2021: Influence of climate change on river discharges over the Sava river watershed in Bosnia and Herzegovina. *Időjárás* 125, 449–462. <https://doi.org/10.28974/idojaras.2021.3.5>
- Heinrich, P., Hagemann, S., Weisse, R., and Gaslikova, L., 2023: Changes in compound flood event frequency in northern and central Europe under climate change. *Front. Clim.* 23, 1967–1985. <https://doi.org/10.3389/fclim.2023.1227613>
- Hosking, J.R.M., and Wallis, J.R., 1997: *Regional Frequency Analysis: An approach based on L-moments*. Cambridge University Press, UK. <http://dx.doi.org/10.1017/cbo9780511529443>
- Hosking, J.R.M., and Wallis, J.R., 1993: Some statistics useful in regional frequency analysis. *Water Resour. Res.* 29, 271–281. <https://doi.org/10.1029/92WR01980>

- Ilinca, C., and Anghel, C.G., 2022: Flood-Frequency Analysis for Dams in Romania. *Water* 14. <https://doi.org/10.3390/w14182884>
- Kavcic, K., Brilly, M., and Sraj, M., 2014: Regional flood frequency analysis in Slovenia. *Geophys. Res. Abstr.* 16. EGU2014-2803.
- Khoi, D.N., Nguyen, V.T., Sam, T.T., Phung, N.K., and Bay, N.T., 2019: Responses of river discharge and sediment load to climate change in the transboundary Mekong River Basin. *Water Environ. J.* 34, 367–380. <https://doi.org/10.1111/wej.12534>
- Kousar, S., Khan, A.R., Ul Hassan, M., Noreen, Z., and Bhatti, S.H., 2020: Some best-fit probability distributions for at-site flood frequency analysis of the Ume River. *J. Flood Risk Manag.* 13. <https://doi.org/10.1111/jfr3.12640>
- Lehmkuhl, F., Schüttrumpf, H., Schwarzbauer, J., Brüll, C., Dietze, M., Letmathe, P., Völker, C., and Hollert, H., 2022: Assessment of the 2021 summer flood in Central Europe. *Environ. Sci. Eur.* 34. <https://doi.org/10.1186/s12302-022-00685-1>
- Leščešen, I., Šraj, M., Basarin, B., Pavić, D., Mesaroš, M., and Mudelsee, M. 2022: Regional Flood Frequency Analysis of the Sava River in South-Eastern Europe. *Sustainability* 14. <https://doi.org/10.3390/su14159282>
- Morlot, M., Brilly, M., and Šraj, M., 2019: Characterisation of the floods in the Danube River basin through flood frequency and seasonality analysis. *Acta hydrotech.* 32, 73–89. <https://doi.org/10.15292/acta.hydro.2019.06>
- Nguyen, V. D., Metin, A.D., Alfieri, L., Vorogushyn, S., and Merz, B., 2020: Biases in national and continental flood risk assessments by ignoring spatial dependence. *Sci. Rep.* 10. <https://doi.org/10.1038/s41598-020-76523-2>
- Pan, X., Yildirim, G., Rahman, A., Haddad, K., and Ouarda, T.B.M.J., 2023: Peaks-Over-Threshold-Based Regional Flood Frequency Analysis Using Regularised Linear Models. *Water* 15. <https://doi.org/10.3390/w15213808>
- Petrović, A.M., Leščešen, I., and Radevski, I., 2024: Unveiling Torrential Flood Dynamics: A Comprehensive Study of Spatio-Temporal Patterns in the Šumadija Region, Serbia. *Water* 16. <https://doi.org/10.3390/w16070991>
- Samantaray, S., and Sahoo, A., 2020: Estimation of flood frequency using statistical method: Mahanadi River basin, India. *H2Open J.* 3, 189–207. <https://doi.org/10.2166/h2oj.2020.004>
- Šraj, M., Viglione, A., Parajka, J., and Blöschl, G., 2016: The influence of non-stationarity in extreme hydrological events on flood frequency estimation. *J. Hydrol. Hydromech.* 64, 426–437. <https://doi.org/10.1515/johh-2016-0032>
- Snizhko, S., Bertola, M., Ovcharuk, V., Shevchenko, O., Didovets, I., and Blöschl, G., 2023: Climate impact on flood changes – an Austrian-Ukrainian comparison. *J. Hydrol. Hydromech.* 71, 271–282. <https://doi.org/10.2478/johh-2023-0017>
- Steinhausen, M., Paprotny, D., Dottori, F., Sairam, N., Mentaschi, L., Alfieri, L., Lüdtke, S., Kreibich, H., and Schröter, K., 2022: Drivers of future fluvial flood risk change for residential buildings in Europe. *Glob. Environ. Change* 76. <https://doi.org/10.1016/j.gloenvcha.2022.102559>
- Tramblay, Y., Arnaud, P., Artigue, G., Lang, M., Paquet, E., Neppel, L., and Sauquet, E., 2023: Changes in Mediterranean flood processes and seasonality *Hydrol. Earth Syst. Sci.* 27, 2973–2987. <https://doi.org/10.5194/hess-27-2973-2023>
- Trobec, T., 2017: Frequency and seasonality of flash floods in Slovenia. *Geogr. Pannonica* 21, 198–211. <https://doi.org/10.5937/gp21-16074>
- Ul Hassan, M., Hayat, O., and Noreen, Z., 2019: Selecting the best probability distribution for at-site flood frequency analysis; a study of Torne River. *SN Appl. Sci.* 1, 1–10. <https://doi.org/10.1007/s42452-019-1584-z>
- Zabret, K. and Brilly, M., 2014: Hydrological regionalisation of flood frequency analyses in Slovenia. *Acta hydrotech.* 27, 139–156. <https://actahydrotechnica.fgg.uni-lj.si/paper/a47kz.pdf>
- Zorzetto, E., Botter, G., and Marani, M., 2016: On the emergence of rainfall extremes from ordinary events. *Geophys. Res. Lett.* 43, 8076–8082. <https://doi.org/10.1002/2016GL069445>

IDŐJÁRÁS

Quarterly Journal of the HungaroMet Hungarian Meteorological Service
Vol. 129, No. 2, April – June, 2025, pp. 177–191

Examination of ERA5 thermodynamic profiles and hodographs in the pre-storm environment of severe thunderstorms producing large hail in Hungary between 2019 and 2023

Kornél Komjáti^{*,1,2,3}, Kálmán Csirmaz^{1,3}, and Hajnalka Breuer²

¹*HungaroMet Hungarian Meteorological Service,
Budapest H-1024, Kitaibel Pál u. 1, Hungary*

²*ELTE Eötvös Loránd University Institute of Geography and Earth Sciences
Department of Meteorology,
Budapest H-1117, Pázmány Péter sétány 1/A, Hungary*

³*Hungarian Association of Stormchasers and Storm Damage Surveyors
Budapest H-1139, Fiastyúk u. 57. 3/3., Hungary*

**Corresponding Author email: komjati.k@met.hu*

(Manuscript received in final form June24, 2024)

Abstract— Validated hail observations are available from the hail suppression system operated by the National Chamber of Agriculture since 2019. Using this dataset, large hail (larger than a walnut) reports were collected from recent years. The environments of hail-producing thunderstorms were reconstructed upon ERA5 reanalysis data, and characteristics were sought between thermodynamic profiles and hodographs that could help recognize the environmental conditions for potentially large hail-producing thunderstorms. During the investigation, 52 cases over a total of 35 days were examined. Although the number of cases did not allow for statistical conclusions, the authors identified similarities among the cases through ensemble sounding and hodograph analysis, which could serve as useful operational tools for forecasters.

Key-words: large hail, sounding, hodograph, supercell

1. Introduction

In Europe and globally, large hail causes significant damage every year (Changnon *et al.*, 2009; Allen *et al.*, 2020; Taszarek *et al.*, 2020), and has a serious economic impact, as well (Púčík *et al.*, 2019). Recent research indicates a growing trend in the occurrence of large hail both in the United States and in Europe (Battaglioli *et al.*, 2023). However, it is difficult to establish global criteria for the environmental conditions necessary for the formation of large hail due to the strong influence of mesoscale processes unique to a region (i.e., low-level jet shear-initiated tornado formation is rare in Europe, due to topography) (Taszarek *et al.*, 2023a).

Investigating the conditions for the formation of large hail poses a significant challenge, as models are limited by microphysical schemes, even in high-resolution simulations (Dennis and Kumjian, 2017; Martius *et al.*, 2018; Raupach *et al.*, 2021). Nevertheless, some features as indicators for large hail have been recognized in past studies. Large near-surface storm-relative inflow contributes to the development of wider updrafts (Peters *et al.*, 2019, 2020), promoting longer residence times of hailstones, although excessively strong storm-relative winds can also be detrimental to hail growth (Kumjian and Lombardo, 2020; Kumjian *et al.*, 2023). Furthermore, the examination of storm-relative hodographs has come to the forefront, namely a straighter hodograph can indicate more prolific hail production in supercells (Kumjian *et al.*, 2021; Nixon and Allen, 2022). However, only from kinematic properties, it cannot be determined whether there is potential for large hail; a proper balance of instability, shear, and relative humidity is needed for their formation (Nixon *et al.*, 2023). Analyzing major hailstorm events in Europe between 2021 and 2022, it was found that it is important for about 65% of CAPE to be positioned below the $-10\text{ }^{\circ}\text{C}$ layer, and these events were also characterized by relatively straight shear profile: sharp wind shift in the inflow layer, and straight, elongated hodograph shape between 1 and 3 km (Púčík *et al.*, 2023a). Furthermore, it was found that cell mergers (Wurman *et al.*, 2007; Komjáti *et al.*, 2023; Púčík *et al.*, 2023a, 2023b; Piasecki *et al.*, 2023) and boundary interactions can also intensify storm severity (Maddox *et al.*, 1980, Markowski *et al.*, 1998, Magee and Davenport, 2020; Púčík *et al.*, 2023b). Numerous researches have shown in the past decades that severe hailstorms occur regularly in the Carpathian Basin, these are based on either observations (Horváth and Geresdi, 2001; 2003) or model simulations (Horváth *et al.*, 2006; 2009; Csirmaz, 2015). All of these studies relate the largest hailstone events to supercell convection but did not provide approaches to assess the specific atmospheric background conditions necessary for very large hail which could then be applied in the operational forecasting workflow.

In this paper, we selected cases characterized by observed damaging hail (walnuts or eggs-sized hail, these categories cover the size range above 3 cm) recorded in the National Chamber of Agriculture (NAK) hail observation

database. Ensemble thermodynamic diagrams and hodographs were prepared using ERA5 reanalysis data provided by the ECMWF (European Centre for Medium-Range Weather Forecasts) integrated forecast system. Despite the relatively small number of cases, distinctive patterns are discernible, which confirm the conclusions based mostly on previous numerical simulation studies presented above. The results are detailed in Section 3.

2. Methodology

For the analysis, we relied on the hail observation data from the NAK, which were reported by generator operators of the hail suppression system, specifying the size of fallen hailstones (wheat, pea, cherry, walnut, egg-sized hail) and the location of each observation (longitude and latitude of the town where the observation took place). The system has been operational in Hungary since 2018, and meteorologist-validated data (hail observations compared against radar data) have been available at HungaroMet since 2019. In this study, we examined weather events where damaging hail has fallen. For this, we analyzed cases falling into the top two categories of the available size-category system (walnuts and eggs-sized hail). These two sizes of hail were uniformly called large hail in this study. The observation period spanned from the 15th of April to the 30th of September every year, and we considered a five-year interval which yielded a total of 35 days characterized by large hail size. Naturally, multiple hail observations were associated with a given day, resulting in a total of 52 cases available for analysis. The authors considered that if there were several large hail observations on a given day (which may also result from the inconsistency of the detection system), then the environment associated with each observation should be examined. As a result, those weather situations where several large hail-producing cells have formed dominate the statistics to an extent in this study. ERA5 data were used for the investigation, namely, to find qualitative relationships between the background conditions provided by the dataset and the hail size produced by storms formed in these environments. The ERA5 reanalyses, according to research in recent years, are considered as one of the most reliable reanalysis datasets (*Li et al.*, 2020; *Taszarek et al.*, 2020, 2021; *Coffer et al.*, 2020), and developed by the ECMWF is available from 1940 to the present, with an hourly frequency, a horizontal grid resolution of $0.25^\circ \times 0.25^\circ$ degrees, and a total of 137 model levels.

Data selection was based on ERA5 grid points closest to observation sites, and the time was chosen to be the nearest hour preceding the observation, thus representing a possible environment for storms producing large hail. Python programs were developed to process the data, and the SHARPPy (v1.4.0b1) software was applied for displaying soundings and hodographs (*Blumberg et al.*, 2017). A composite hodograph was also created from the u and v wind

components of ERA5 data, using the 75th percentiles of the datasets at each given level in order to examine the vertical wind profile from a storm-relative perspective. For visualization, the Sam Brandt Hodograph Plotter [1 – GitHub] was utilized, and a relative vertical wind profile was created for the right-moving cell (conclusions drawn from left-moving cells were similar). To determine the storm-relative winds, we shifted the coordinate system to the endpoint of the storm motion vector. Consequently, this location became the reference point (origin), rendering the storm motion vector to be represented as 0. From this point, we recalculated the environmental winds for creating the storm-relative hodograph.

In order to confirm the results extracted from 52 cases, we evaluated them in six additional case studies. Among these six cases, we provide a more detailed presentation of June 12, 2018 (Section 3.3), with the results from the other 5 cases presented in the Appendix section (Appendix A1-A5). ERA5 data were obtained from the nearest grid point to these observations, and displayed on the rawinsonde.com website [2 – Rawinsonde] (Taszarek *et al.*, 2023b).

3. Results

3.1. Ensemble of ERA5 sounding

Having examined the ensemble of sounding data, we found some characteristics that may generally promote the formation of large hail (*Fig. 1*). Our first observation was that in the near-surface layer (up to approximately 850 hPa), the ensemble of the analysis profiles exhibited greater spread, indicating that large hail-producing thunderstorms can also occur in a relatively drier environment near the surface as opposed to the expected relatively moist environment. The mean dewpoint deficit on the lowest level was 6.3 °C, and the 75th percentile of the dewpoint deficit was 9.4 °C. In drier cases, only air parcels driven by strong forcing mechanisms could reach the lifting condensation level, thereby promoting the formation of fewer but more intense cells with wider updrafts (Mulholland *et al.*, 2021). Secondly, in this layer (particularly in the lower few hundred meters), northerly winds dominated in most cases, which could have facilitated surface drying. Our next observation was that between 850 and 700 hPa (at the approximate top of the inflow layer – Thompson *et al.*, 2007) the ensemble of the dew point profiles was close to the temperature profiles (reduced spreading), indicating a relatively humid environment in this layer in the cases under study. The mean dewpoint deficit was 2.4 °C and the 75th percentile of the dewpoint values reached 7.0 °C in this layer. Moistening at the top of the inflow layer could have aided in the rapid growth of hailstones (Kumjian *et al.*, 2021). In the mid-troposphere, the ensemble of profiles again exhibited greater spread, with cases where a strong mid-level drying characterized the environment (mean dewpoint deficit = 10.9 °C, and the 75th percentile of the dewpoint deficit = 16.3 °C at 500 hPa). So, large hail

formed by rather varied moisture and CAPE profiles, very similarly to the results found by *Nixon et al.* (2023). Furthermore, mid-level dryness – if it is not too large to suppress convection - can enhance downdraft, which will create stronger cold pools, thus increasing secondary convection and formation of more graupel particles that can affect hail formation (*Miao and Yang, 2022*).

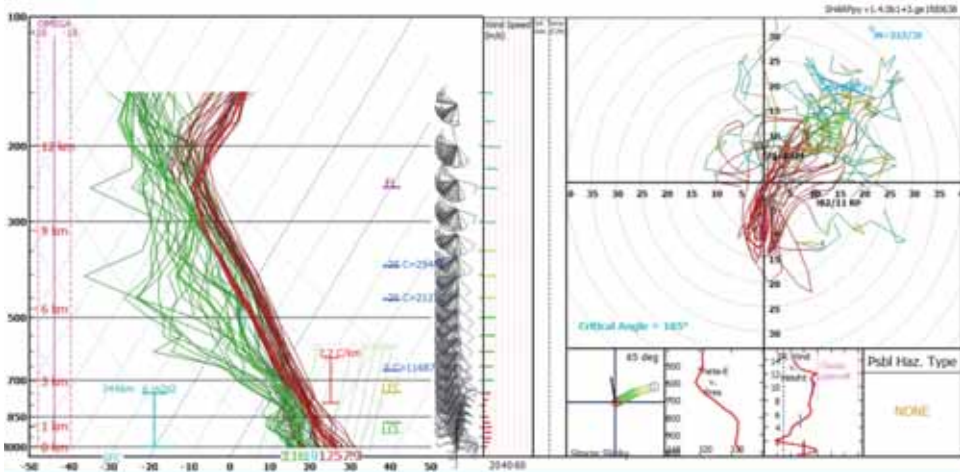


Fig. 1. Ensemble sounding and hodograph based on large hail cases between 2018 and 2023 in Hungary. On the thermodynamic diagram (left panel), the red lines indicate the temperature profiles and the green lines depict the dew point profile. The colors of the hodograph sections represent different layers (red: 0–3 km; green: 3–6 km; yellow: 6–9 km; cyan: 9–15 km). The bold lines represent the first date of the dataset. For the interpretation of the insets, see the help (*Blumberg et al., 2017*).

Examining the ensemble hodograph, we found that northerly winds dominated in the near-surface layer (as shown in the skew-T diagrams), and then the wind quickly veered (turned counterclockwise) within the lowest 1 km layer, followed by typically straight hodograph shape in the upper levels. To further analyze the hodographs, we created a composite storm-relative hodograph representing the 75th percentile of the u and v components of the datasets at each given level. The results are discussed in the following section.

3.2. Composite hodograph

The shape of the obtained storm-relative composite hodograph exhibits similarities with hodographs presented in previous studies (*Nixon and Allen, 2022; Kumjian et al., 2023; Púčik et al., 2023*) (*Fig. 2*). The main similarity lies in the weaker 0–1 km wind shear (based on the presented articles, strong wind shear in the 0–1 km layer is more typical of tornado cases), as well as the elongated and

relatively straight hodograph observed especially between 1 and 3 km. However, it is interesting to note that a dominant northerly wind component appears below 500 m, which quickly veers with height within the inflow layer. The vorticity induced by wind shear in this layer is relatively large and streamwise for right-moving supercells (500 m mean streamwise vorticity = 0.009 s^{-1}). Therefore, this sharp wind shift could provide the necessary helical updrafts in the inflow layer, which could be important for supercells producing large hail. It remains unclear from the results whether a northerly wind component near the surface is a necessary criterion. In this layer, a relatively high ($\sim 15 \text{ ms}^{-1}$) storm-relative inflow was apparent, which facilitated the development of wide updrafts (Peters *et al.*, 2019; 2020). However, storm-relative winds decreased with height, and weak storm-relative winds were observed in the hail growth zone. Despite the low number of cases, characteristics that appeared on the composite hodograph are corroborated by the results of the aforementioned previous studies.

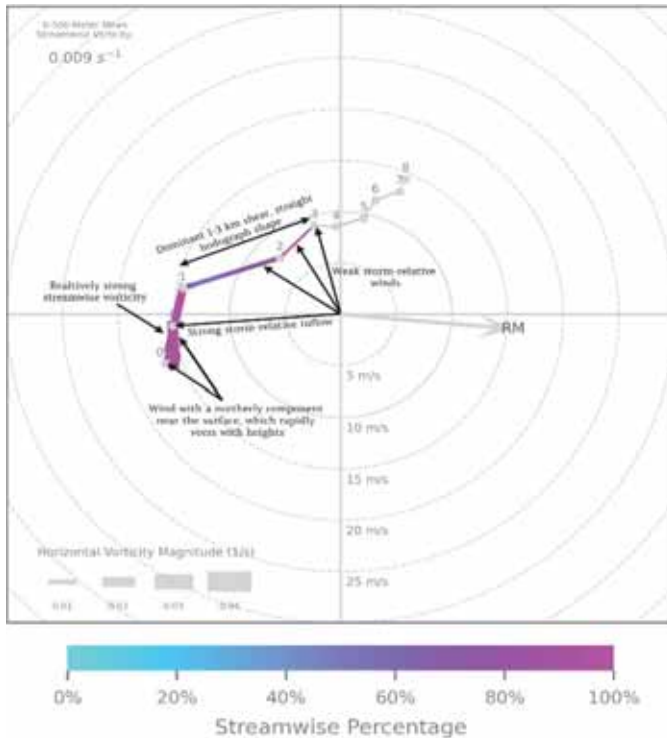


Fig. 2. Composite storm-relative hodograph created from the 75th percentile of the u and v components of each given level. The thickness of the hodograph represents the horizontal vorticity magnitude generated by the vertical wind shear, and the colors depict the streamwiseness of the horizontal vorticity relative to the inflow. The gray arrow represents the original storm motion for the right-moving (RM) supercell.

3.3. Archive case of 12 June 2018

Radiosondes are launched at 0000 and 1200 UTC every day. In Hungary, the launches take place in Budapest and Szeged (situated 170 km distance apart), making it very difficult to validate the conclusions drawn from reanalysis with measurement data. In the absence of proper proximity soundings, we present some cases from the period preceding the start of the NAK data collection period (i.e., before 2019), where large hail was reported by eyewitnesses, and nearby ERA5 soundings and hodographs are presented, generated by the rawinsonde.com website from the grid points closest to the observation location.

On June 12, 2018, an elongated frontal zone approached the Carpathian Basin from the west, with a warm, moist, unstable air mass accumulating in the warm sector. The most favorable conditions for thunderstorm development were primarily in the northwestern and northeastern thirds of the country. A small cluster of thunderstorms reached the Hungarian border from Austria at 1200 UTC (*Fig. 3a*), with its outflow gradually spreading southward and southeastward (*Fig. 3b*). Along the outflow boundary at 1430 UTC, new storms initiated (*Fig. 3c*), and developed into supercells as they moved along the boundary (*Fig. 3d*).

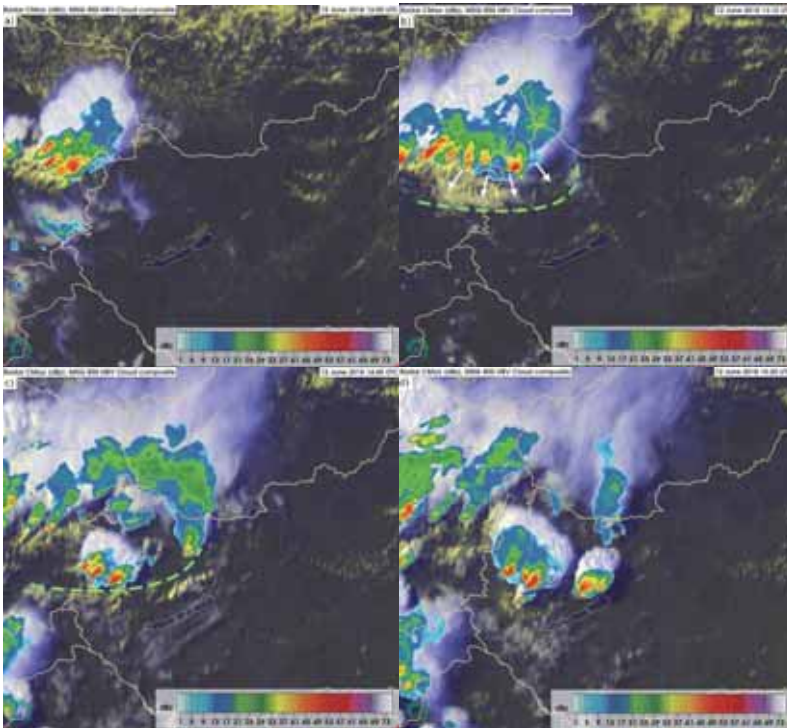


Fig. 3. The outflow boundary (dashed green line) initiated new supercells (depicted by column maximum radar reflectivity field) overlaid on visible spectrum satellite images on 12 June 2018 between 1200 and 1520 UTC (a–d). The white arrows represent the outflow motion of the boundary.

Due to the outflow boundary, northern winds dominated near the surface, but this was limited only to a shallow layer. The wind profile quickly veered due to warm air advection, and we found a relatively straight, elongated hodograph shape, especially in the 1–3 km layer (*Fig. 4*). The characteristics consistent with the above-mentioned results (*Fig. 1*) are evident in both the thermodynamic profile and the hodograph. Namely: a dry layer near the surface, moistening at the top of the inflow layer, mid-level dry conditions, a significant portion of CAPE located below the $-10\text{ }^{\circ}\text{C}$ layer, northerly and veering winds near the surface, strong ($\sim 15\text{ ms}^{-1}$) storm-relative inflow, streamwise vorticity in the inflow layer, relatively straight hodograph, and small storm-relative winds in the hail growth zone (approximately the $-10\text{ }^{\circ}\text{C}$ to $-30\text{ }^{\circ}\text{C}$ layer).

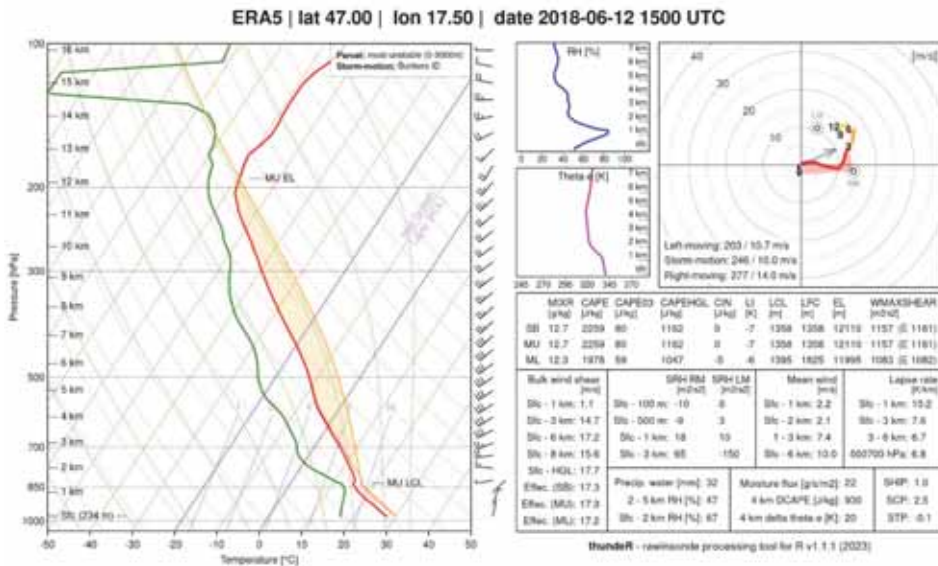


Fig. 4. ERA5 sounding and hodograph for June 12, 2018, at 1500 UTC generated by rawinsonde.com webpage. The red line on the left panel represents the environmental temperature profile, and the green line depicts the dew point profile. The yellow shaded area represents the total amount of potential energy available to the most unstable air parcel. The wind barbs show the environmental wind at each given level. The colors of the hodograph (right top panel) represent different layers (purple: 0–1 km; red: 1–3 km; orange: 3–6 km; yellow: 6–9 km; cyan: 9–12 km). The gray arrow depicts the mean motion vector, the empty circles represent the motion direction for right-mover (RM) and left-mover (LM) supercells. For the interpretation of the insets, see the help on the rawinsonde.com webpage.

Based on observations, large hail was also reported in Ajka (Veszprém county) on the Köpönyeg.hu Facebook page [3 – Köpönyeg.hu] produced by a supercell (*Fig. 5*). According to the ESSL (European Severe Storms Laboratory) observation guide [4 – ESSL], the largest hailstone could have reached a diameter of 4–5 cm.



Fig. 5. Large hail observation from a supercell on June 12, 2018 around 1600 UTC.

4. Conclusion

In this study, we examined thunderstorms that produced large hail. We investigated the environmental characteristics of the storms using ERA5 data and attempted to find similarities in the thermodynamic and kinematic characteristics of each case. Based on the ensemble diagrams (*Fig. 1*) and the hodograph created from the 75th percentile of the dataset (*Fig. 2*), we found the following characteristics in the environment of thunderstorms producing large hail:

- Large hail can form by various moisture profiles, and a considerable portion of the cases is characterized by mid-level dryness and an inverted V profile near the ground (high cloud base) with an average 6.3 °C dew point deficit.

The 75th percentile of the dew point deficit was 9.4 °C, and the 25th percentile of the dewpoint deficit was 3.1 °C near the surface.

- A significant portion (~60%, similar to *Púčik et al.*, 2023b) of CAPE is generated below the -10°C layer (more than 50% of the cases).
- Strong storm-relative inflow (~15 ms⁻¹) near the surface (more than 60% of the cases).
- Sufficiently large (>15 m/s) 0–6 km vertical wind shear (more than 80% of the cases).
- Typically northerly winds near the surface, which quickly veer in the lowest 1 km (more than 50% of the cases)
- Strong streamwise environmental vorticity in the lowest 500 m (mean streamwise vorticity = 0.009 s⁻¹)
- Straight 1–3 km hodograph profile, weak winds at the top of the inflow layer relative to the storm (more than 80% of the cases).

However, these conclusions were based on a small number of cases, and although most of the results can be supported by previous studies, significantly more data would be needed to strengthen these results. It must be further emphasized that there can be cases where not all the conditions have to be fulfilled for large hail formation, as the cases were specifically selected when damaging hail occurred. Although the aforementioned criteria can be good indicators for their timely recognition, thus aiding the public warning system.

The ERA5 data only allowed the examination of environmental kinematic and thermodynamic characteristics, however, the authors would like to emphasize that cloud microphysical processes and PBL characteristics also play an important role in the formation of large hail. Our future plans include a comparison of the results of large hail events with those cases where only smaller hailstones were observed. In addition, it may be worthwhile to expand the dataset with cherry-sized hail (>2 cm) detections, thus a larger data set would be available to determine stronger results. Furthermore, it is worth noting upon the case of 12 June 2018, that small-scale processes or weather objects (in that specific case: an outflow boundary) can also contribute to the intensification of thunderstorms. These processes may not necessarily appear in NWP model forecasts and especially not in reanalyses and thus are not visible in the preliminary environment either.

Acknowledgments: The authors are grateful to the HungaroMet Hungarian Meteorological Service for making the data available for research. We are also grateful to our colleague András Imre Vaszkó for assistance in exploring archival cases. Hajnalka Breuer was supported by the Hungarian Scientific Research Fund under the grant FK132014. The research was supported by the DIMOP_PLUSZ-2.3.1-23-2023-00001 "Developing an environmental monitoring system using installed data collection network and creating a climate data repository with associated service environment" Project, implemented by HungaroMet Hungarian Meteorological Service.

References

- Allen, J.T., Giammanco, I.M., Kumjian, M.R., Punge, H.J., Zhang, Q., Groenemeijer P., Kunz, M., and Ortega, K., 2020: Understanding hail in the Earth system. *Rev. Geophys.* 58, e2019RG000665. <https://doi.org/10.1029/2019RG000665>
- Battaglioli, F., Groenemeijer, P., Púčik, T., Taszarek, M., Ulbrich, U., and Rust, H., 2023: Modeled Multidecadal Trends of Lightning and (Very) Large Hail in Europe and North America (1950–2021). *J. Appl. Meteorol. Clim.* 62, 1627–1653. <https://doi.org/10.1175/JAMC-D-22-0195.1>
- Blumberg, W.G., Halbert, K.T., Supinie, T.A., Marsh, P.T., Thompson, R.L., and Hart, J.A., 2017: SHARPy: An Open-Source Sounding Analysis Toolkit for the Atmospheric Sciences, *Bulletin of the American Meteorological Society*, 98(8), 1625–1636. <https://doi.org/10.1175/BAMS-D-15-00309.1>
- Changnon, S., Changnon, D., and Hilberg, S.D., 2009: Hailstorms across the nation: An atlas about hail and its damages. *Illinois State Water Survey Contract Rep.* 2009(12), 92.
- Coffer, B.E., Taszarek, M., and Parker, M.D., 2020: Near-Ground Wind Profiles of Tornadoic and Nontornadoic Environments in the United States and Europe from ERA5 Reanalyses. *Wea. Forecast.* 35, 2621–2638. <https://doi.org/10.1175/WAF-D-20-0153.1>
- Csirmaz, K., 2015: A new hail size forecasting technique by using numerical modeling of hailstorms: A case study in Hungary. *Időjárás* 119, 443–474.
- Dennis, E.J. and Kumjian, M.R., 2017: The impact of vertical wind shear on hail growth in simulated supercells. *J. Atmos. Sci.* 74, 641–663. <https://doi.org/10.1175/JAS-D-16-0066.1>
- Horváth, Á. and Geresdi, I., 2001: Severe convective storms and associated phenomena in Hungary. *Atmos. Res.* 56, 127–146. [https://doi.org/10.1016/S0169-8095\(00\)00094-6](https://doi.org/10.1016/S0169-8095(00)00094-6)
- Horváth, Á. and Geresdi, I., 2003: Severe storms and nowcasting in the Carpathian basin. *Atmos. Res.* 67–68, 319–332. [https://doi.org/10.1016/S0169-8095\(03\)00065-6](https://doi.org/10.1016/S0169-8095(03)00065-6)
- Horváth, Á., Geresdi, I., and Csirmaz, K., 2006: Numerical simulation of a tornado producing thunderstorm: a case study. *Időjárás* 110, 279–297.
- Horváth, Á., Geresdi, I., Németh, P., Csirmaz, K., and Dombai, F., 2009: Numerical modeling of severe convective storms occurring in the Carpathian Basin. *Atmos. Res.* 93, 221–237. [10.1016/j.atmosres.2008.10.019](https://doi.org/10.1016/j.atmosres.2008.10.019)
- Komjáti, K., Csirmaz, K., Breuer, H., Kurcsics, M., and Horváth, Á., 2023: Supercell interactions with surface baroclinic zones in the Carpathian Basin, 11th European Conference on Severe Storms, Bucharest, Romania, 8–12 May 2023, ECSS2023-39. <https://doi.org/10.5194/ecss2023-39>
- Kumjian, M.R. and Lombardo, K., 2020: A hail growth trajectory model for exploring the environmental controls on hail size: Model physics and idealized tests. *J. Atmos. Sci.* 77, 2765–2791. <https://doi.org/10.1175/JAS-D-20-0016.1>
- Kumjian, M.R., Lombardo, K., and Loeffler, S., 2021: The evolution of hail production in simulated supercell storms. *J. Atmos. Sci.* 78, 3417–3440. <https://doi.org/10.1175/JAS-D-21-0034.1>
- Kumjian, M., Lombardo, K., Nixon, C., and Allen, J., 2023: Does Low-level Vertical Wind Shear Matter for Hail Production? 11th European Conference on Severe Storms, Bucharest, Romania, 8–12 May 2023, ECSS2023-91. <https://doi.org/10.5194/ecss2023-91>
- Li, F., Chavas, D.R., Reed, K.A., and Dawson II, D.T., 2020: Climatology of Severe Local Storm Environments and Synoptic-Scale Features over North America in ERA5 Reanalysis and CAM6 Simulation. *J. Climat.* 33, 8339–8365. <https://doi.org/10.1175/JCLI-D-19-0986.1>
- Maddox, R.A., Hoxit, L.R., and Chappell, C.F., 1980: A study of tornadoic thunderstorm interactions with thermal boundaries. *Mon. Weather Rev.* 108, 322–336. [https://dx.doi.org/doi:10.1175/1520-0493\(1980\)108%3C0322:ASOTTI%3E2.0.CO;2](https://dx.doi.org/doi:10.1175/1520-0493(1980)108%3C0322:ASOTTI%3E2.0.CO;2)
- Magee, K.M. and Davenport, C.E., 2020: An observational analysis quantifying the distance of supercell-boundary interactions in the great plains. *J. Operat. Meteor.* 8(2), 15–38. <https://doi.org/10.15191/nwajom.2020.0802>
- Markowski, P.M., Rasmussen, E.N., and Straka, J.M., 1998: The occurrence of tornadoes in supercells interacting with boundaries during VORTEX-95. *Wea. Forecasting* 13, 852–859. [https://doi.org/10.1175/1520-0434\(1998\)013%3C0852:TOOTIS%3E2.0.CO;2](https://doi.org/10.1175/1520-0434(1998)013%3C0852:TOOTIS%3E2.0.CO;2)

- Martius, O., Hering, A., Kunz, M., Manzato, A., Mohr, S., Nisi, L., and Trefalt, S., 2018: Challenges and recent advances in hail research. *Bull. Amer. Meteorol. Soc.*, 99, ES51–ES54. <https://doi.org/10.1175/BAMS-D-17-0207.1>
- Miao, J. and Yang, M., 2022: The impacts of mid-level moisture on the structure, evolution and precipitation of afternoon thunderstorms: A real-case modeling study at Taipei on 14 June 2015. *J. Atmos. Sci.* 98, 129–152. <https://doi.org/10.1175/JAS-D-21-0257.1>
- Mulholland, J.P., Peters, J.M., and Morrison, H., 2021: How Does LCL Height Influence Deep Convective Updraft Width? *Geophys. Res. Lett.* 48, e2021GL093316. <https://doi.org/10.1029/2021GL093316>
- Nixon, C.J. and Allen, J.T., 2022: Distinguishing between hodographs of severe hail and tornadoes. *Wea. Forecasting* 37, 1761–1782. <https://doi.org/10.1175/WAF-D-21-0136.1>
- Nixon, C.J., Allen, J.T., and Taszarek, M., 2023: Hodographs and Skew Ts of Hail-Producing Storms. *Wea. Forecasting* 38, 2217–2236. <https://doi.org/10.1175/WAF-D-23-0031.1>
- Peters, J.M., Nowotarski, C.J., and Morrison, H., 2019: The role of vertical wind shear in modulating maximum supercell updraft velocities. *J. Atmos. Sci.*, 76, 3169–3189. <https://doi.org/10.1175/JAS-D-19-0096.1>
- Peters, J.M., Nowotarski, C.J., Mulholland, J.P., and Thompson, R.L., 2020: The influences of effective inflow layer streamwise vorticity and storm-relative flow on supercell updraft properties. *J. Atmos. Sci.* 77, 3033–3057. <https://doi.org/10.1175/JAS-D-19-0355.1>
- Piasecki, K., Matczak, P., Taszarek, M., Czernecki, B., Skop, F., and Sobisiak, A., 2023: Giant hail in Poland produced by a supercell merger in extreme instability – A sign of a warming climate? *Atmos. Res.* 292. <https://doi.org/10.1016/j.atmosres.2023.106843>
- Púčik, T., Castellano, C., Groenemeijer, P., Kühne, T., Rädler, A. T., Antonescu, B., and Faust, E., 2019: Large hail incidence and its economic and societal impacts across Europe. *Mon. Weather Rev.* 147, 3901–3916. <https://doi.org/10.1175/MWR-D-19-0204.1>
- Púčik, T., Groenemeijer, P., Singer, M., Ryva, D., Stanek, M., Pistotnik, G., Kaltenberger, R., and Holzer, A., 2023a: Damage survey, environment and storm-scale evolution of the giant hail and F4 tornado producing supercell on 24 June 2021, 11th European Conference on Severe Storms, Bucharest, Romania, 8–12 May 2023, ECSS2023-143. <https://doi.org/10.5194/ecss2023-143>
- Púčik, T., Groenemeijer, P., Taszarek, M., and Battaglioli, F., 2023b: Pre-storm environments and storm-scale properties of the major hailstorms of 2021 and 2022 in Europe., 11th European Conference on Severe Storms, Bucharest, Romania, 8–12 May 2023, ECSS2023-124. <https://doi.org/10.5194/ecss2023-124>
- Raupach, T.H., Martius, O., Allen, J.T., Kunz, M., Lasher-Trapp, S., Mohr, S., Rasmussen, K.L., Trapp, R.J., and Zhang, Q., 2021: The effects of climate change on hailstorms. *Nat. Rev. Earth Environ.* 2, 213–226. <http://dx.doi.org/10.1038/s43017-020-00133-9>
- Taszarek, M., Allen, J.T., Púčik, T., Hoogewind, K.A., and Brooks, H.E., 2020: Severe Convective Storms across Europe and the United States. Part II: ERA5 Environments Associated with Lightning, Large Hail, Severe Wind, and Tornadoes. *J. Climat.* 33, 10263–10286. <https://doi.org/10.1175/JCLI-D-20-0346.1>
- Taszarek, M., Pilguy, N., Allen, J.T., Gensini, V., Brooks, H.E., and Szuster, P., 2021: Comparison of Convective Parameters Derived from ERA5 and MERRA-2 with Rawinsonde Data over Europe and North America. *J. Climat.* 34, 3211–3237. <http://dx.doi.org/10.1175/JCLI-D-20-0484.1>
- Taszarek, M., Allen, J., Nixon, C., Dowdy, A., and Battaglioli, F., 2023a: Do severe storms across Australia, Europe and the United States share similarities? A comparison of atmospheric profiles and environmental predictors, 11th European Conference on Severe Storms, Bucharest, Romania, 8–12 May 2023, ECSS2023-25. <https://doi.org/10.5194/ecss2023-25>
- Taszarek, M., Czernecki, B., and Szuster, P., 2023b: thundeR - a rawinsonde package for processing convective parameters and visualizing atmospheric profiles, 11th European Conference on Severe Storms, Bucharest, Romania, 8–12 May 2023, ECSS2023-28. <https://doi.org/10.5194/ecss2023-28>
- Thompson, R.L., Mead, C.M., and Edwards, R., 2007: Effective storm-relative helicity and bulk shear in supercell thunderstorm environments. *Wea. Forecasting* 22, 102–115. <https://doi.org/10.1175/WAF969.1>

Wurman, J., Richardson, Y., Alexander, C., Weygandt, S., and Zhang, P.F., 2007: Dual-Doppler and single-Doppler analysis of a tornadic storm undergoing mergers and repeated tornadogenesis. *Mon. Weather Rev.* 135, 736–758, <https://doi.org/10.1175/MWR3276.1>

Online sources:

[1 – GitHub] <https://github.com/SamBrandtMeteo/Storm-Relative-Hodograph-Plotter>

[2 – Rawinsonde] http://rawinsonde.com/ERA5_Europe/

[3 – Köpönyeg.hu]

<https://www.facebook.com/photo/?fbid=10156507851324312&set=a.473986179311>

[4 – ESSL] https://www.essl.org/cms/wp-content/uploads/ESSL_hail_size_comparisons.pdf

Appendix

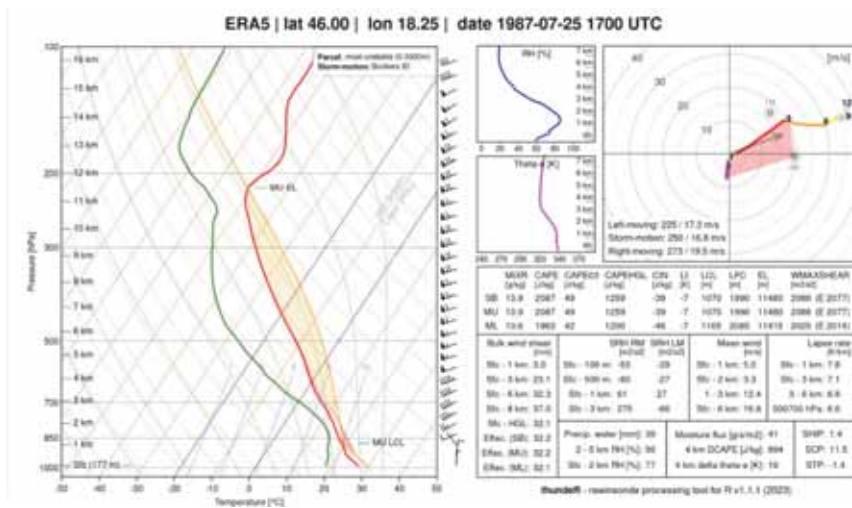


Fig. A1. Same as Fig. 4, but at 1700 UTC on July 25, 1987.

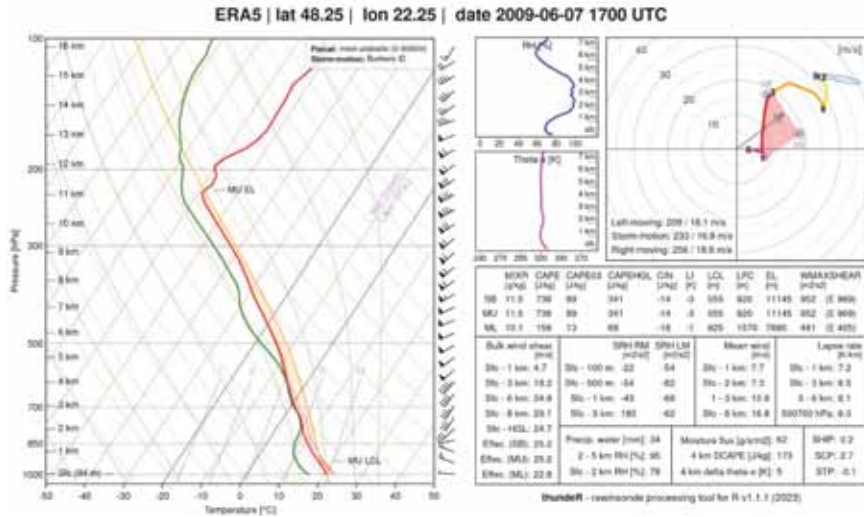


Fig. A2. Same as Fig. 4, but at 1700 UTC on June 7, 2009.

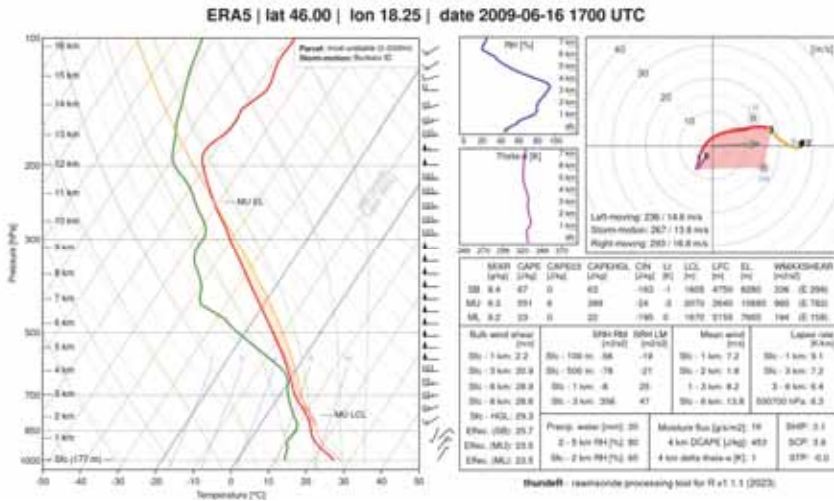


Fig. A3. Same as Fig. 4, but at 1700 UTC on June 16, 2009.

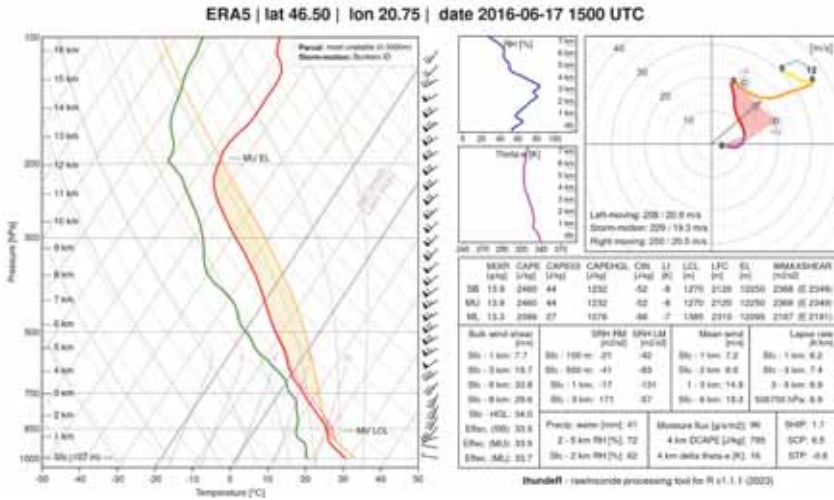


Fig. A4. Same as Fig. 4, but at 1500 UTC on June 17, 2016.

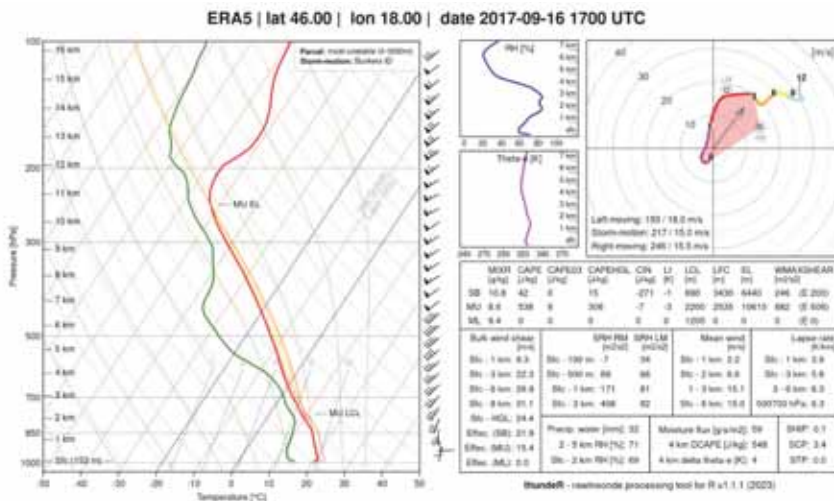


Fig. A5. Same as Fig. 4, but at 1700 UTC on September 16, 2017.

IDŐJÁRÁS

*Quarterly Journal of the HungaroMet Hungarian Meteorological Service
Vol. 129, No. 2, April – June, 2025, pp. 193–200*

Evaluation of long-term temporal variations in Hungarian PM₁₀ and PM_{2.5} emissions based on national inventories applied for air quality management

Krisztina Labancz^{1,*}, László Bozó^{1,2}, and Gábor Kis-Kovács¹

¹*HungaroMet Hungarian Meteorological Service
Kitaibel Pál str. 1., 1024 Budapest, Hungary*

²*Hungarian University of Agriculture and Life Sciences
Institute of Environmental Sciences, Hungary*

**Corresponding Author email: labancz.k@met.hu*

(Manuscript received in final form March 25, 2025)

Abstract—Accession to the European Union has resulted in a remarkable step forward in air quality protection in Hungary. At present, particulate matter means the most significant environmental health risk, and it is Hungary's most problematic pollutant: its concentration exceeds the EU limit values for longer periods under certain conditions. It is presented how the rates and contributors of the PM₁₀ and PM_{2.5} emissions varied in Hungary during the two decades of the 2000–2021 period. Special attention is paid to the residential combustion sector which is a key category in particulate matter emissions. Price elasticity of demand of natural gas and other fuels are investigated together with the latest comprehensive population census on conventional stoves and boilers used in the Hungarian households to determine the possible measures that could be taken to improve and change the residential heating habits.

Key-words: air quality measures, particulate matter emissions, residential combustion, heating habits, Hungary.

1. Introduction

Accession to the European Union has resulted in a significant step forward in air quality protection in Hungary. Industrial emission and pollution related electricity and heat production have been significantly reduced. Consequently, residential solid fuel combustion, transport, agriculture, and illegal waste combustion have become the most significant emission sources (e.g., European Environment Agency, 2023).

In Hungary, three important factors have essential effects on PM concentrations: local anthropogenic emissions, long-range transboundary transport and meteorological conditions (Ferenczi *et al.*, 2021). Compiling national emission inventories based on comparable international standards of UN and EU is a basic associated tool for harmonizing model estimations on the level of air pollution and rate of deposition. Further, it can contribute to evaluate the risks for human health and ecosystems (Przybysz *et al.*, 2014; Simon *et al.*, 2020). Among pollutants of anthropogenic origin, PM₁₀ and PM_{2.5} play a distinguished role in many European countries.

2. Trend of PM emissions in the Hungarian inventory

Particulate matter (PM) is the general term used to describe solid particles and liquid droplets suspended in the air. The chemical composition and size of these airborne particles vary widely. Four types of particles should be reported in the inventory: TSP (total suspended material, i.e. the mass concentration of particulate matter), PM₁₀, PM_{2.5}, and BC (black carbon).

Small aerosol particles, especially black carbon, play an important role in the formation of smog. In winter, in addition to sulfur-dioxide, one of the characteristic components of smog during the heating period is black carbon, which is formed during the imperfect combustion of carbonaceous fuels. Greater particles are emitted into the air directly, mainly from residential heating and construction sites of buildings and roads.

Particulate matter contains microscopic solids or liquid droplets that are so small that they can be inhaled and cause serious health problems (Saini *et al.*, 2022). Some particles, less than 10 micrometers in diameter, can get deep into the lungs and some may even get into the bloodstream. Of these, particles less than 2.5 micrometers pose the greatest risk to health, as other risky substances (heavy metals, bacteria, carcinogens) can bind on their surface.

At present, particulate matter means the most significant environmental health risk and it is Hungary's most problematic pollutant: its concentration exceeds the EU limit values for longer periods under certain conditions. *Fig. 1* shows the trend of aerosol particle emissions between 1990 and 2021 in Hungary,

compared to the level of 2000. There is no definite trend for particulates, emissions vary from year to year. However, between 2015 and 2020, particulate emissions were characterized by a decrease, which began to increase again by the year 2021.

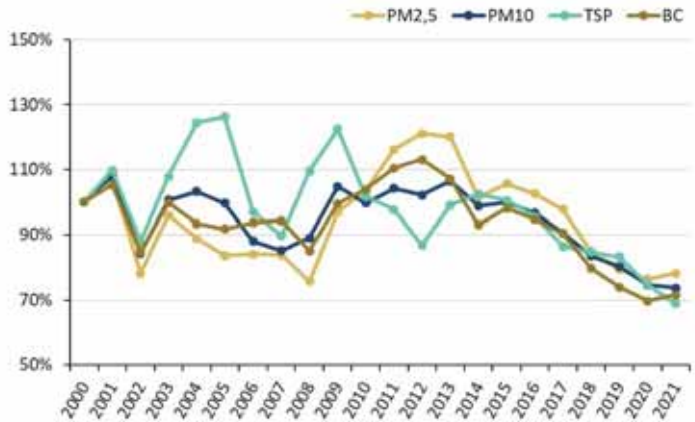


Fig. 1. Changes in particulate emissions in Hungary, compared to the level of 2000.

Hungary still has a lot of work to do in reducing PM emissions. According to the latest inventory report, the assumed reduction compared to the 2005 level will not be realized based on the current trend. Fig. 2 shows the reduction commitment made by Hungary compared to the level of 2005 and the real emissions.

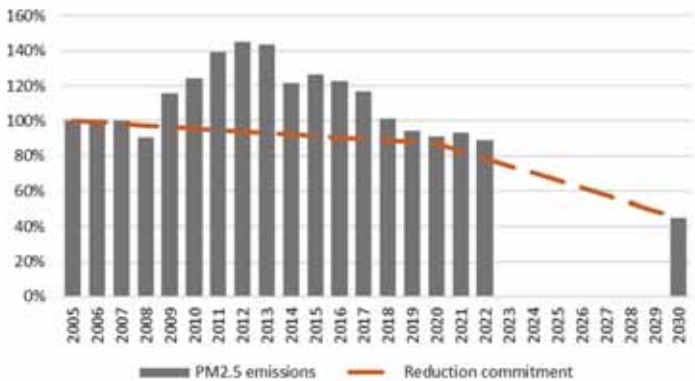


Fig. 2. PM_{2.5} reduction commitment compared to the level of 2005 and emissions in Hungary.

3. Distribution of PM emissions between inventory sources

In the next few figures, instead of the official breakdown of the four main sectors, emission ratios of the sectors according to the actual end users are shown in more detail. Graphs show the dominant role of non-industrial combustion in particulate emissions. Non-industrial combustion contains the use of fuels by households and institutions as well as agricultural heatings. *Figs. 3 and 4* show PM₁₀ and PM_{2.5} emissions, respectively, between 2000 and 2021 in Hungary in sectorial splitting.

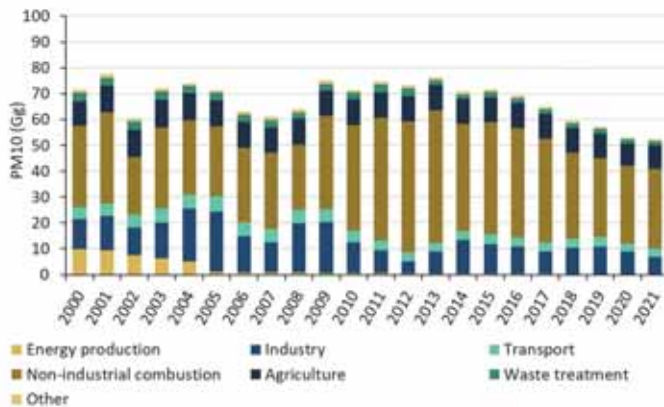


Fig. 3. PM₁₀ emissions between 2000 and 2021 (in a sectorial splitting different from the official four sectors).

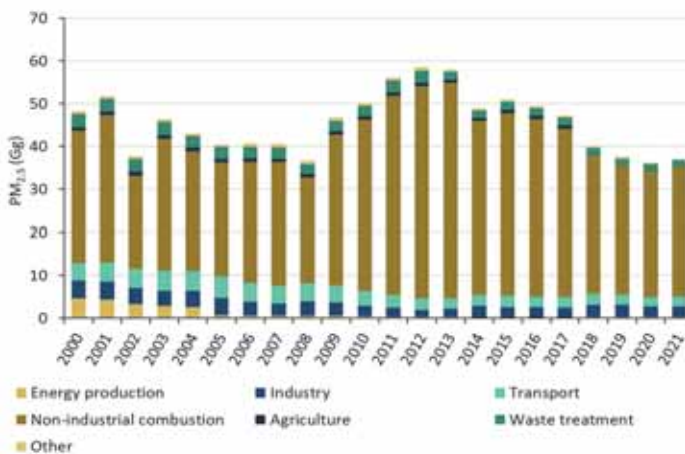


Fig. 4. PM_{2.5} emissions between 2000 and 2021 (in a sectorial splitting different from the official four sectors).

Both figures, but especially PM_{2.5} emissions, which have more dangerous health effects, show the dominant role of household burning. Based on the 2021 data, more than half of the total PM₁₀ emissions (58%) come from non-industrial combustion (mainly from residential heating), the same ratio for PM_{2.5} is 78%, and 68% of BC (soot) emissions can be linked to this source.

4. Composition of fuels used in residential heating in Hungary

Fortunately, natural gas is the dominant fuel in Hungary. According to the 2016 microcensus survey, natural gas was used in nearly 62% of homes. In addition, 38% of the apartments (this means almost one and a half million apartments) are heated with wood (also) and 3% with coal (also). If we add to this the 16% share of district heating, 2% of electricity, etc., we are well over 100%, which means that an apartment can have several types of heating materials. Almost one-fifth of households, therefore, use both piped gas and firewood, and can even switch between heating materials according to their price changes.

Particulate emissions must be considered in the case of solid burning (coal, wood and wood waste, or possibly other waste). Given that the vast majority of solid fuel heating devices currently operating in Hungary are decades old, while the prevalence of modern, low-emission technologies (e.g., eco-fireplaces, pellet burning, wood gasification boilers) can be put at a maximum of a few percent, the trend of emissions is basically determined by the amount of fuel used. *Fig. 5* shows the evolution of the coal and biomass fuel amounts used in households and the emissions from them between 2005 and 2021 in Hungary.

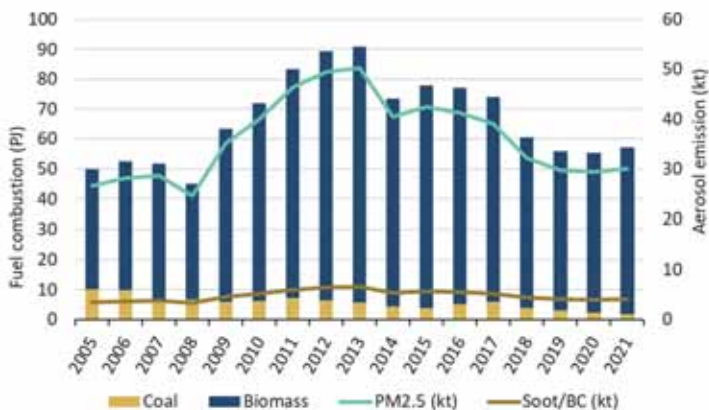


Fig. 5. Aerosol (PM_{2.5} and BC) emissions from residential solid burning between 2005 and 2021 in Hungary.

Let us examine the effects of price changes. *Fig. 5* indicates an increase of biomass combustion in households. The price of natural gas started to increase in 2005 which may have caused the increase in the use of fuel wood/biomass, which was relatively cheaper compared to natural gas. This led to increasing PM emissions from 2008. After 2014, however, the price advantage of wood gradually decreased, so the use of natural gas increased again, and the use of firewood – and with it the emission of particles – began to slowly decrease. *Fig. 6* indicates the changes in the usage and prices of natural gas and fuel wood.

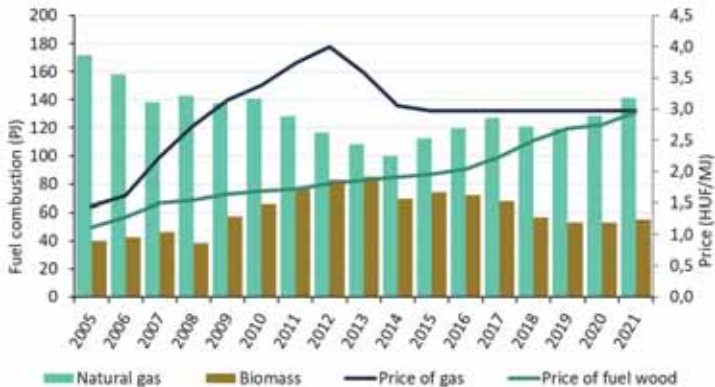


Fig. 6. The effect of fuel price changes on consumption between 2005 and 2021 in Hungary.

5. Waste burning in Hungarian households

Based on the investigations of the Clean Air Action Group of Hungary (2015), unfortunately one third of the population burns waste in Hungary with changing frequency during the year. Most people burn garden waste, 13% burn household garbage, 6% burn treated wood, rags, clothing, and footwear. Plastics (in addition to household waste) are burned by 3% and rubber by 1%. In a representative poll, 54% of the respondents considered that lack of knowledge, 35% that irresponsibility, and 15% that poverty are the main causes of irregular residential waste burning. The poll data is confirmed by the experiences of a ‘Do not burn campaign’: in the examined area of Eastern Hungary, a third of the waste disappears in the winter - in the stoves. *Fig. 7* shows the amount (in tons) of municipal waste collected by the waste collecting company during the year.

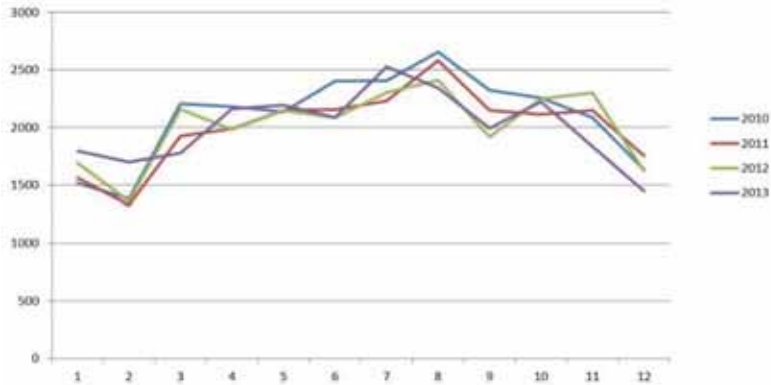


Fig. 7. Amount of officially collected municipal waste in four years in Hajdúság, Eastern Hungary. Vertical axis indicates the quantity in tons, while horizontal axis indicates the months of the year.

6. Conclusions

Particulate matter can be considered as the most significant environmental health risk in Hungary: its concentration exceeds the EU limit values for longer periods under certain conditions. It is obvious that Hungary still has a lot to do in reducing PM emissions. It should be taken into account that meteorological conditions have significant influence on the measured PM concentrations and their temporal variations. In addition, on annual average, the influence of transboundary contributions in PM concentrations could be dominant, and local regulatory policy may only bring limited results (Ferenczi and Bozó, 2017). State of the atmospheric environment could be evaluated through involving relevant monitoring and modeling activities, partly based on official emission inventories.

Public opinion formation might help to persuade the population on cleaner wood burning and the cessation of illegal waste burning. Many municipalities set good examples in front and prohibits the debris and garden waste burning. Legislation is needed to prohibit the sale of low-calorific and high-sulfur coals for residential heating purposes. Support for energy modernization of buildings is to be continued so that air pollution from heating could be reduced by half or even a third, if adequate thermal insulation of the buildings is also supported.

Acknowledgements: The research was funded by the Sustainable Development and Technologies National Programme of the Hungarian Academy of Sciences (FFT NP FTA).

References

- Clean Air Action Group, 2015: Air Pollution from Residential Burning (in Hungarian).
https://www.levego.hu/sites/default/files/Pollution_from_residential_burning_hungarian_final.pdf
- European Environment Agency, 2023: Hungary – Air Pollution Fact Sheet.
<https://www.eea.europa.eu/themes/air/country-fact-sheets/2023-country-fact-sheets/hungary-air-pollution-country>
- Ferenczi, Z. and Bozó, L., 2017: Effect of the long-range transport on the air quality of greater Budapest area. *Int. J. Environ. Pollut.* 62, 407–416. <https://doi.org/10.1504/IJEP.2017.089428>
- Ferenczi, Z., Imre, K., Lakatos, M., Molnár, Á., Bozó, L., Homolya, E. and Gelencsér, A., 2021: Long-term characterization of urban PM₁₀ in Hungary. *Aerosol Air Qual. Res.* 21, 210048-210062. <https://doi.org/10.4209/aaqr.210048>
- Przybysz, A.; Sæbø, A.; Hanslin, H.M.; and Gawroński, S.W., 2014: Accumulation of particulate matter and trace elements on vegetation as affected by pollution level, rainfall and the passage of time. *Sci. Total Environ.* 481, 360–369. <https://doi.org/10.1016/j.scitotenv.2014.02.072>
- Saini, M., Joon, M., and Saini, S.K., 2022: Human Health Effects of Particulate Matter. In: (eds Sonwani, S., Shukla, A.) Airborne Particulate Matter. Springer, Singapore.
https://doi.org/10.1007/978-981-16-5387-2_9
- Simon, E., Molnár, V.É., Tóthmérész, B. and Szabó, Sz., 2020: Ecological Assessment of Particulate Material (PM₅ and PM₁₀) in Urban Habitats. *Atmosphere* 11, 559.
<https://doi.org/10.3390/atmos11060559>

IDŐJÁRÁS

*Quarterly Journal of the HungaroMet Hungarian Meteorological Service
Vol. 129, No. 2, April – June, 2025, pp. 201–217*

Changing rainfall patterns and their impact on cereal crops in the Szentes district

Dorottya Szám^{1,2,*}, Gábor Keve¹, Árpád Fekete³, and Zsolt Hetesi^{4,5}

¹*Faculty of Water Sciences, Department of Regional Water Management
Ludovika University of Public Service*

Bajcsy-Zsilinszky út 12–14., Baja, H-6500, Hungary

²*National Laboratory for Water Science and Water Security, Faculty of Water Sciences Ludovika
University of Public Service*

Bajcsy-Zsilinszky út 12–14., Baja, H-6500, Hungary

³*Faculty of Water Sciences, Department of Hydraulic Engineering
Ludovika University of Public Service,*

Bajcsy-Zsilinszky út 12–14., Baja, H-6500, Hungary

⁴*Faculty of Water Sciences, Department of Water and Environmental Security
Ludovika University of Public Service*

Bajcsy-Zsilinszky út 12–14., Baja, H-6500, Hungary

⁵*Faculty of Natural Sciences, Institute of Mathematics and Informatics
University of Pécs*

Ifjúság útja 6. F/221., Pécs, H-7624, Hungary

**Corresponding Author email: szam.dorottya@uni-nke.hu*

(Manuscript received in final form April 8, 2024)

Abstract— One of the most significant impacts of climate change on domestic agriculture is an adverse change in rainfall patterns and an increased frequency of droughts. In our study, we analyzed the daily rainfall data at the automatic hydro-meteorological measuring station of the Lower Tisza Water Directorate (ATIVIZIG) in Szentes from 1981 to 2000 and 2001 to 2020. The focus of our study was the change in precipitation patterns caused by climate change and the phenology-dependent water demand and related yield of field cereal crops (wheat, maize). The yields of wheat and maize grown on the two largest arable land areas in the Szentes District and its wider region, the Southern Great Plain, between 2003 and 2020 showed a moderately strong correlation with changes in annual rainfall for the farms studied. This points to a strong dependence on rainfall for yields, also taking into account the risk of rainfall extremes. We found that in the second period under study, the dispersion of both annual and monthly rainfall totals increased strongly but in an insignificant way. The number of days with high rainfall increased by 19.3% and the

number of days with extreme rainfall increased by 40.9%. Even larger increases were observed for the highest five-day rainfall totals (62.1%).

Key-words: rainfall patterns, drought, global warming, Southern Great Plain region, *Triticum aestivum*, *Zea mays*, *Helianthus annuus*

1. Introduction

In a number of studies, the increasing frequency of extreme weather events has been consistently highlighted (Hetesi *et al.*, 2016; Stott, 2016), including extreme precipitation patterns in the Carpathian Basin (Hetesi *et al.*, 2023; Jánosi *et al.*, 2023). There is a typically strong correlation between precipitation patterns and crop yields, especially in areas where the only source of water is natural precipitation (Varga-Haszonits and Varga, 2005). The amount of water available for arable crops is not only a major determinant in their survival but also in their productivity. Their growth, development, and subsequent achievement of optimum yields require sufficient water (mainly through natural precipitation), which enhances the domestic application of water-saving agrotechnical solutions (Hetesi *et al.*, 2022).

In addition to the amount of precipitation, its optimal temporal distribution is also important. The critical periods in common wheat (*Triticum aestivum*) are the tillering stage (Nyiri, 1993) and the period of generative organ development. During this period, water shortage is particularly limiting for further development and subsequent yield. If the amount of available water is insufficient, the yield quality will deteriorate along with the amount of genetically available yield (Alaei *et al.*, 2010; Xuemei *et al.*, 2010; Nouri *et al.*, 2011; Ragheid *et al.*, 2011;). In maize (*Zea mays*), adequate water supply is important from the early growth period. While the plant is small, the rows are not closed, so there is a high loss of water through direct evaporation from the soil (Lacolla *et al.*, 2023). The entire reproductive (grain filling) period requires the most moisture; rain fed production requires its temporal alignment with the peak of seasonal rainfall. Continued warming may cause an asynchrony large enough to threaten yields, particularly from exposure of the silk-tasseling phase to hot, dry conditions (Harrison *et al.*, 2011). In Hungary, the irrigation effect of maize is significant, with the crop's water requirements almost always greater than the rainfall of the growing season (Tamás *et al.*, 2022).

Too little precipitation can lead to drought stress, which in combination with other abiotic stress factors (e.g., extreme heat) can have an accumulative effect, causing greater damage (Keles and Oncel, 2002; Barnabás *et al.*, 2008). In addition to the lack of precipitation, extreme precipitation also has a detrimental effect on the development of cereals. Excessive precipitation and the high humidity that often accompanies it can facilitate the growth and transmission of many hydrophilic plant pathogenic fungi (Pál-Fám and Rudolf, 2014). Moreover,

high precipitation also favors weed infestation, which causes significant agricultural damage (Varga *et al.*, 2002; Márton *et al.*, 2013).

The Szentes District investigated in this study is located in Csongrád-Csanád County, part of the Southern Great Plain region of Hungary. The region has excellent agricultural endowments, the largest area under wheat production (209 706 ha) and the highest total harvested weight (1 107 162 t) in the country (KSH, 2020, 2022). Comparably, maize ranks second among the regions, after the Northern Great Plain region, in terms of area under cultivation (221 541 ha) and total harvested weight (1 821 828 t) (KSH, 2020, 2022).

Our objective was to investigate the precipitation patterns in the Szentes District of the region, and to show their becoming more extreme during the year. In addition, we analyzed the impact of varying rainfall on wheat and maize yield averages using the example of a large farm located on the outskirts of the village of Derekegyház. These two arable crops were therefore chosen, because they cover the largest share of the area under cultivation both in the region and on the farm under study.

2. Materials and methods

Our study was conducted in the Szentes District in the Southern Great Plain region (Fig. 1). Szentes is the third most populous settlement in the county, situated on the left bank of the River Tisza, and has been a Tisza crossing point since 1903. It has low-lying, inhabited suburban settlements, which are on flood plains exposed to floods and inland waterways. Both the water level of the river and the local measurement of precipitation are a priority for water management and disaster prevention. The Lower Tisza Water Management Directorate (ATIVIZIG, 2024) measures daily rainfall at the Felsőveker hydrometeorological station in the municipality. As it is standard, the rainfall totals are automatically read at exactly 07:00 every day with an accuracy of tenths of a millimeter.

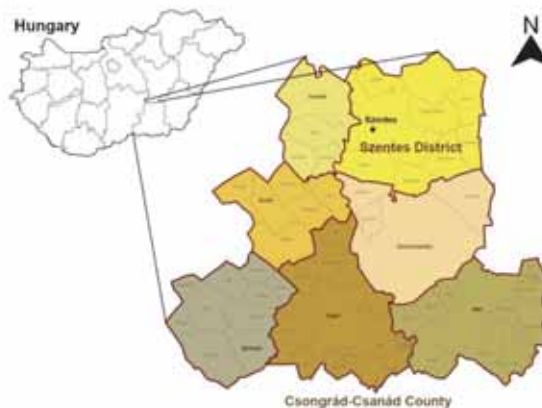


Fig. 1. Study area: the Szentes District in Csongrád-Csanád County, marked in yellow.

First, we looked at annual and monthly variations in precipitation. To this end, the period under study was divided into two equal time intervals (1981–2000; 2001–2020). The precipitation totals and their standard deviations were then compared. Our hypothesis was that the effect of climate change in weather extremes would be observed: in the second period, we would observe a larger variance in both annual and monthly precipitation totals; and that the second period would have a higher number of off-average values (weather records).

Precipitation extremes were investigated by calculating the main climatological indices for the period 1981–2000 and 2001–2020. *Table 1* summarizes the trends indices in Szentes, indicating the method of calculation. It is noted that the four parameters in the first four rows of the table are not extreme in nature, but rather refer to the variation in total precipitation. One of the most important of the indices is the standardized precipitation index, the calculation of which is recommended by the World Meteorological Organization (WMO) in order to characterize meteorological drought and for early warning systems for meteorological services of member countries (WMO, 2012).

To monitor droughts, the Standardized Precipitation Index (SPI) was determined for the two study periods. Computation of the SPI involves fitting a probability density function (PDF) to total precipitations for the stations of interest. In this study, the gamma distribution is applied, and defined by its frequency or PDF as:

$$G(x) = \int_0^x g(x)dx = \frac{1}{\beta^\alpha \Gamma(\alpha)} \int_0^x x^{(\alpha-1)} e^{(-x/\beta)} dx \quad \text{for } x > 0, \quad (1)$$

where x is the precipitation amount, α and β are shape and scale parameters, and $\Gamma(\alpha)$ is the Gamma function (*McKee et al.*, 1993). The α and β parameters have to be estimated, to each time scale of interest (1981–2020) and for each year. The maximum likelihood estimation was also employed. The resulting parameters were used to find the cumulative probability of an observed precipitation event for a timescale. This was then used in turn to obtain SPI values classified into different ranges of above and below normal values, in this way indicating the severity of the drought or non-drought event (*Table 2*). Several characteristics of droughts such as magnitude, duration or intensity can be derived based on the SPI values. In order to account for the probability q of zero rainfall to occur, the cumulative distribution function (CDF) for the Gamma distribution is modified as:

$$H(x) = q + (1 - q) G(x). \quad (2)$$

Table 1. Abbreviation and detailed method of calculation of the precipitation indices used in this study

Precipitation index	Meaning, definition	Calculation	Units of measurement
DD	Number of dry days, i.e., when precipitation does not exceed 1 mm	$n (R_{day} < 1 \text{ mm})$	day
RR0.1	Number of days with a daily rainfall total of 0.1 mm or above	$n (R_{day} \geq 0.1 \text{ mm})$	day
RR1	Number of days with a daily rainfall total of 1 mm or above	$n (R_{day} \geq 1 \text{ mm})$	day
RR5	Number of days with a daily rainfall total of 5 mm or above	$n (R_{day} \geq 5 \text{ mm})$	day
RR10	Number of days with a daily rainfall total of 10 mm or above	$n (R_{day} \geq 10 \text{ mm})$	day
RR20	Number of days with a daily rainfall total of 20 mm or above	$n (R_{day} \geq 20 \text{ mm})$	day
RX1	Maximum daily rainfall total		mm
RX5	Maximum rainfall total within 5 consecutive days	$\text{Max}(R_{day}^i, i + 1, i + 2, i + 3, i + 4)$	mm
SPI	Standardized Precipitation Index	Eqs. 1 and 2.	–
SDII	Simple Day Intensity Index: the average rainfall rate on „wet days” ($R \geq 1 \text{ mm}$) during the period of interest (here year)	$(\sum P)/RR1$ where $\sum P$ is the yearly precipitation	mm/day
CDD	The longest period without precipitation, when consecutive daily rainfall totals are less than 1 mm	$\text{Max}(R_{day}^i, i + 1, \dots, i + n)$ when $R_{day} < 1 \text{ mm}$	day
CWD	The longest period of precipitation when consecutive daily rainfall totals reach at least 1 mm	$\text{Max}(R_{day}^i, i + 1, \dots)$ when $R_{day} \geq 1 \text{ mm}$	day
R75	Number of days with moderate precipitation	$R_{day} > R_{75\%}$ where $R_{75\%}$ is the upper quartile of daily precipitation in the period under consideration	day
R95	Number of very precipitation days	$R_{day} > R_{95\%}$ where $R_{95\%}$ is the 0.95 percentile of daily precipitation in the period under consideration	day
DS5	Number of dry periods longer than 5 days		1
DS10	Number of dry periods longer than 10 days		1
DS5N	Number of days during dry spells longer than 5 days		day/period

Table 2. Changes in the main climatological indices for the periods 1981–2000 and 2001–2020. (Source of data: ATIVIZIG, 2024).

	1981–2000	2001–2020	Change (%)
DD	1505 day	1590 day	+5.6
RR0.1	2340 day	2513 day	+7.4
RR1	1505 day	1590 day	+5.6
RR5	614 day	683 day	+11.2
RR10	285 day	340 day	+19.3
RR20	66 day	93 day	+40.9
RX1	52.3 mm	75 mm	+43.4
RX5	95.2 mm	154.3 mm	+62.1
SPI	-0.23	+0.24	-
CDD	44 day	46 day	+4.5
CWD	9 day	8 day	-11.1
SDII	6.38 mm/day	6.93 mm/day	+8.7
R75	1735 day	1776 day	+2.4
R95	351 day	364 day	+3.7
DS5	334	345	+3.3
DS10	155	154	-0.6
DS5N	4163	4150	-0.3

The calculated precipitation probabilities were transformed into the corresponding standard normal values, from which the SPI values were subsequently calculated. Additional descriptions can be found in *Edwards and McKee (1997)*. The drought classification was based on the SPI (*McKee et al., 1993*).

Finally, we tested whether there is a significant correlation between rainfall and yields in wheat, maize, and sunflower fields. The rainfall data were obtained from the ATIVIZIG measuring station in Szentes and the yields from a 300 ha farm on the outskirts of the village of Derekegyház. These three crops were chosen because they account for the largest share of the farm's production area. Likewise, these three crops are the most widely grown in the Southern Great Plain region. The dependence of wheat and maize yields on water availability is a well-known fact in the literature. Both crops are rain-fed. Maize prefers more humid conditions than wheat and is also drought-sensitive. Sunflowers (*Helianthus annuus*) are moderately drought tolerant compared to wheat and maize. The

rainfall requirements of sunflowers are highly dependent on their phenological stage. As the plants grew during July, transpiration increased alongside the expanding leaf area; therefore, sunflower water use increased and reached its highest level in July or August. However, during the mowing period following pan maturation, precipitation in the pan may be conducive to fungal infections (*Gulya et al.*, 2018). Thus, the dependence of sunflower yield on precipitation was used as a control in our study, and no correlation between the two variables was expected. In contrast, for wheat and maize, we hypothesized that yields would be strongly dependent on rainfall.

In our research, the normality of the samples was checked using Shapiro-Wilk tests, which can also be applied to samples with a small number of elements. Where normality was met, we compared the standard deviations of the samples using an F-test. Where normality was not met, Levene's test was used to determine the homogeneity of variance. At several sites, a two-sample Kolmogorov-Smirnov test was used. This less well-known statistical test compares the continuous distribution of two samples. This does not specify the common distribution (e.g., normal or abnormal) (*Naaman*, 2021). The test's null hypothesis is that the two samples come from a population with the same distribution. The null hypothesis can be rejected if the value obtained is greater than the critical value from the table.

Statistical tests (linear trend estimates, F-tests, Shapiro-Wilk tests, correlation analyses) were performed at a significance level of $\alpha = 0.05$ in all cases not specifically indicated. In exceptional cases, different levels of significance were used to demonstrate the conclusiveness of the computational results. These are indicated in all cases. We used a significance level lower than the usual $\alpha = 0.05$, because the two-sample Kolmogorov-Smirnov tests are more robust, weaker statistical tests (*Marrozzi*, 2009, 2013).

3. Results and discussion

Looking at the development of the annual precipitation sum (*Fig. 2*), the year 2000 was a year of extreme drought, even at the national level, and one of the worst years for Hungarian agriculture due to the lack of precipitation. The annual rainfall at the Felsőveker station was less than 300 mm (299.6 mm), which was extremely low by national standards. Furthermore, it highlighted the meteorological drought vulnerability of the Southern Great Plain region due to the lack of precipitation. Szeged, located approximately 40 km south of Szentes as the crow flies, recorded the lowest annual precipitation in 2000 in national comparison, 203.3 mm (*Szentes*, 2023).

The year 2010 was exceptionally wet, with a national average of more than one and a half times the multi-year average (169%) (HungaroMet, 2024). At Felsőveker, a total rainfall of 848.4 mm was recorded. In May this year,

unprecedented flooding occurred on smaller rivers, and a further flood wave was still flowing in June. The River Tisza, which borders Szentes, also experienced flooding. September and December were also extremely wet months. In Szentes, nine people were forced to leave their homes, which had become unsafe due to the flooding (Nagy, 2011).

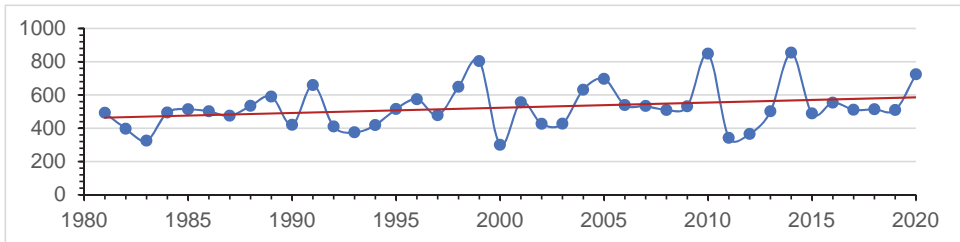


Fig. 2. Annual rainfall totals (mm) in Szentes between 1981 and 2020 (Source of data: ATIVIZIG, 2024).

The year 2011 brought a reversal of the trend, with prolonged periods of drought and precipitation levels of less than half the long-term average. The national precipitation total in 2011 was 404.4 mm, which is only 4.3 mm more than the second lowest annual value (year 2000) since measurements began to be taken (Fekete and Keve, 2020). The central region was the driest in the country (HungaroMet, 2024). At the Szentes station, 341.9 mm of precipitation was recorded in 2011, which is much lower than the national value.

Year 2014 (HungaroMet, 2024) was even wetter than 2010, when a total of 854.0 mm of precipitation was recorded at the hydrometeorological station. July 2014 was one of the five wettest Julys in the national statistics, which have been kept since 1901. Although this month is one of the wettest months of the year in a large part of the country, it is also often a period of severe drought (Ambrózy *et al.*, 1990). The highest July precipitation in 2014, 237.6 mm, was recorded very close to the station at Pankota near Szentes. The month of September 2014 was also very wet, with several properties in Szentes at risk of flooding, low-lying suburban houses and farms in particular. Two thousand sandbags were transported to the Szentes area by the disaster management team, whose units from Szeged and Hódmezővásárhely also took part in the clean-up. In Szentes, firefighters pumped rainwater from three locations. According to climate research studies, these record years are not clearly due to climate change, but they are an indication of the weather becoming more extreme.

At the national level, annual rainfall totals have shown a downward trend since 1901. In contrast, Szentes shows a small, but not significant ($R^2 = 0.0787$)

increase in annual precipitation totals between 1981 and 2020. The results of the Shapiro-Wilk tests [$W(20) = 0.96$; $p = 0.555$; $W(20) = 0.9$; $p = 0.039$] indicate that the annual precipitation totals for the period 1981–2000 follow a normal distribution. The distribution of the data for 2001–2020 is very close to a normal distribution, but is not normally distributed at the 0.05 significance level. Nevertheless, an F-test was used to compare the dispersion of rainfall amounts over the two time intervals. Our hypothesis was that the extremes of precipitation would move in a wider range and occur more frequently. However, the results of the F-test [$SD_1 = 120.05$, $SD_2 = 137.70$, $F(19,19) = 0.8$, $p = 0.556$] did not show that the precipitation extremes increased significantly.

We also examined how annual rainfall totals varied during the growing season relevant for crop water requirements (from March 1 to October 31) (Fig. 3). Similarly, the year 2000 was considered the driest year, while the highest rainfall was recorded in 2014. There is no significant increasing trend in rainfall amounts in this comparison ($R^2 = 0.0507$). Our two rainfall amount samples (1981–2000; 2001–2020) are normally distributed [$W(20) = 0.93$, $p = 0.163$; $W(20) = 0.93$, $p = 0.125$], and therefore an F-test was used. Likewise, the F-test did not reveal any significant difference [$SD_1 = 99.31$, $SD_2 = 122.80$, $F(19,19) = 0.7$, $p = 0.363$] between the sample variances. The variances within the growing season were lower than the variances in annual rainfall totals.

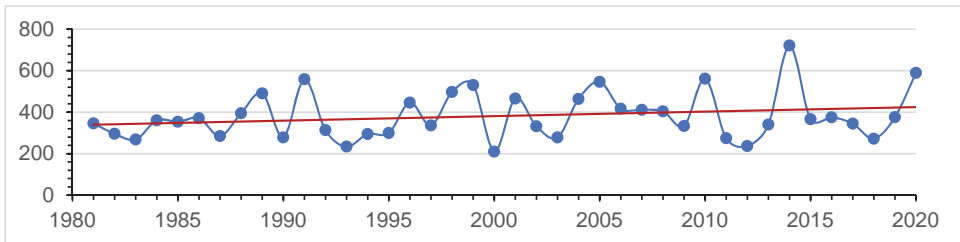


Fig. 3. Trends in rainfall (mm) per vegetation period (from March 1 to October 31) in Szentes between 1981 and 2020 (Source of data: ATIVIZIG, 2024).

Similarly, there is no significant trend (increase) in the number of precipitation days per year between 1981 and 2020 ($R_2 = 0.0015$). The record year of 2010 had an exceptionally high number of precipitation days 114, while the years 1983, 2000, and 2011 had much fewer than 60 precipitation days on average (Fig. 4).

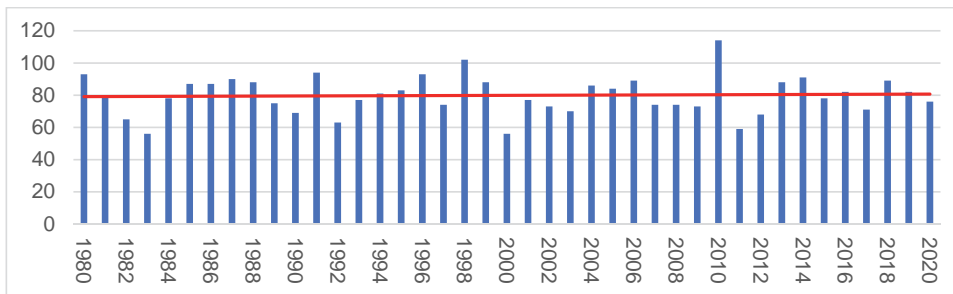


Fig. 4. Changes in the number of precipitation days between 1980–2020 (Source of data: ATIVIZIG, 2024).

The monthly number of days with precipitation (excluding outliers) follows a normal distribution between 1981 and 2020 (Fig. 5). Outliers, i.e., values exceeding one and a half times the width of the interquartile range from the lower to the upper limit of the range, are marked by circles in Fig. 5. Outlier days were: March 1988 (19 days), July 2014 (18 days), and October 2003 (20 days). In October 2003, the national rainfall was well above the multi-year average, at around 90 mm. The high precipitation was accompanied by cold weather, with snow falling in several municipalities across the country on October 23–24, with snow cover of more than 10 cm covering the surface for several days (HungaroMet, 2024). At the Felsőveker measuring station, 126.4 mm of precipitation was recorded in October.

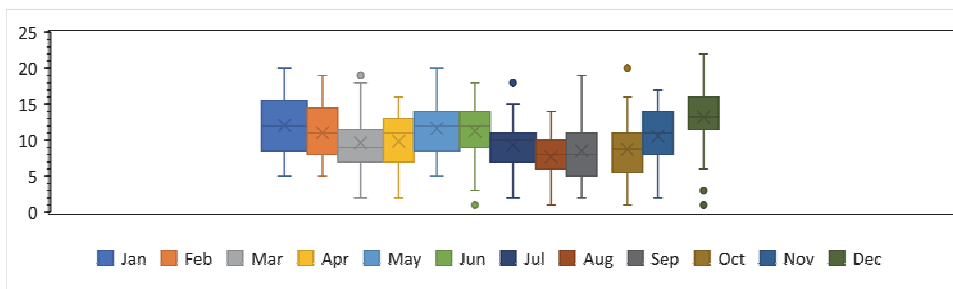


Fig. 5. Changes in the number of precipitation days per month between 1981 and 2020 (Source of data: ATIVIZIG, 2024).

Outlier days were recorded in June 2000 (1 day), December 2013 (1 day) and December 2016 (3 days). It is noteworthy that five of the six outlier months fell in the second half of the period under study (2001–2020).

Two-sample Kolmogorov-Smirnov tests show that there is no significant difference in the distribution of daily precipitation between 1981–2000 and 2001–2020. There is an increase in the number of days with low rainfall (maximum 10 mm per day) and an increase in the number of days with extreme rainfall, which merits further research.

For the extreme precipitation study, increases were observed for most climatological indices (*Table 2, Fig. 6*). This is in line with the spatial results from observed data on the change in annual precipitation totals (1981–2020) (HungaroMet, 2021a). The number of precipitation days (RR0.1) increased by 7.4%. A precipitation day is defined here as a daily precipitation sum reaching 0.1 mm. The number of days with high rainfall ($R_{day} \geq 10$ mm) increased by 19.3%. The number of extreme rainfall days (when the daily rainfall total reaches 20 mm) has increased even more (40.9%). Increases in RR10 and RR20 have been shown in several previous studies (Bartholy and Pongrácz, 2004; 2005a; 2005b) for several domestic stations (including Szeged, which is the closest to Szentes) in the period 1976–2001. However, a further study (No. T-049824 OTKA grant, final report) shows that RR10 and RR20 values are already showing diverging trends in the European region. In addition, climate models for long-term Hungarian projections highlight the seasonal variability of the RR1 and RR10 indices. They show an increase in RR1 in summer and a decrease in RR1 in winter for the period 2071–2100 compared to the reference period 1961–1990 (Pongrácz *et al.*, 2012).

The record for the highest daily rainfall (RX1) was 75 mm in the second period under study (September 13, 2014). The highest 5-day rainfall was also recorded between September 10 and 14, 2014, with a value of 154.3 mm. By comparison, this value is approximately twice the average monthly 30-day rainfall total for June 1991–2020, which is the highest average rainfall total for any of the months (HungaroMet, 2021b). This is a significant increase compared to the record 5-day rainfall total of 95.2 mm in 1981–2000.

The longest period without rainfall between 1981–2000 was 44 days, but this record was also broken between 2001–2020 with a 46-day period. The length of the rainfall-free and rainfall-rich periods is important for determining drought periods. Two-sample Kolmogorov-Smirnov tests show no significant difference in the distribution of the length of the rainy season ($D_{max} = 0.22$; $K_S = 0.47$; $p = 0.98 > 0.05$) and the length of the dry season ($D_{max} = 0.11$; $K_S = 0.65$; $p = 0.79 > 0.05$).

The simple daily rainfall intensity index (SDII) shows an increase of +8.7% in the second period. This means that the average amount of precipitation per day of precipitation has increased by this amount.

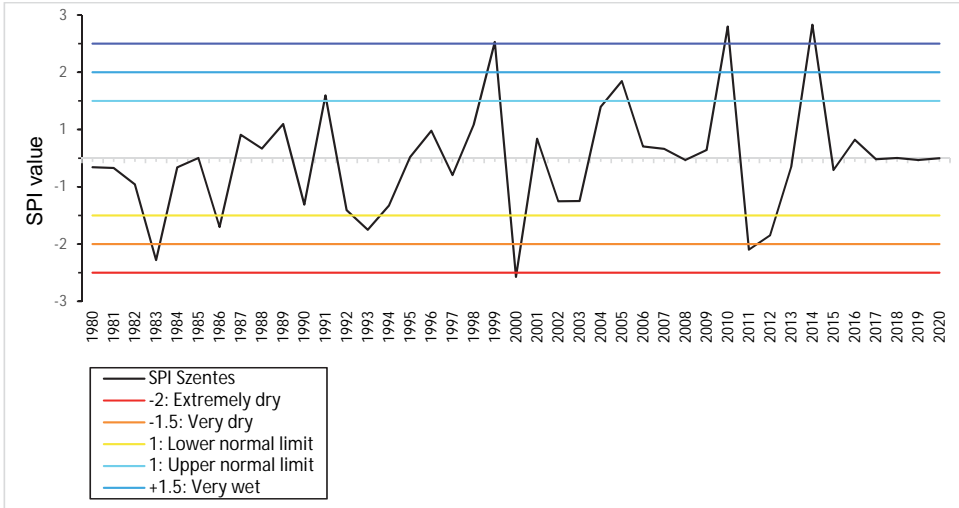


Fig. 6. Change of SPI values in Szentes between 1980–2020 (Source of data: ATIVIZIG, 2024).

In further examination of extreme precipitation events using the Kolmogorov-Smirnov test we found that the distribution of the precipitation amount neither for days with high precipitation ($D_{max} = 0.1231$; $K_S = 0.7016$; $p = 0.7085 > 0.05$) nor for days with extreme precipitation ($D_{max} = 0.1455$; $K_S = 0.7628$; $p = 0.6057 > 0.05$) differed significantly in the two periods (Fig. 7). It is noteworthy, however, that for nine of the ten days with the highest daily precipitation, totals fell in the period 2001–2020.

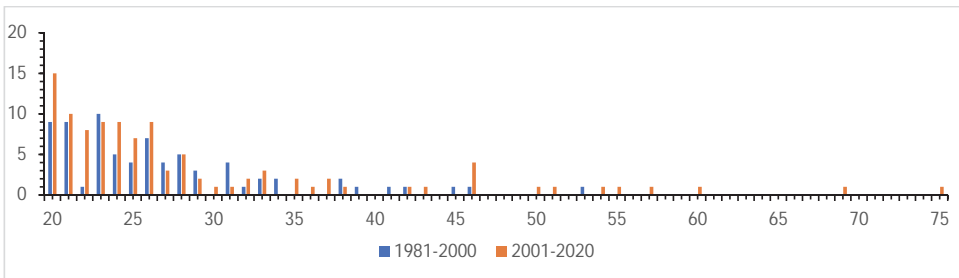


Fig. 7. Distribution (%) of rainfall totals on days with extreme precipitation (>20 mm) between 1981–2000 and 2001–2020 (Source of data: ATIVIZIG, 2024).

Since national laws only consider the effect of daily maximum temperatures and rainfall totals on drought development, drought statistics may be biased by days with intense rainfall, ignoring the rolling effect of precipitation. An increase in the frequency of dry days may result in a similar rolling effect, which can be explained by soil water resources, soil water holding capacity, and its finite nature.

In our study, we investigated whether there is a significant relationship (correlation) between annual precipitation and the yield of wheat and maize fields on the farm near the municipality of Derekegyháza, which share the two largest area shares. *Fig. 8* shows how sensitive the yield of different crops is to rainfall. A medium strong correlation ($R^2 = 0.32$) is observed for maize, which is considered a drought indicator crop, and a medium strong correlation ($R^2 = 0.20$) for wheat. As a control, the yields of the sunflower fields occupying the third largest area of the farm were also examined. Our original hypothesis was supported by the fact that sunflower yields did not show any correlation ($R^2 = 4 * 10^{-5}$) with rainfall.

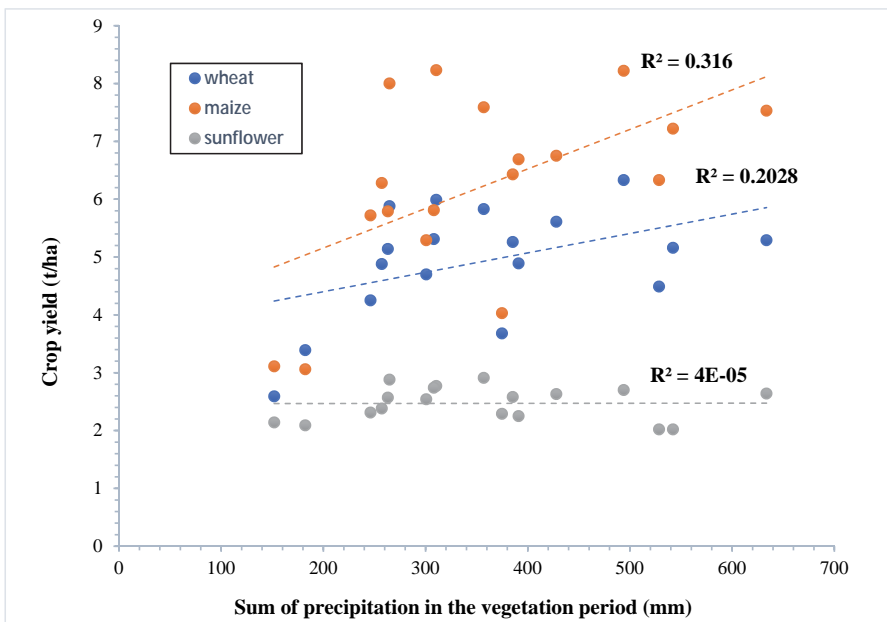


Fig. 8. Yields (t/ha) of maize, wheat, and sunflower on a farm near Derekegyház and annual precipitation data in Szentes between 1978 and 2020 (Source of data: ATIVIZIG, 2024; Derekegyház farm, 2023).

The lowest yields shown in *Figure 7* belong to the years 2003 and 2007, when the growing season rainfall did not even reach 200 mm. The year with the highest rainfall was 2014, when a total of 633.6 mm of rainfall was recorded during the growing season. Even so, this is not the year with the highest average yields, which points to the impact of the high rainfall not being clearly positive (+78% compared to the growing season average). The highest yield averages typically occurred in years close to the multi-year rainfall average (2016, 2018, 2020).

A similar positive correlation was found between maize yield ($R^2=0.21$) and wheat yield ($R^2 = 0.10$) and annual precipitation between 2006 and 2019 in a study in Poland, but Poland has a rainier climate than Hungary (*Wójcik-Gront and Gozdowski, 2023*).

The lack of a strong correlation can be explained by several factors, the most important of which is the phenological, phase-dependent water demand of plants, which varies during the growing season. The water requirements of plants are more or less constant and are a well-known varietal characteristic. Like many abiotic environmental factors, rainfall is optimal for crops within a range. Too much rainfall can lead to anaerobic soil conditions and soil erosion, as the soil has a finite capacity to absorb water. It can also increase the growth and spread of weeds, pests, and pathogens that require a wet and humid environment. Among pathogens, fungal diseases such as rust (*Puccinia sorghi*, *Puccinia striiformis*, *Puccinia triticina*) and fusarium (*Fusarium* sp.) are particularly susceptible to humid conditions. Among pests, aphids (*Aphidoidea*) and leafbeetles (*Oulema* sp.) are also important.

It is also worth comparing wheat and maize crop yields with buying-in prices (*Fig. 9*). It can be seen that the two driest years (2003, 2012) had the lowest yields, which drove up buying-in prices. In the years with better yields, prices fell.

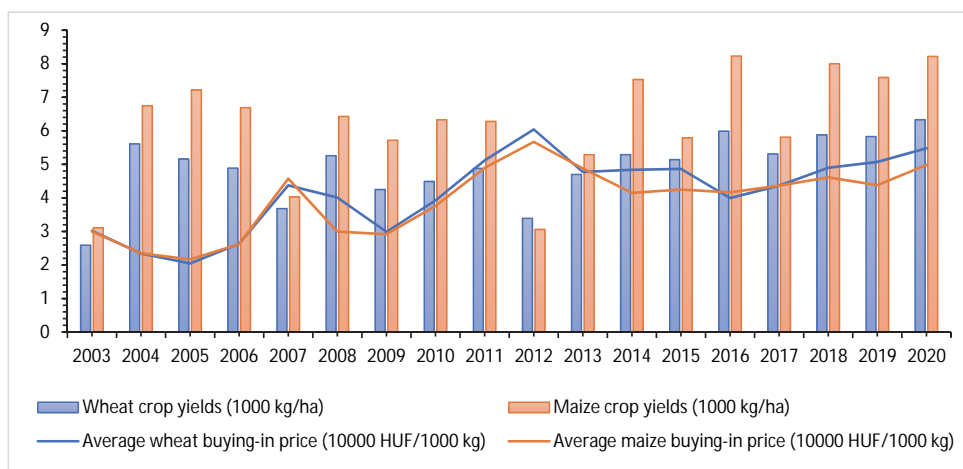


Fig. 9. Trends in wheat and maize crop yields and average buying-in prices 2003–2020. (Source of data: KSH, 2024; Derekegyház farm, 2023).

An even more accurate relationship between crop yields and buying-in prices would be obtained by inflation-adjusted prices. However, the drought year of 2012 is still striking, with only 182.3 mm of rainfall in the vegetation period and prices at a record high (wheat: 60 425 HUF/10 000 kg, maize: 56 697 HUF/10 000 kg). The previous year, also dry, was also low, with 246.1 mm of rainfall. Thus, the high buying-in price in 2012 probably reflects the rolling effect of the drought, just as the fall in prices was delayed, the rise in yields appeared with a lag. Limited storage time also plays a role in this.

4. Conclusions

No clear upward trends in annual and monthly rainfall totals were observed over the period 1981–2020; we did, however, demonstrate a non-significant but still notable increase in the frequency of rainfall extremes. Dividing the period under study into two equally long periods, we found that the number of days with high precipitation increased by 19.3% and the number of days with extreme precipitation increased by 43.4%. The increase in the frequency of intense rainfall periods is even more significant. The highest five-day precipitation index was 62.1% higher in the second period (154.3 mm). There was also a change in the distribution of rainfall totals. The probability of the occurring two extreme conditions, the frequency of dry days and, in parallel, the frequency of extreme precipitation days increased.

It would also be worth looking at the number of days with precipitation over a longer time horizon. It is questionable whether the already significant decrease in the national average (17 days per 120 years between 1901 and 2020) can be observed here. It would also be worth knowing how the frequency of extreme precipitation events has changed.

The dependence of wheat and maize yields on the amount of precipitation is shown using the example of the average yields of a large farm from 2003 to 2020. The drought-sensitive nature of maize, which prefers humid conditions, was shown by the dependence of the yield average on higher precipitation. Wheat yield averages were found to be less dependent on precipitation than maize, which is consistent with the lower water requirement of the crop. This result confirms the role of intra- and inter-annual rainfall forecasting in crop protection.

Acknowledgements: The research presented in the article was carried out within the framework of the Széchenyi Plan Plus program with the support of the RRF 2.3.1 21 2022 00008 project.

Conflict of interests: The authors declare no conflict of interests.

References

- Alaei, M., Zaefizadeh, M., Khayamezhad, M., and Alaei, Z., 2010: Evaluation of Germination Properties of Different Durum Wheat Genotypes under Osmotic Stress. *Middle-East J. Sci. Res.* 6, 642–646.
- Ambrózy, P., Koflanovits, E., and Kövér, B., 1990: A csapadék-eloszlás időbeli átrendeződése Magyarországon. *Időjárás* 94, 156–167. (in Hungarian)
- ATIVIZIG, 2024: Szentés csapadékkadatok napai, havi és éves bontásban. (in Hungarian)
- Barnabás, B., Jäger, K., and Fehér, A., 2008: The effect of drought and heat stress on reproductive processes in cereals. *Plant Cell Environ.* 31, 11–38.
<https://doi.org/10.1111/j.1365-3040.2007.01727.x>
- Bartholy J. and Pongrácz R., 2004: Extrém csapadékindexek XX. századi tendenciái a Kárpát-medence térségében. *Földtani Kutatás* 41, (3–4.), 57–68. (In Hungarian)
- Bartholy J. and Pongrácz R., 2005a: Néhány extrém éghajlati paraméter globális és a Kárpát-medencére számított tendenciája a XX. században. *AGRO-21 Füzetek* 40, 70–93. (In Hungarian)
- Bartholy J., and Pongrácz R., 2005b: Tendencies of extreme climate indices based on daily precipitation in the Carpathian Basin for the 20th century. *Időjárás* 109, 1–20.
- Fekete, Á. and Keve, G., 2020: Baja éves csapadékösszegeinek statisztikai vizsgálata az 1989–2018-as időszakra. In: (ed. Szlávik, L.) XXXVII. Országos Hidrológiai Vándorgyűlés dolgozatai. Budapest, Magyarország: Magyar Hidrológiai Társaság 1–9., 9. (in Hungarian)
- Gulya, T., Mathew, F.M., Harveson, R.M., and Markell, S., 2018: Diseases of Sunflower (*Helianthus annuus*). 2018. Diseases of Sunflower. In: (eds. McGovern, R.J., Elmer, W.H.) Handbook of Florists' Crops Diseases. pp. 787–837. https://doi.org/10.1007/978-3-319-39670-5_27
- Harrison, L., Michaelson, J., Funk, C., and Husak, G.J., 2011: Effects of temperature changes on maize production in Mozambique. *Climate Res.* 46, 211–222. <https://doi.org/10.3354/cr00979>
- Hetesí, Zs., Szám, D., and Vicze, I., 2016: Káros jelenségek az éghajlatváltozás folyamatai között. In: Horváth B. (ed.): Ökológiai lábnyom és fenntarthatatlanság. L'Harmattan Kiadó, 221–238. (in Hungarian)
- Hetesí, Zs., Mrekva, L. and Szám, D., 2022: Agroforestry: a Possible Response to the Challenges of Climate Extremes. *Georgikon for Agriculture: A Multidisciplinary Journal in Agricultural Sciences* 26(3), 120–126.
- Hetesí, Zs., Szám, D., Lakatos, B., Belényesi, M., Birinyi, E., Mikus, G., and Kristóf, D., 2023: A 2022-es aszály éghajlati, tájhasználati okai és következményei. *Agrofórum – A Növénytermesztők és Növényvédők Havilapja* 34(2), 18–22. (in Hungarian)
- HungaroMet, Hungarian Meteorological Service, 2021a: Hőmérséklet és csapadéktrendek. (in Hungarian)
https://www.met.hu/eghajlat/eghajlatvaltozas/megfigyelt_hazai_valtozasok/homerseklet_es_csapadektrendek/csapadekosszegek/
- HungaroMet, Hungarian Meteorological Service, 2021b: Magyarország csapadék viszonyai. (in Hungarian)
https://www.met.hu/eghajlat/magyarorszag_eghajlata/altalanos_eghajlati_jellemzes/csapadek/
- HungaroMet, Hungarian Meteorological Service, 2024: Elmúlt évek időjárása. (in Hungarian)
https://www.met.hu/eghajlat/magyarorszag_eghajlata/eghajlati_visszatekinto/elmult_evek_idoja_rasa/main.php?no=12&ful=4
- Jánosí, A., Fekete, Á., and Szám, D., 2023: Markov-láncok alkalmazása az aszályos napok valószínűségének megállapítására Budapest térségében. *Hadmérnök* 18(3), 69–81. (in Hungarian)
<https://doi.org/10.32567/hm.2023.3.6>
- Keles, Y. and Oncel, I., 2002: Response of antioxidative defence system to temperature and water stress combinations in wheat seedlings. *Plant Sci.* 163, 783–790.
[https://doi.org/10.1016/S0168-9452\(02\)00213-3](https://doi.org/10.1016/S0168-9452(02)00213-3)
- KSH, Hungarian Hungarian Central Statistical Office, 2020: 19.1.2.1. Földterület művelési ágak, valamint vármegye és régió szerint [ezer hektár]. (in Hungarian)
https://www.ksh.hu/stadat_files/mez/hu/mez0068.html
- KSH, Hungarian Hungarian Central Statistical Office, 2022: A fontosabb növények vetésterülete. (in Hungarian) <https://www.ksh.hu/s/kiadvanyok/a-fontosabb-novenyek-vetesterulete-2022-junius-1/>
- KSH, Hungarian Hungarian Central Statistical Office, 2024: 1.1.1.13. Gabonafélék felvásárlási átlagára [Ft/tonne]. (in Hungarian) https://www.ksh.hu/stadat_files/ara/hu/ara0013.html

- Lacolla, G., Caranfa, D., Corato, U.D., Cucci, G., Mastro, M.A., and Stellacci, A.M., 2023: Maize Yield Response, Root Distribution and Soil Desiccation Crack Features as Affected by Row Spacing. *Plants* 12, 1380. <https://doi.org/10.3390/plants12061380>
- Marozzi, M., 2009: Some notes on the location-scale Cucconi test. *J. Nonparam. Stat.* 21, 629–647. <https://doi.org/10.1080/10485250902952435>
- Marozzi, M., 2013: Nonparametric Simultaneous Tests for Location and Scale Testing: A Comparison of Several Methods. *Commun. Stat. Simulation and Computation*, 42 (6), 1298–1317. <https://doi.org/10.1080/03610918.2012.665546>
- Márton, L., Lehoczy, É., and Wágner, G., 2013: Study on the weeds of maize in the infected field with *Cirsium Arvense* (L.) scop. *Acta Agraria Debreceniensis* 51, 131–135. <https://www.doi.org/10.34101/actaagrar/51/2077>
- McKee, T.B., Doesken, N.J., and Kleist J., 1993: The relationship of drought frequency and duration to time scales. Proc. 8th Conf. on Applied Climatology, January 17–22., 1993. American Meteorological Society, Massachusetts, 179–184.
- Naaman, M., 2021: On the tight constant in the multivariate Dvoretzky-Kiefer-Wolfowitz inequality. *Stat. Prob. Lett.* 173, 109088. <https://doi.org/10.1016/j.spl.2021.109088>
- Nagy, S., 2011: 2010–2011. évi kül- és belterületi belvízi védekezés tapasztalatai Szentes kistérségben. *Műszaki Katonai Közlöny* 21, 760–776. (in Hungarian)
- Nouri, A., Etmnan, A., Silva, J.A., and Mohammadi, R., 2011: Assessment of yield, yield-related traits and drought tolerance of durum wheat genotypes (*Triticum turjidum* var. Durum Desf.). *Australian J. Crop Sci.* 5, 8–16.
- Nyíri, L., 1993: Földműveléstan. Mezőgazda Kiadó, Budapest, 47–85. (in Hungarian)
- Pál-Fám, F. and Rudolf, K., 2014: Gombakórokozók a kukoricán és előfordulásuk csapadékos években. *Agrofórum Extra* 57, 84–87. (in Hungarian)
- Pongrácz, R., Bartholy, J., Kis, A., Miklós, E., and Törék, O. 2012: Extrém Éghajlati Indexek várható tendenciái modellszimulációk eredményei alapján. *Léggör* 57, 166–169. (in Hungarian)
- Ragheid, A., Tahar, B., and Abdellah, A., 2011: Smart irrigation system for wheat in Saudi Arabia using wireless sensors network technology. *Int. J. Water Res. Arid Environ.* 1, 478–482.
- Stott, P.A., Christidis, N., Otto, F.E.L., Sun, Y., Vanderlinden, J-P., Jan van Oldenborgh, G., Vautard, R., Storch, H., Walton, P., Pascal, Y. W., and Zwiers, F., 2016: Attribution of extreme weather and climate-related events. *WIREs Climate Change* 7, 23–41. <https://doi.org/10.1002/wcc.380>
- Szentes, O., 2023: Szárazság Magyarországon 2022-ben és a múltban. *Léggör* 68(1), 9–19. (in Hungarian) <https://doi.org/10.56474/legkor.2023.1.2>
- Tamás, A., Radócz, L., Horváth, É., and Zagyi, P., 2022: A termesztéstechnológiai tényezők hatása a kukorica (*Zea mays* L.) terméseredményeire polifaktoriális tartamkísérletben. *Növénytermelés* 71, 67–80. (in Hungarian)
- T-049824 OTKA grant, final report, 2002–2009: Regionális modellbecslésekkel előállított éghajlatváltozási forgatókönyvek a Kárpát-medence térségére. Supervisor: Bartholy, J., Eötvös Loránd University, Budapest, Hungary. (in Hungarian)
- Varga, P., Béres, I., and Reisinger, P., 2002: Három veszélyes gyomnövény hatása a kukorica termésalakulására három eltérő csapadékkellátottságú évben. In: XII. Keszthelyi Növényvédelmi Fórum p. 42. (in Hungarian)
- Varga-Haszonits, Z. and Varga, Z., 2005: Nyugat-Magyarország éghajlati viszonyai és a kukorica.. *Agro-21 Füzetek*, 43. 71–79 (in Hungarian)
- WMO, World Meteorological Organization, 2012: Standardized Precipitation Index – User Guide. Available: https://www.droughtmanagement.info/literature/WMO_standardized_precipitation_index_user_guide_en_2012.pdf
- Wójcik-Gront, E. and Gozdowski, D. 2023: Effect of Climate Change in Years 2006–2019 on Crop Yields in Poland. *Europ. J. Sustain. Develop.* 12, 225–236. <https://www.doi.org/10.14207/ejsd.2023.v12n4p225>
- Xuemei, J.I., Jianlin, W., David, C.L., Colin, L.D.J., Anthony, G.C., Richard A.R., and Rudy, D., 2010: Importance of pre-anthesis anther sink strength for maintenance of grain number during reproductive stage water stress in wheat. *Plant, Cell and Environment* 33, 926–942. <https://doi.org/10.1111/j.1365-3040.2010.02130.x>

IDŐJÁRÁS

*Quarterly Journal of the HungaroMet Hungarian Meteorological Service
Vol. 129, No. 2, April – June, 2025, pp. 219–240*

Changes in precipitation conditions in Slovakia during northern and southern cyclonic situations in the 1991–2020 period

Peter Zaujec^{1,2,*} and Martin Halaj³

¹*Comenius University in Bratislava, Faculty of Natural Sciences
Department of Physical Geography and Geoinformatics
Ilkovičova 6, 842 15 Bratislava, Slovakia*

²*Slovak Hydrometeorological Institute
Jeséniova 17, 833 15 Bratislava, Slovakia*

³*Slovak Hydrometeorological Institute
Zelená 5, 974 04 Banská Bystrica, Slovakia*

**Corresponding Author email: zaujec8@uniba.sk*

(Manuscript received in final form May 21, 2024)

Abstract— In Slovakia, the spatial distribution of precipitation is inhomogeneous, which is mainly caused by the prevailing airflow of individual synoptic types in combination with a diverse georelief. The article examines the precipitation conditions of Slovakia for all northern and southern types of cyclonic situations in the period 1991–2020. In the selected area we worked with precipitation totals from 798 stations provided by the Slovak Hydrometeorological Institute. We processed the separate dataset in Microsoft Excel and created distinct layers of precipitation totals for all the situations studied in ArcGIS software using a Python script. From the separate datasets, we created precipitation fields for the average annual precipitation total and fields for the percentage of the average annual precipitation fallen during all northern and all southern types of cyclonic situations out of the total average annual precipitation fallen during the whole period under study and for each decade, respectively. Based on the results obtained, we can observe changes in the frequency of occurrence and in the spatial distribution of precipitation, especially for southern, but also for northern cyclonic types of situations. These findings can be used in practice in several fields, especially in synoptic meteorology, climatology, and hydrology.

Key-words: precipitation conditions, climate change, northern and southern cyclonic situations, Slovakia

1. Introduction

In terms of geographical location, Slovakia lies in a temperate climate zone in the middle of Central Europe (Fig. 1), where different air masses (arctic, polar, tropical) alternate throughout the year. The distance from the Atlantic Ocean or the surrounding seas means that Slovakia's climate is transitional between oceanic and continental. It is, therefore, very important what synoptic situation brings atmospheric precipitation to our area.



Fig. 1. Location of Slovakia within Europe. (Source: Freeworldmaps, (2023), own modification)

Slovakia is a very rugged country in terms of relief. It is made up of the lowlands of the Pannonian Basin, basins, and the Carpathian Mountains. These lowlands, basins, and mountain ranges are part of a vertically and horizontally extensive geomorphological system on the surface of the earth, namely the Alpine-Himalayan system. This extends from northern Africa, across Europe, into southern Asia. In terms of geomorphology, Slovakia is divided into sub-systems, provinces, sub-provinces, areas, units, sub-units, and parts (Mazúr and Lukniš, 1978).

The orographic conditions and the diversity of the georelief of Slovakia imply considerable contrasts not only in altitude but also in temperature, precipitation, soils, geological composition, vegetation cover (Lukniš *et al.*, 1972). We were interested in the different precipitation patterns at the level of geomorphological units, depending on the altitude and mass of the geomorphological unit, uneven distribution of precipitation can occur at different distances from it. Precipitation is a key element of climate that determines the availability of freshwater, and soil moisture levels and can have a significant

impact on society (Nikolova et al., 2013). The knowledge gained about precipitation variability can carry important information about climate change.

In addition, knowledge of the behavior of different types of cyclonic situations can help us in issuing both meteorological and hydrological warnings. Therefore, the main aim of article is to investigate the changes in precipitation ratios and different distributions of precipitation in Slovakia under northern and southern types of cyclonic situations.

2. Theoretical background

The average annual rainfall is variable, mainly due to the topography, even though Slovakia is a relatively small country. In Slovakia, the average annual rainfall ranges from less than 500 mm in town Galanta, town Senec, and the eastern part of riverine island Žitný ostrov to about 2 000 mm in the High Tatras (SHMIa, 2023).

The spatial distribution, variability, and trends of precipitation have been of interest to several authors around the world (Arora et al., 2006; Meseguer-Ruiz et al., 2019). In addition, in recent years, authors have also been interested in the extremity of precipitation events themselves, which are generally increasing (Casanueva et al., 2014; Iqbal et al. 2019; Markovič et al., 2021)

For our purposes of calculating the share of the average annual precipitation fallen during different types of cyclonic situations in the total average annual precipitation, we have prepared a map of the average annual precipitation fallen during the period 1991–2020 (Fig. 2). Maps of average annual totals can also be found processed by the authors Faško and Št'astný (2002) for the period from 1961 to 1990 or in the Climate Atlas (Bochníček et al., 2015) for the period from 1981 to 2010.

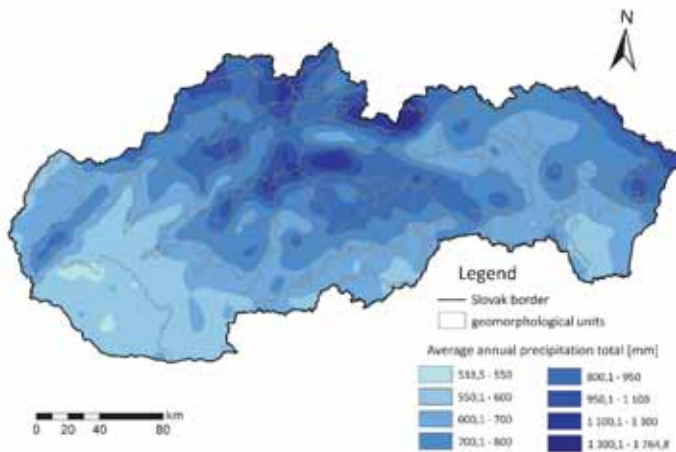


Fig. 2. Average annual precipitation between 1991 and 2020 (Source: SHMI data, own processing).

Sobíšek et al. (1993) define weather typing as a system of synoptic types that have been created using daily synoptic maps for meteorological forecasts, climatological assessments, etc. Classification of synoptic types is the assignment of a classification type to each day, even if the weather on that day does not meet the characteristics of that type (*Benco*, 2009). This is because both the atmospheric circulation and the synoptic type itself are dynamic and constantly changing mechanisms.

In the past, different synoptic classification of weather situations were used for territory of Czechoslovakia. The oldest was by *Hess* and *Brezovský* (1952), in *Katalog der Grosswetterlagen Europas*. This classification, originally developed for the western German territory, did not gain widespread acceptance in our local climatic conditions. Subsequently, several modified synoptic classification were created by *Rein* (1959), *Brádka et al.* (1961), and *Červený* (1965).

At present, the synoptic classification according to the Hydrometeorological Institute under the then leadership of J. Brádka, described in detail in the *Catalogue of Weather Situations of the Czechoslovak Socialist Republic* (*Brádka et al.*, 1968), is valid for our territory. This contains 25 sample synoptic situations, of which 10 are anticyclonic and 15 cyclonic. All types are characterized by a certain flow direction or its short-term changes, the pressure field regime, the way of transition of individual frontal systems, and the air masses flow or their alternation. A detailed description of all types of cyclonic situations can be found on the SHMI website (SHMIb, 2023). Cyclonic situations differ from each other not only in their characteristics, and the trajectory of movement, but also in the spatial distribution of precipitation, different intensities of precipitation, and different occurrences within a calendar year. Since 1991, the Czech and Slovak sides started to prepare their proposals for the types of situations throughout the year separately (Czech Meteorological Society, 2023).

The northern types of cyclonic situations are characterized by the predominant flow from northern directions into our area. NWc (northwest cyclonic situation) and Nc (north cyclonic situation) bring moisture and associated precipitation processes to our area mainly from the northeast Atlantic region. The NEc (northeast cyclonic situation) has a moisture source in the Mediterranean area, which can be deduced from the prevailing flow in *Fig. 3*. The center of the cyclone in this type of situation is generally in the Balkan region, based on which the prevailing northeasterly flow is in our area.

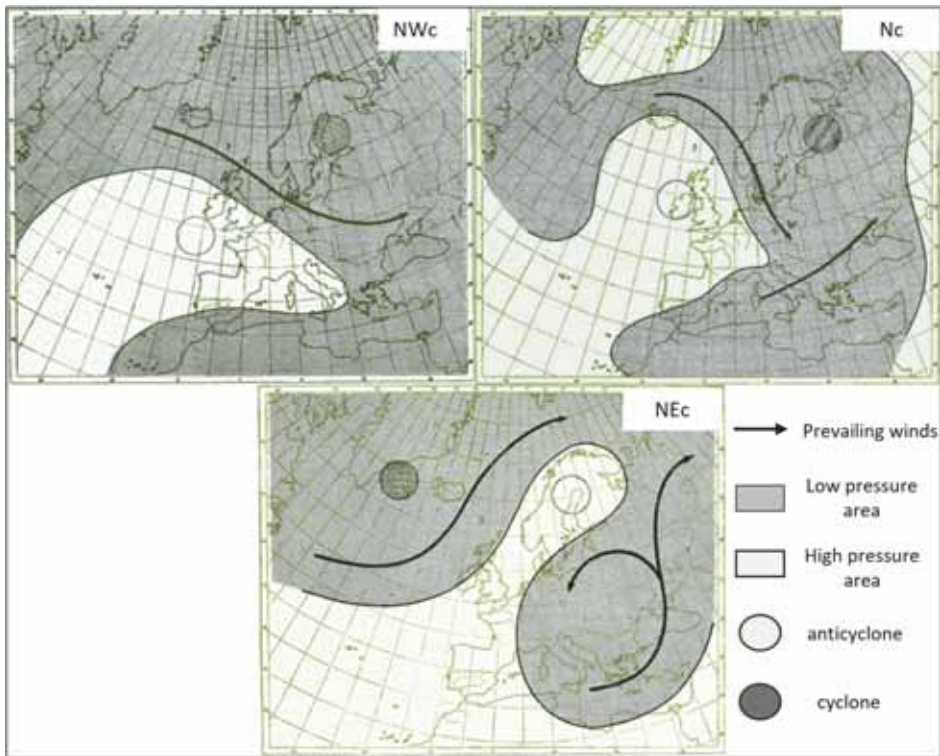


Fig. 3. Schematic representation of the surface pressure field in Europe during different northern types of cyclonic situations (Source: SHMI, own processing).

The southern types of cyclonic situations are characterized by the opposite of the northern types by the flow from the southern directions into our area (Fig. 4). SEc (southeast cyclonic situation) brings to our area precipitation from the Adriatic region, where the center of its “controlling” cyclone is generally located. Situations SWc1, SWc2, and SWc3 (southwesterly cyclonic situation of type 1, type 2, and type 3) bring moisture to our area mainly from the eastern Atlantic region. The SWc1 situation is more meridional compared to the more zonal SWc2 and SWc3 situations, which may give rise to shallow frontal waves in the northern Italy area, which advance northwards across our territory in this type of situation.

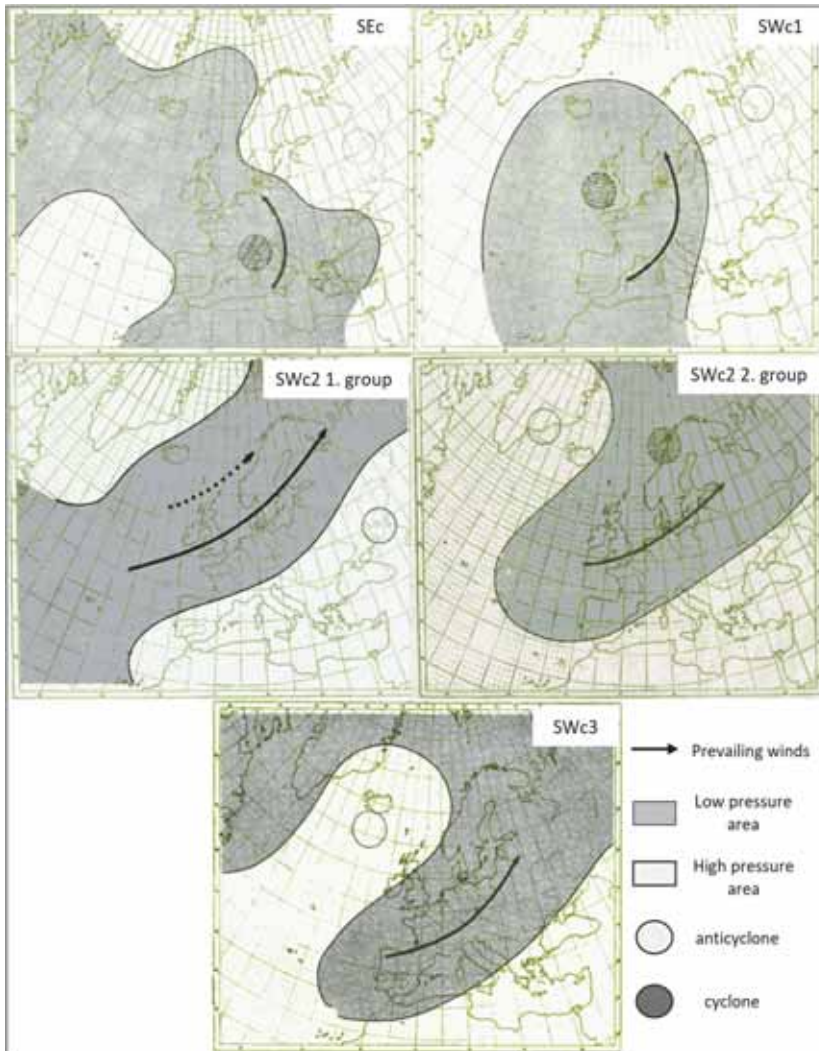


Fig. 4. Schematic representation of the surface pressure field in Europe during individual southern cyclonic types (Source: SHMI, own processing).

However, in this case it is a traditional (subjective) classification. Due to continuous development (objective), algorithmic methods of circulation classification are commonly used in most European countries. Among a number of algorithmic methods, the Simulated Annealing and Diversified Randomisation (SANDRA) classification scheme (Philipp *et al.*, 2007) is a quite reliable and widely used alternative. SANDRA is based on conventional k-means clustering. It is numerically less expensive and overcomes many limitations of established

automatic clustering methods (*Hansen and Belušić, 2021*). Numerous studies have been developed in Europe, investigating the relationship between climatological variables and circulation patterns expressed by different classifications of circulation types. The differences in the construction of various types lie in their adaptation to the geographical and atmospheric conditions of the domain or subdomain. A comparison of circulation type classifications from the COST733 action "Harmonisation and Applications of Weather Types Classifications for European Regions" can be found in *Beck and Phillip (2010)*. The use of the traditional subjective method (e.g., in the case of the Czech Republic and Slovakia) is still applied despite the advanced classification methods (*Řehoř et al., 2020*). A comparison of traditional subjective and objective classification methods analyzed for conditions in Central Europe can be found in *Řehoř et al. (2021)*. The reason for choosing a traditional subjective classification method was to maintain consistency with previous publications to which this paper is directly related.

3. Material and methods

The analysis of changes in precipitation conditions was based on precipitation totals from the SHMI precipitation gauging stations throughout Slovakia in the period 1991–2020. The station network had 798 stations over the 30 years under study, with precipitation totals measured steadily at approximately 600 stations each year. Station network was relatively evenly distributed, except for the highest parts of Slovakia. For the statistical treatment of all northern and southern types of cyclonic situations, we used a classification of synoptic types based on the Catalogue of Weather Situations of Czechoslovakia (*Brádka et al., 1968*) available in the Calendar of Individual Weather Situations (SHMIb, 2023). Since 1991, the Czech and Slovak sides started to prepare their proposals for the types of situations throughout the year independently (Czech Meteorological Society, 2023). Therefore, it was important to investigate the issue from 1991 at the earliest, so that the homogeneity of the data would not be disturbed.

In the Microsoft Excel environment we statistically processed the individual weather situations studied, for which we used the aforementioned calendar of the synoptic classification. Based on it, we recorded the number of days with the occurrence of southern and northern cyclonic situations together but also individually. Then we created a line graph with a linear trend, which showed the evolution of the total number of days of all southern and northern types of situations in the studied period. We further detailed each situation (NWc, Nc, NEc, SEc, SWc1, SWc2, and SWc3). For each year under study, warm half-year (April to September) and cold half-year (October to March), we recorded the number of days with the occurrence of each situation. After then we created a line graph for each situation that displayed the 5-year moving averages of the number of days with that

situation in the year, warm half-year, and cold half-year. Because of the huge variability in the occurrence of individual northern and southern cyclonic situations, we preferred to work only with the 5-year moving averages, since using a linear trend would result in a coefficient of determination (R^2) close to 0.

However, annual and daily precipitation totals (from 7.00 a.m. to 7.00 a.m. of the following day) were the subject of the main treatment. Additional but important data were geographic coordinates, indications, and names of rain gauge stations. Precipitation totals were sorted in the Microsoft Excel environment based on the cyclonic types studied according to the calendar of individual weather situations (SHMIb, 2023). Furthermore, annual and daily precipitation totals were processed in ArcGIS software using the Topo to Raster interpolation method. The aforementioned method calculates an estimate of the interpolated value from four adjacent points using an iterative finite difference method (ArcGIS, 2024). According to Šercl (2008), the isolines produced by this interpolation most closely resemble the isolines that would be a map would be drawn by an experienced expert. In addition, a script in Python environment was used to streamline the creation of the individual partial raster for spatial distribution of precipitation (referred to as rasters hereafter). A simplified flowchart of the processing of the resulting maps is shown in *Fig. 5*. The detailed methodology can be found in the work on Precipitation conditions of Slovakia in northern and southern cyclonic situations (Zaujec, 2022). However, this article is based on adjusted partial rasters that were created only when processing the average annual precipitation totals of all individual cyclonic situations (Halaj and Zaujec, 2023).

To create maps of average annual precipitation totals of all northern and southern cyclonic types, respectively, we summed all partial raster of the entire period and divided them by the number of years of the period under study (the entire 30-year period, or 10 years). We then obtained the resulting raster from which we could create individual maps (*Figs. 9 and 10*). In each quadrant representing a decade or the whole period, respectively, we chose the same 8-class scale with an assignment of the value of the maximum and minimum rainfall totals in the period under study.

In *Figs. 11 and 12* are presented the proportion of the average annual precipitation fallen during all northern cyclonic types, and southern cyclonic types out of the total average annual precipitation for the whole period (1991–2020). We also used similarly processed partial raster for the average annual rainfall in Slovakia (e.g., *Fig. 2*, but also for the average annual rainfall in individual decades) for each decade (1991–2000, 2001–2010, 2011–2020). Similar to the previous type of results, we divided the resulting maps into 4 quadrants, with each map consisting of the same 8-class scale with the maximum and minimum fraction of precipitation of all northern and southern cyclonic situations, respectively, assigned to the total mean annual precipitation. So, what does the changes in precipitation ratios and overall distribution of precipitation totals look like across all northern and southern cyclonic types over the last few decades?



Fig. 5. Simplified scheme of data processing into map form.

4. Results

Over the 30 years from 1991–2020, all cyclonic types occurred on a total of 6582 days, of which the northern and southern types studied accounted for more than 42%. However, there has been a decline in the occurrence of cyclonic types of situations over the period studied, at the expense of an increase in anticyclonic types (Fig. 6).

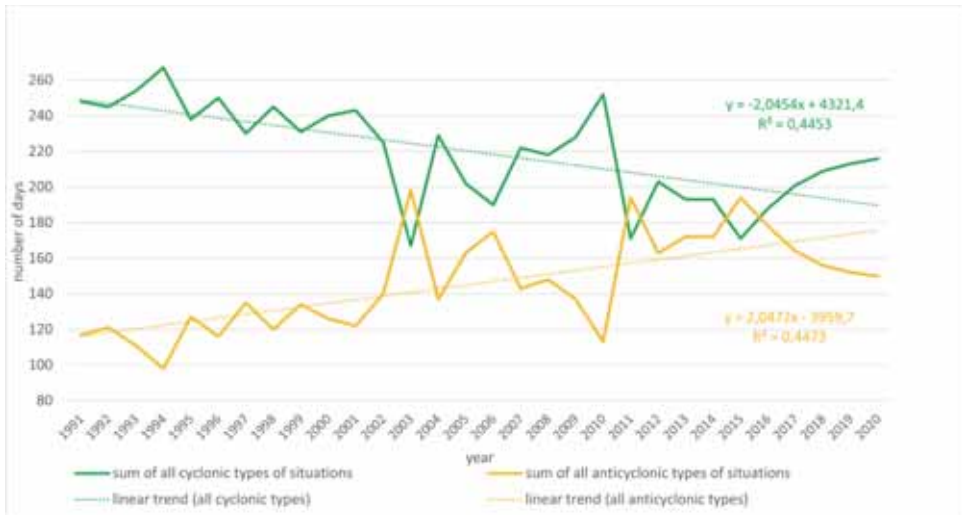


Fig. 6. Number of days with all cyclonic and all anticyclonic situations between 1991–2020 (Source: SHMI data, own processing).

Of the specific northern and southern types of cyclonic situations studied, the NEc situation occurred most frequently, specifically on 720 days. On the contrary, the SWc3 situation occurred the least, in 250 days. In total, all situations occurred on 2794 days, of which the northern situations occurred on 1636 days and the southern situations on 1158 days. The situations studied occurred most frequently in 2001 (128 days) and in the lowest number of days in 2015 (42 days). Interestingly, all but the southern and northern situations declined over the study period (*Fig. 7*). From the trend line, we can read a more pronounced reduction of southern over northern cyclonic situations. However, it is worth mentioning the significant variability in the occurrence of southern and even more northern types of cyclonic situations from year to year.

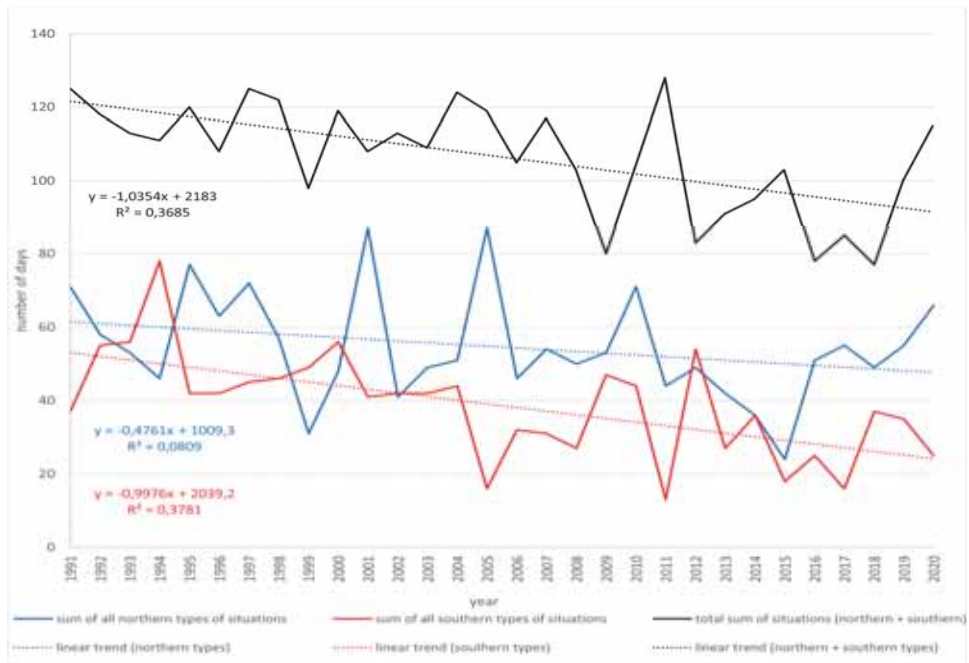


Fig. 7. Number of days with all northern and southern cyclonic situations between 1991–2020 (Source: SHMI data, own processing).

The NWc situation occurred on 577 days during the period under study, with the lowest occurring towards the end of the first decade and the beginning of the second decade, respectively, based on 5-year moving averages. Conversely, at the end of the period under study, this type of situation occurred the most, on an average of 23 days per year. For the most frequently occurring situation NEc (720 days per period), we can see that the situation generally occurred most frequently in the first decade under study, but it was significantly less in the last

decade as we can see in *Fig. 8*. Overall, the Nc situation occurred on 339 days, and similar to the NEc type, the most frequent occurrence was in the first decade studied and the least frequent occurrence was in the last years studied. For the NEc and Nc situation, we observed a significant decrease in occurrence over the study period, which was also reflected in the overall decrease of all northern cyclonic situation types between 1991 and 2020 (*Fig. 7*).

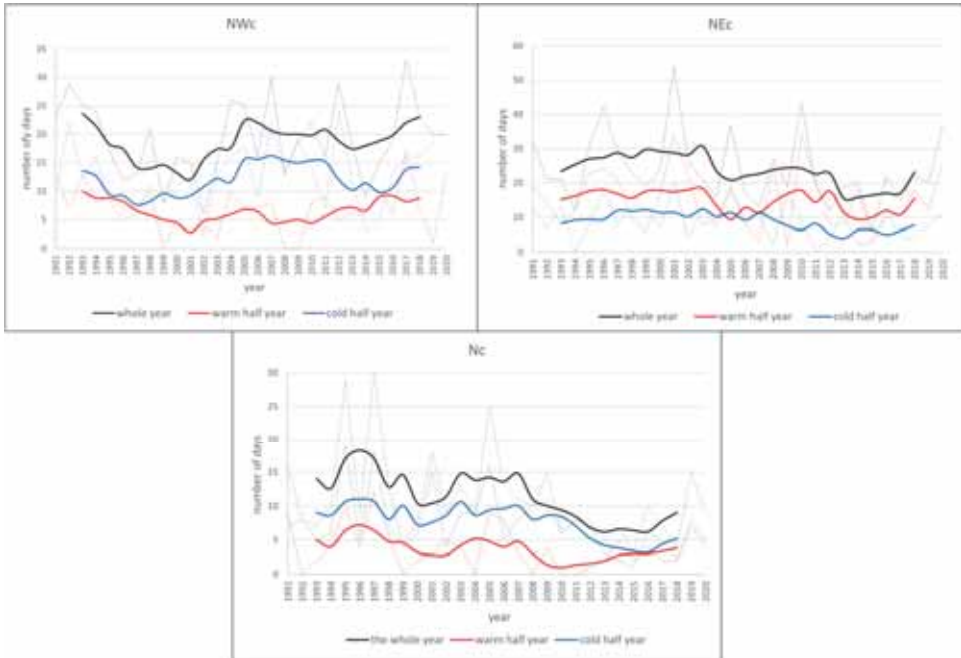


Fig. 8. Number of days with individual northern cyclonic situations between 1991–2020 (rough curves = 5-year moving averages) (Source: SHMI data, own processing).

The SEc situation occurred on 281 days during the study period, occurring most frequently in the middle of the first decade studied and least frequently in the middle of the second decade. The different SWc types occurred differently over the study period, as can be read from *Fig. 9*. Of these, the SWc2 situation occurred most frequently at 352 days, followed by the SWc1 situation at 275 days, and the SWc3 situation occurred least frequently at 250 days. It is worth noting the significant decrease in the type of SWc3 situation, which occurred on only 14 days in the last decade, while in 6 years of the mentioned decade, this situation did not occur even once. In comparison, in the first and second decade, the situation occurred on 135 and 101 days, respectively. This situation is the main cause of the overall decline in all southern cyclonic situation types combined (*Fig. 7*).

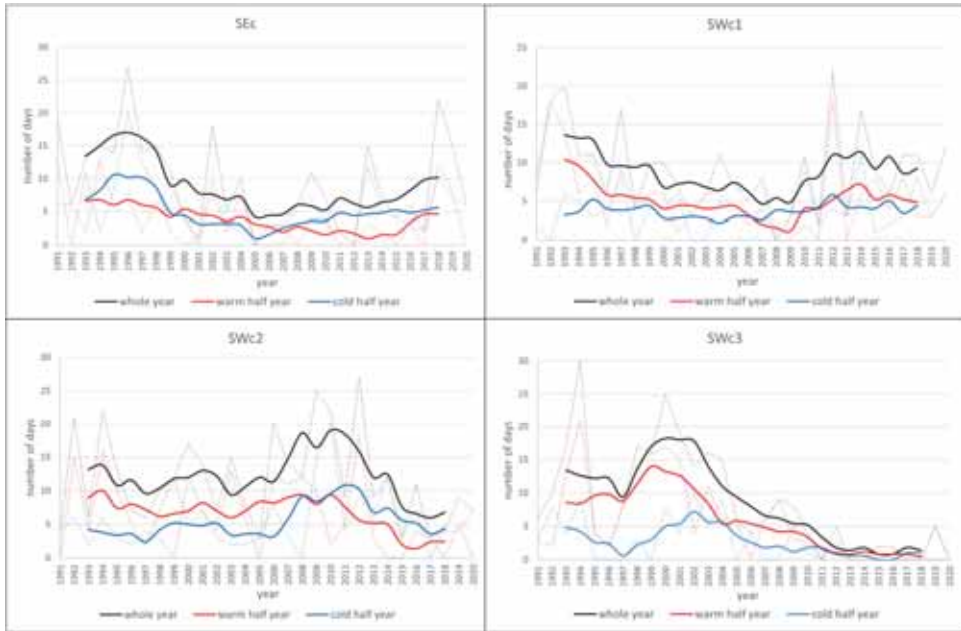


Fig. 9. Number of days with individual southern cyclonic situations between 1991–2020 (rough curves indicate 5-year moving averages) (Source: SHMI data, own processing).

The average annual precipitation for all northern cyclonic types between 1991–2020 ranged from about 68 mm at the boundary between the geomorphological units Podunajská pahorkatina and Podunajská rovina, to about 530 mm in the geomorphological unit Tatry (Fig. 10). The decade 1991–2000 (576 days of occurrence) was the driest in terms of average annual precipitation. In contrast, the decade 2001 to 2010 (589 days of occurrence) was the wettest decade for all northern cyclonic types. The last decade studied, 2011–2020 (471 days of occurrence), was the most similar to the average over the entire 30-year period studied.

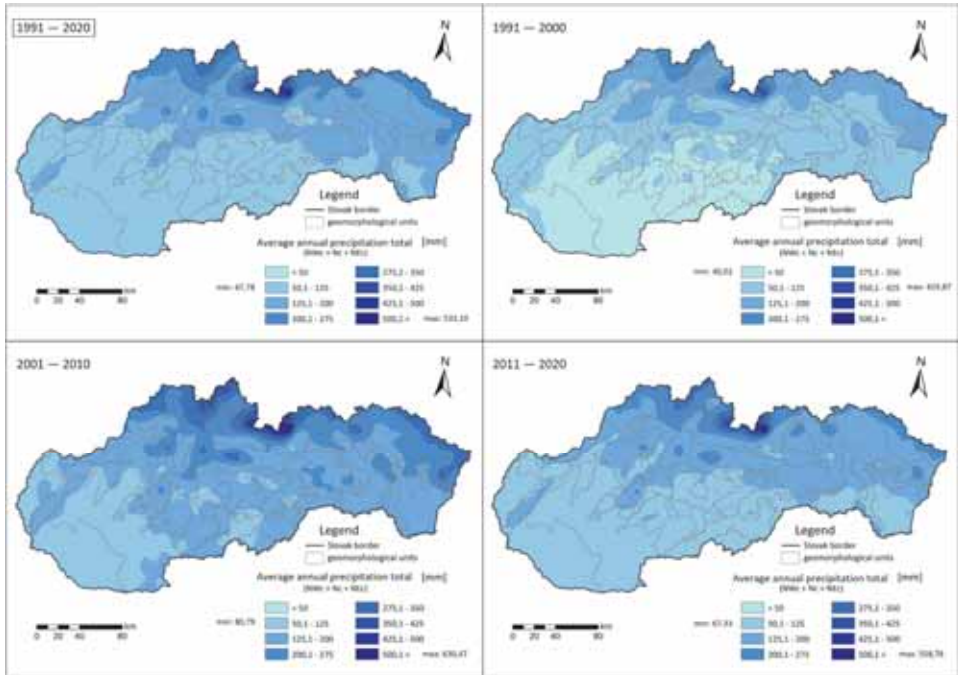


Fig. 10. Average annual precipitation total for all northern cyclonic types from 1991 – 2020 (full period and individual decades) (Source: SHMI data, own processing).

The average annual precipitation for all southern cyclonic types between 1991–2020 ranged from about 78 mm in the geomorphological unit Východoslovenská nížina to more than 200 mm in the geomorphological units Starohorské vrchy, Nízke Tatry, and Tatry (*Fig. 11*). The decade 1991–2000 (506 days of occurrence) was the wettest in terms of average annual precipitation for the southern types. In contrast, the driest decade for all southern cyclonic types was the last decade 2011–2020, when these situations occurred on only 286 days. The middle decade studied, 2001–2010 (366 days of occurrence), was the most similar to the average over the entire 30-year period studied.

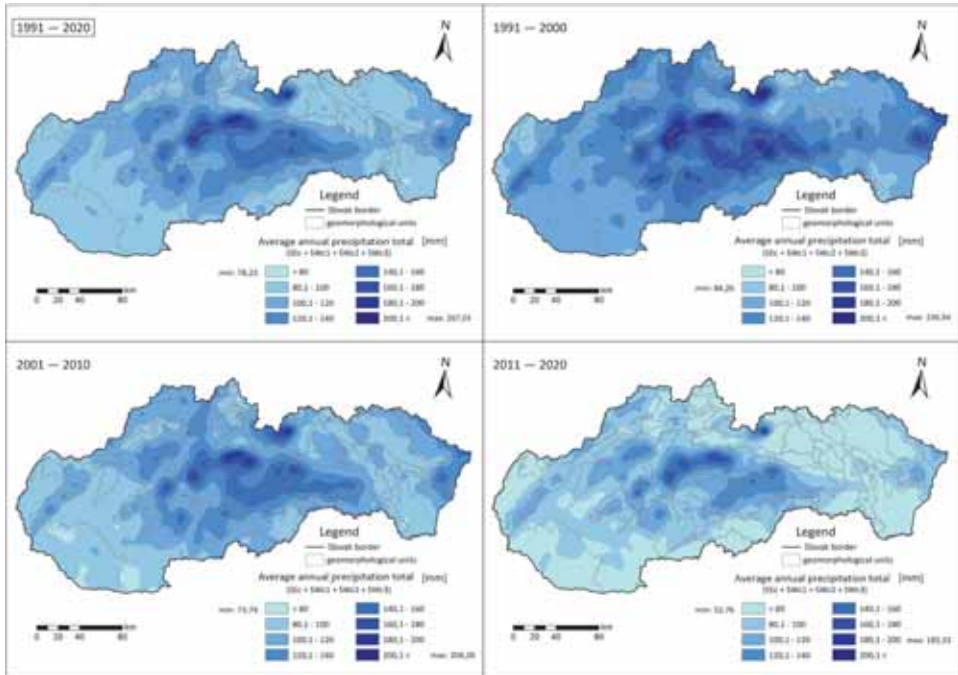


Fig. 11. Average annual precipitation for all southern cyclonic types from 1991–2020 (full period and individual decades) (Source: SHMI data, own processing).

The proportion of the average annual precipitation fallen during all northern cyclonic types out of the total average annual precipitation during the period 1991–2020 ranged from less than 12% in the geomorphological units Zvolenská kotlina and Horehronské podolie, to more than 32% in the geomorphological units Čergov and Busov (Fig. 12). In general, the highest proportion of average annual precipitation falling during all northern types of cyclonic situations out of the total average annual precipitation was in the second studied decade from 2001–2010, where it was also more than 40% in Čergov. In the geomorphological units in the north of the territory, especially in the border area with Poland, the significantly increased percentage of the average annual precipitation fallen during all northern types of cyclonic situations from the total average annual precipitation can be attributed to the enhanced windward effect of the individual mountain ranges.

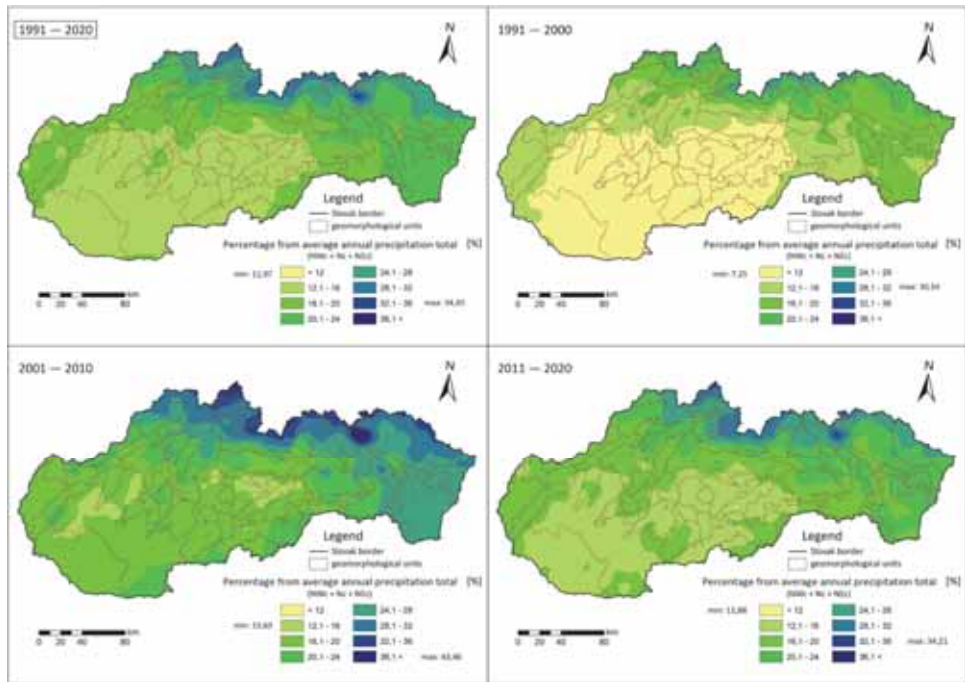


Fig. 12. Percentage of average annual precipitation fallen during all northern cyclonic types out of the total average annual precipitation for the whole period (1991–2020) or for each decade (1991–2000, 2001–2010, 2011–2020). (Source: SHMI data, own processing).

The percentage of the average annual precipitation fallen during all southern cyclonic types out of the total average annual precipitation in the period 1991–2020 ranged from less than 10% in the geomorphological units Oravské Beskydy, Podbeskydská brázda, Podtatranská brázda, Skorušinské vrchy, Spišská Magura, and Pieniny, to more than 18.5% in the geomorphological units Revúcka vrchovina, Stolické vrchy, and Zvolenská kotlina (Fig. 13). The highest percentage of the average annual precipitation fallen during all southern cyclonic types out of the total average annual precipitation of cyclonic situations was during the first studied decade in the period 1991–2000, where in most of the geomorphological units of the southern half of Slovakia the mentioned percentage was more than 20%. This was due to the very frequent occurrence of southern cyclonic types in this decade (506 days of occurrence). On the contrary, in the following decades, a significant decrease in the studied situations was recorded, which was also reflected in the actual decrease of the percentage of the average annual precipitation falling during all southern types out of the total average annual precipitation.

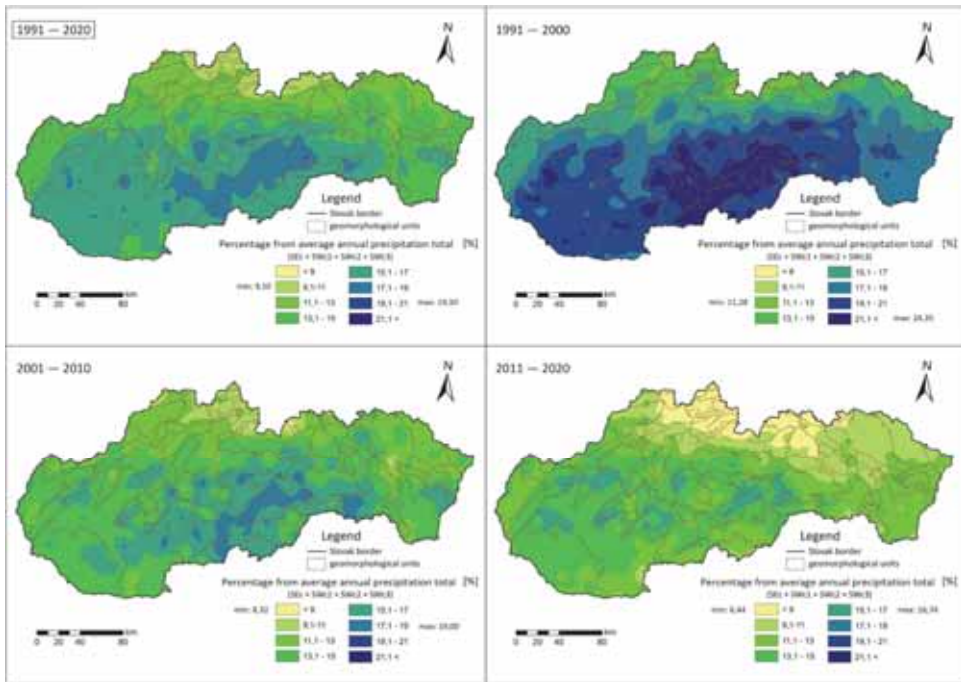


Fig. 13. Percentage of average annual precipitation fallen during all southern cyclonic types out of the total average annual precipitation for the whole period (1991–2020) or for each decade (1991–2000, 2001–2010, 2011–2020). (Source: SHMI data, own processing).

5. Discussion and conclusion

In terms of statistical processing, we can conclude that all northern cyclonic types (NWc, Nc and, NEc) occurred in 1636 days between 1991–2020, while all southern types (SEc, SWc1, SWc2, and SWc3) occurred in 1158 days. In both cases, there was a decrease in the occurrence of weather events over the study period, but the decrease is more pronounced for the southern types (Fig. 8). Such results confirm the changes in the general circulation of the atmosphere in our area and help to capture trends or predictions of the future climate on the territory of Slovakia. The North Atlantic Oscillation (NAO) may be one of the reasons for the decrease in days with the occurrence of the studied situations, especially meridional types. In recent decades, its positive phase prevails over the negative phase, as confirmed by *Lešková et al.* (2012), and even the frequency of the extremely positive phase could increase in the winter months in the future, according to *McKenna and Maycock* (2022). When the NAO is in the negative

phase, the flow is more meridional. On the contrary, when the phase is positive, the flow is more zonal (Labudová *et al.*, 2013).

Noting the resulting maps of mean annual precipitation for all northern and southern types of cyclonic situations from the total average annual precipitation, respectively, we see only small areas of intervals for the highest precipitation totals for the northern types of cyclonic situations (NWc + Nc + NEc) compared to large areas of intervals for the lowest precipitation totals (mainly the southern half of Slovakia). In contrast, there was almost no difference between the size of the areas representing the areas of the intervals for the highest and lowest precipitation totals for the southern types of cyclonic situations (SEc + SWc1 + SWc2 + SWc3). This is probably due to the absence of significant vertically and horizontally massive mountain ranges in the southern part of Slovakia. Because of this, from the southern directions, these types of situations are not weakened by mountain ranges further north and are even often precipitation amplified by outflow movements in the central part of Slovakia (suitably located mountain ranges with respect to the flow direction) and are thus not weakened as in the case of the northern types, which "crash" into higher geomorphological units already at the border with Poland.

In the next part of the results, we investigated the percentage of the mean annual precipitation fallen during all northern and southern cyclonic situations, respectively, out of the total average annual precipitation. Noting the result maps of this part of the results alone, we see higher differences between the maximum and minimum percentages for the northern types of cyclonic situations (NWc + Nc + NEc) than for the southern types (SEc + SWc1 + SWc2 + SWc3). One reason for this may be the more pronounced windward and leeward effect for the northern types of cyclonic situations partly mentioned in the previous paragraph. Another cause is the more frequent occurrence of northern types of cyclonic situations. For the southern types, there was a significant decrease in the proportion of total precipitation out of the total mean precipitation over the decades, which correlated with a rapid decline in the number of days with southern types of cyclonic situations. For the northern types, we also observed a decrease in the number of days between the first (1991–2000) and the last decade (2011–2020), but the percentage of total precipitation increased for these types in the last decade studied. This suggests to us that the average daily precipitation for the northern cyclonic types was higher than in the first decade under study (if we consider a minimal change in the total average annual precipitation). This may be due to the higher air temperature in the near-surface layer of the atmosphere caused by global warming, which directly affects the ability of the air to take up water vapour (there is an increase in water vapour content of about 6–7% per 1 °C for the same relative humidity) (Pecho and Faško, 2010). However, as Lapin *et al.* (2010) point out, higher average air temperature does not only cause a higher risk of heavy precipitation under cyclonic weather conditions or intense convection but also a higher risk of drought under anticyclonic weather conditions. Droughts

are particularly accentuated by increasing evapotranspiration due to rising temperatures and increasing frequency of heat waves in central Europe (*Lapin et al.*, 2015; *Tomczyk and Bednorz*, 2016).

Climate change has resulted in a change in the occurrence of more extreme weather events (Ministry of the Environment of the Slovak Republic, 2018). For example, the period 1980–2016 was characterized by high variability in rainfall (152% of normal in 2010, 74% of normal in 2003), which caused episodes of severe drought on the one hand and local or regional floods on the other (*Gnida et al.*, 2017). One of the adverse consequences of this change is that it can cause changes in hydrological processes, thereby increasing the likelihood of extreme events such as droughts and floods (*De Sá Silva et al.*, 2022). Therefore, we also consider it very important to study changes in precipitation ratios for different types of cyclonic situations in an attempt to understand, prepare for, or adapt to ongoing and also incoming climate change.

Although works of similar focus in Slovakia can be found in the earlier past (*Brázdil and Faško*, 1993). *Hoy et al.* (2014) investigated large-scale synoptic types in relation to precipitation in Europe and concluded that changes in precipitation totals are related to changes in the frequency of synoptic types, but predominantly during the winter half-year. However, similar work can also be found in neighboring Poland where the variability of precipitation in relation to individual situations was addressed in the area of the High Tatras and they identified 3 types of cyclonic situations (namely 2 of them are Nc and NEc), which are responsible for the most extreme precipitation in the mentioned area (*Niedźwiedz et al.*, 2015). However, the first work in Slovakia that set up a systematic treatment of precipitation totals in different types of cyclonic situations was by *Mészáros* (2015), focusing on situations from southerly directions. In addition, *Mészáros* (2019) developed this work with results for windward and leeward positions and the occurrence of different types of southern cyclonic situations. A similar methodology has been developed in the works by *Kasza* (2018) - northern directions and *Halaj* (2019) - western directions. The subject of the work was mainly the average annual rainfall totals during the different situations studied. The identified precipitation total and the cumulative precipitation total forecast from the ECMWF model (European Centre for Medium-Range Weather Forecasts) were confronted by *Polčák and Mészáros* (2018) on the example of a specific cyclonic situation. The aforementioned work was followed by *Zaujec* (2020), where the influence of georelief on the precipitation totals of the Podunajská nížina under NWc and SEc situations was investigated in detail. Based on a 40-year period, windward, leeward and neutral positions were identified for all northern and southern cyclonic situation types using an innovative methodology (*Zaujec*, 2022). A partially new output was the grouping of cyclonic situations based on their prevailing flow (*Mészáros et al.*, 2022). As the methodological approach was adopted in the then work and encountered its limitations, it had to be modified. This occurred in the

- De Sá Silva, A.C.R., Bimbato, A.M., Balestieri, J.A.P., and Vilanova, M.R.N., 2022: Exploring environmental, economic and social aspects of rainwater harvesting systems: A review. *Sustain. Cities Soc.* 76(23), 103475. <https://doi.org/10.1016/j.scs.2021.103475>
- Fáško, P. and Šťastný, P., 2002: Average annual rainfall totals. In Atlas of the landscape of the Slovak Republic. Bratislava: Ministry of the Environment of the Slovak Republic, Banská Bystrica: Slovak Environmental Agency. 344 p. ISBN 80-88833-27-2.
- Freeworldmaps, 2023: Europe physical map. [online]. [cit. 2024-01-10]. Available on the internet: <https://www.freeworldmaps.net/europe/>
- Gnida, M., Grajciar, M., Chocholová, L., Košovský, P., Malatinská, L., ... and Hlásny, T., 2017: The Seventh National Communication of the Slovak Republic on Climate Change. Under the United Nations Framework Convention on Climate Change and the Kyoto Protocol. Ministry of Environment of the Slovak Republic and Slovak Hydrometeorological Institute, Bratislava. [online]. [cit. 2024-01-10]. Available at: https://unfccc.int/sites/default/files/resource/976840315_Slovakia-NC7-17NC_SVK.pdf
- Halaj, M., 2019: Effect of relief on the distribution of precipitation in Slovakia in western cyclonic situations. Bratislava. Diploma thesis. Comenius University in Bratislava. Faculty of Natural Sciences, 83 p. [online]. (in Slovak) [cit. 2023-10-10]. Available at: <https://opac.crzp.sk/?fn=detailBiblioForm&sid=BCA102CB6C4CA54D4BE6A175C35B>
- Halaj, M., and Zaujec, P., 2023: Priestorové rozloženie atmosférických zrážok na Slovensku počas rôznych typov synoptických situácií v období 1991–2020. *Meteorologický časopis* 26(1), 15–25. (in Slovak)
- Hansen, M., and Belusić, D., 2021: Tailoring circulation type classification outcomes. *Int. J. Climatol.* 41, 6145–6161. <https://doi.org/10.1002/joc.7171>
- Hess P. and Brezowsky H., 1952: Katalog der grosswetterlagen europas. Deutscher Wetterdienst. 39 p. (in German)
- Hoy, A., Schucknecht, A., Sepp, M., and Matschullat, J., 2014: Large-scale synoptic types and their impact on European precipitation. *Theor. Appl. Climatol.* 116, 19–35. <https://doi.org/10.1007/s00704-013-0897-x>
- Iqbal, Z., Shahid, S., Ahmed, K., Termizi I., and Nadeem N., 2019: Spatial distribution of the trends in precipitation and precipitation extremes in the sub-Himalayan region of Pakistan. *Theor. Appl. Climatol.* 137, 2755–2769. <https://doi.org/10.1007/s00704-019-02773-4>
- Kasza, R., 2018: Effect of relief on the distribution of precipitation in Slovakia in northern cyclonic situations. Diploma thesis. Comenius University in Bratislava. Faculty of Natural Sciences. 67 p. (in Slovak) [online]. [cit. 2023-10-10]. Available at: <https://opac.crzp.sk/?fn=detailBiblioForm&sid=EEE57057A47611A7EF7ACC4E9AC3>
- Labudová, L., Šťastný, P. and Trizna, M., 2013: The north atlantic oscillation and winter precipitation totals in Slovakia. *Moravian Geographical Reports* 21(4), 38–49. <https://doi.org/10.2478/mgr-2013-0019>
- Lapin, M., Damborská, I., Gera, M., Hrvol, J., and Melo, M., 2015: Trends of evapotranspiration in Slovakia, including scenarios up to 2100. In: International Bioclimatological Conference: Toward Climatic Services. Slovak Bioclimatological Society SAS, Nitra, 5 p. <http://www.sbks.sk/doc/papers/Lapin%20Trends%20of%20evapotranspiration.pdf>
- Lapin, M., Gera, M., and Kremler, M., 2010: Temperature and Air Humidity Scenarios for Slovakia and Possible Impacts in the Cities. *Život. Prostr.* 44(3), 227–231. (in Slovak) http://publikacie.uke.sav.sk/sites/default/files/2010_5_227_231_lapin.pdf
- Lešková, L., Šťastný, P., and Trizna, M., 2012: Analýza vplyvu Severoatlantickej oscilácie na sezónne úhrny zrážok v zrážkových oblastiach Slovenska. *Meteorologický časopis* 15(2), 75–80. (in Slovak) https://www.shmu.sk/File/ExtraFiles/MET_CASOPIS/2012-2_MC.pdf
- Lukniš, M. 1972: Slovakia 2. Nature. Bratislava: Obzor. ISBN 65-043-72-I (in Slovak)
- Markovič L., Fáško P., and Pecho J., 2021: Climatology of the extreme heavy precipitation events in Slovakia in the 1951–2020 period. *Acta Hydrologica Slovaca* 22(2), 294–303. <https://doi.org/10.31577/ahs-2021-0022.02.0033>
- Mazúr E. and Lukniš M., 1978: Regional Geomorphological Division of the SSR. *Geografický časopis*, 30(2), 101–125. (in Slovak) https://www.sav.sk/journals/uploads/10251027GC_1978_2_1_Mazur%20et%20al.pdf

- McKenna, CH., and Maycock, A., 2022: The Role of the North Atlantic Oscillation for Projections of Winter Mean Precipitation in Europe. *Geophys. Res. Lett.* 49(19). e2022GL099083. <https://doi.org/10.1029/2022GL099083>
- Meseguer-Ruiz, O., Ponce-Philimon, P.I., Guijarro, J.A., and Sarricolea, P., 2019: Spatial distribution and trends of different precipitation variability indices based on daily data in Northern Chile between 1966 and 2015. *Int. J. Climatol.* 39, 4595–4610. <https://doi.org/10.1002/joc.6089>
- Mészáros, J., 2015: Effect of relief on the distribution of precipitation in Slovakia in southern cyclonic situations. Bratislava. Diploma thesis. Comenius University in Bratislava, Faculty of Natural Sciences. (in Slovak) [online]. [cit. 2024-01-17]. Available at: <https://opac.crzp.sk/?fn=detailBiblioFormChildI103R7&sid=4A220BA9C567A84919003CD1351D&seo=CRZP-detail-kniha>
- Mészáros, J., 2019: Spatial patterns of distribution of atmospheric precipitation in Slovakia in southern cyclonic situations during the period 1991–2015. Bratislava. Rigorous thesis. Comenius University in Bratislava, Faculty of Natural Sciences. (in Slovak) [online]. [cit. 2024-01-17]. Available at: <https://opac.crzp.sk/?fn=detailBiblioForm&sid=5379D0B7E3C25FE39D32B84ABF03>
- Mészáros, J., Halaj M., Polčák N., and Onderka M., 2022: Mean annual totals of precipitation during the period 1991–2015 with respect to cyclonic situations in Slovakia. *Időjárás* 126, 267–284. <https://doi.org/10.28974/idojaras.2022.2.6>
- Ministry of the Environment of the Slovak Republic, 2018: Stratégia adaptácie Slovenskej republiky na zmenu klímy. (in Slovak) [online]. [cit. 2024-02-25]. Available at: <https://www.minzp.sk/files/odbor-politiky-zmeny-klimy/strategia-adaptacie-sr-zmenu-klimy-aktualizacia.pdf>
- Niedzwiedz, T., Lupikasza, E., Pińskwar, I., Kundzewicz, Z., and Malarzewski, L., 2015: Variability of high rainfalls and related synoptic situations causing heavy floods at the northern foothills of the Tatra Mountains. *Theor. Appl. Climatol.* 119, 273–284. <https://doi.org/10.1007/s00704-014-1108-0>
- Nikolova, N., Faško, P., Lapin, M., and Švec, M., 2013: Changes in snowfall/precipitation-day ratio in Slovakia and their linkages with air temperature and precipitation. *Contribut. Geophys. Geodesy* 43(2), 141–155. <https://doi.org/10.2478/congeo-2013-0009>
- Oudar, T., Cattiaux, J. and Douville, H., 2020: Drivers of the northern extratropical eddy-driven jet change in CMIP5 and CMIP6 models. *Geophys. Res. Lett.* 47(8). e2019GL086695 <https://doi.org/10.1029/2019GL086695>
- Pecho, J. and Faško, P., 2010: Hazards of extreme summer rainfall. Slovak Hydrometeorological Institute. [online]. [cit. 2024-01-10]. Available at: <https://www.shmu.sk/sk/?page=2049andid=142>
- Phillip, A., Dekka-Marta, P.M., Jacobeit, J., Fereday, D.R., Jones, P.D., Moberg, A., and Wanner, H., 2007: Long-term variability of daily North Atlantic–European pressure patterns since 1850 classified by simulated annealing clustering. *J. Climate* 20, 4065–4095. <https://doi.org/10.1175/JCLI4175.1>
- Polčák, N., and Mészáros, J., 2018: The effect of relief on the distribution of atmospheric precipitation in Slovakia in the southern cyclonic situations. *Geografický časopis* 70(3), 259–272. (in Slovak) <https://doi.org/10.31577/geogrcas.2018.70.3.14>
- Rein, F., 1959: Weather typing with regard to dynamic climatology. *Studia Geophysica et Geodaetica* 3, 177–194. (in Russian) <https://doi.org/10.1007/BF02585561>
- Řehoř, J., Brázdil, R., Trnka, M., Řezníčková, L., Balek, J., and Možný, M., 2020: Regional effects of synoptic situations on soil drought in the Czech Republic. *Theor. Appl. Climatol.* 141, 1383–1401. <https://doi.org/10.1007/s00704-020-03275-4>
- Řehoř, J., Brázdil, R., Lhotka, O., Trnka, M., Balek, J., Štěpánek, P., and Zahradníček, P., 2021: Precipitation in the Czech Republic in light of subjective and objective classifications of circulation types. *Atmosphere* 11, 1536. <https://doi.org/10.3390/atmos12111536>
- Šercl, P., 2008: Assessment of methods for area precipitation estimates. *Meteorologické zprávy* 61(2), 33–43. (in Czech) <https://www.chmi.cz/files/portal/docs/reditel/SIS/casmz/assets/2008/Meteor-2008-02.pdf>
- Shepherd, T.G., 2014: Atmospheric circulation as a source of uncertainty in climate change projections. *Nat. Geosci.* 7, 703–708. <https://doi.org/10.1038/NGEO2253>
- SHMIA, 2023: Climatic conditions of Slovakia. (in Slovak) [online]. [cit. 2024-02-26]. Available on the internet: <https://www.shmu.sk/sk/?page=1064>

- SHMib.*, 2023: Types of weather situations. (in Slovak) [online]. [cit. 2024-02-26]. Available on the internet: <https://www.shmu.sk/sk/?page=8androk=2020>
- Sobišek, B.*, 1993: Meteorologický slovník výkladový & terminologický. Praha: Ministerstvo životního prostředí České republiky. 594 p. ISBN 80-85368-45-5. (in Czech)
- Tomczyk, A. M., and Bednorz, E.*, 2016: Heat waves in Central Europe and their circulation conditions. *Int. J. Climatol.* 36, 770–782. <https://doi.org/10.1002/joc.4381>
- Zaujec, P.*, 2020: Influence of the relief on the precipitation conditions of the Podunajská nížina during the period 1991 – 2018. Bratislava. Bachelor thesis. Comenius University in Bratislava, Faculty of Natural Sciences. 55 p. (in Slovak) [online]. [cit. 2024-01-10]. Available at: <https://opac.crzp.sk/?fn=detailBiblioForm&sid=C4B2143D4F9CE1498D0864B8E130>
- Zaujec, P.*, 2022: Precipitation conditions of Slovakia in northern and southern cyclonic situations. Bratislava. Diploma thesis. Comenius University in Bratislava, Faculty of Natural Sciences. [online]. [cit. 2024-01-10]. Available at: <https://opac.crzp.sk/?fn=detailBiblioForm&sid=2F8FD603D177BA679134FA795407> (in Slovak)

INSTRUCTIONS TO AUTHORS OF *IDŐJÁRÁS*

The purpose of the journal is to publish papers in any field of meteorology and atmosphere related scientific areas. These may be

- research papers on new results of scientific investigations,
- critical review articles summarizing the current state of art of a certain topic,
- short contributions dealing with a particular question.

Some issues contain “News” and “Book review”, therefore, such contributions are also welcome. The papers must be in American English and should be checked by a native speaker if necessary.

Authors are requested to send their manuscripts to

Editor-in Chief of IDŐJÁRÁS
P.O. Box 38, H-1525 Budapest, Hungary
E-mail: journal.idojaras@met.hu

including all illustrations. MS Word format is preferred in electronic submission. Papers will then be reviewed normally by two independent referees, who remain unidentified for the author(s). The Editor-in-Chief will inform the author(s) whether or not the paper is acceptable for publication, and what modifications, if any, are necessary.

Please, follow the order given below when typing manuscripts.

Title page should consist of the title, the name(s) of the author(s), their affiliation(s) including full postal and e-mail address(es). In case of more than one author, the corresponding author must be identified.

Abstract: should contain the purpose, the applied data and methods as well as the basic conclusion(s) of the paper.

Key-words: must be included (from 5 to 10) to help to classify the topic.

Text: has to be typed in single spacing on an A4 size paper using 14 pt Times New Roman font if possible. Use of S.I.

units are expected, and the use of negative exponent is preferred to fractional sign. Mathematical formulae are expected to be as simple as possible and numbered in parentheses at the right margin.

All publications cited in the text should be presented in the *list of references*, arranged in alphabetical order. For an article: name(s) of author(s) in Italics, year, title of article, name of journal, volume, number (the latter two in Italics) and pages. E.g., *Nathan, K.K.*, 1986: A note on the relationship between photo-synthetically active radiation and cloud amount. *Időjárás* 90, 10–13. For a book: name(s) of author(s), year, title of the book (all in Italics except the year), publisher and place of publication. E.g., *Junge, C.E.*, 1963: *Air Chemistry and Radioactivity*. Academic Press, New York and London. Reference in the text should contain the name(s) of the author(s) in Italics and year of publication. E.g., in the case of one author: *Miller* (1989); in the case of two authors: *Gamov* and *Cleveland* (1973); and if there are more than two authors: *Smith et al.* (1990). If the name of the author cannot be fitted into the text: (*Miller*, 1989); etc. When referring papers published in the same year by the same author, letters a, b, c, etc. should follow the year of publication. DOI numbers of references should be provided if applicable.

Tables should be marked by Arabic numbers and printed in separate sheets with their numbers and legends given below them. Avoid too lengthy or complicated tables, or tables duplicating results given in other form in the manuscript (e.g., graphs). *Figures* should also be marked with Arabic numbers and printed in black and white or color (under special arrangement) in separate sheets with their numbers and captions given below them. JPG, TIF, GIF, BMP or PNG formats should be used for electronic artwork submission.

More information for authors is available: journal.idojaras@met.hu

Published by the HungaroMet Hungarian Meteorological Service

Budapest, Hungary

ISSN 0324-6329 (Print)

ISSN 2677-187X (Online)